THE Marquardt CORPORATION

12 MARCH 1964

REPORT 6033

COPY NO. 50

(Title -- Unclassified)

HYDROGEN RELIQUEFIERS FOR LUNAR STORAGE SYSTEMS

UNCLASSIFIED

(Title -- Unclassified)

HYDROGEN RELIQUEFIERS FOR LUNAR STORAGE SYSTEMS

Contract NAS 8-5298

Project 325

PREPARED BY

T. A. Sedgwick

R. McGlone A. Malek

CHECKED BY

A. Rose

APPROVED BY

W. P. Boardman, Jr.
Manager, Advanced Product
Development Department

UNCLASSIFIED

THE Marquardt CORPORATION
VAN NUYS, CALIFORNIA

MAC A1158

FOREWORD

This report was prepared by The Marquardt Corporation, Van Nuys, California under National Aeronautics and Space Administration Contract NAS 8-5298. The work was administered under the direction of the Propulsion and Mechanics Branch of the Propulsion and Vehicle Engineering Division of the George C. Marshall Space Flight Center, Huntsville, Alabama. Mr. Robert Middleton was Technical Supervisor for the Propulsion and Mechanics Branch. Dr. Aaron Rose was Program Manager for The Marquardt Corporation.

This is the final report for studies begun in June 1963 and concluded in February 1964. The chief contributors to these studies and their fields of interest are: T. A. Sedgwick, system application and heat transfer studies; A. Malek and E. J. Yates, component design studies; and R. McGlone, cycle studies.

CONTENTS

MAC A 658

ILLUSTRATIONS

ILLUSTRATIONS (Continued)

I. SUMMARY

General criteria are developed for the application of reliquefiers to eliminate propellant boil off losses in space and lunar storage systems. Combination of these criteria with conservative estimates of the mass and performance of reliquefiers for liquid hydrogen storage systems at lunar equatorial sites indicates the following: For a storage duration of 12 lunar days (approximately one earth year) the total masses which must be transported to supply a fixed mass of liquid hydrogen at the end of the storage period can be reduced 14 and 28 percent by the use of reliquefiers for 20 and 10-foot diameter storage tanks, respectively. Operation of these reliquefiers only during the lunar night results in unvented tank pressure increases during the daylight hours of only 5 and 12 psi, respectively, and is, therefore, considered feasible. This mode of operation permits the reliquefier waste heat to be radiated to space using comparatively low radiator temperatures. This in turn permits the use of relatively simple reliquefier cycles which could not otherwise be employed.

Preliminary reliquefier component analysis and design studies tend to substantiate the initial reliquefier mass and performance estimates. These studies also indicate that nuclear power systems presently under development, such as SNAP 2, result in a mass chargeable to the reliquefier which is a small fraction of the mass of hydrogen recovered by reliquefaction. More advanced nuclear power systems will result in an almost negligible fraction of the total mass chargeable to the reliquefaction system.

II. INTRODUCTION

The objective of the studies reported herein is the evaluation of the feasibility of employing hydrogen reliquefiers to reduce or eliminate boil off losses from lunar and space liquid hydrogen storage systems. The emphasis is on storage periods of the order of one earth year at a lunar equatorial site. The sequence of presentation of the studies conducted to accomplish this objective is as follows: The general conditions under which the use of a reliquefier is advantageous are derived. The criterion employed is that the use of a reliquefier shall result in a reduction in the total mass which must be transported in order to supply a given mass of hydrogen at the end of a specified storage period. The resulting conditions are combined with preliminary estimates of the performance and mass of a reliquefier for a lunar equatorial site. From this combination, it is shown that substantial savings in the total mass transported can be effected. The remainder of the studies reported constitute an initial verification of the reliquefier performance and mass estimates. The feasibility of operating the reliquefier only during the lunar night is first confirmed. This result provides a basis for the selection of radiator temperature levels and thereby has a fundamental influence on the selection of potential reliquefier cycles for the comparative cycle study which follows. Finally, the results of representative cycle analyses are employed as the bases for component analyses and conceptual design studies.

Wherever the thermodynamic properties of hydrogen are required, parahydrogen data and 20.4°K equilibrium hydrogen data are used interchangeably. The justification for this and the conversion factors and enthalpy datum shifts associated with the several sources of data employed are presented in Appendix A.

MAC A-68

III. APPLICATION STUDIES

A. Reliquefier Application Criteria

1. General Criteria

The fundamental assumptions and principal results of a comparative analysis of two liquid storage systems--one with a reliquefier and one without a reliquefier--are presented herein. The reader is referred to Appendix B for a detailed derivation of the results. The purpose of the analysis is to determine under what conditions the use of a reliquefier will result in a reduction in the total mass which must be transported in order to supply a given mass of liquid at the end of a specified storage period. It is, of course, only valid to compare the best storage system with a reliquefier to the best storage system without a reliquefier. Accordingly, the total mass transported is minimized for each of the two systems.

In spite of the frequent reference to liquid hydrogen in Appendix B, the analysis is in fact applicable to liquid storage systems in general. Further, the results are independent of the environmental conditions and the storage tank construction. It is assumed merely that these are the same for both storage systems.

In the case of the storage system without a reliquefier, the total mass transported is minimized with respect to the mass of insulation employed on the storage tank. The minimization is primarily a trade between the insulation mass and the mass of the boil off losses. The boil off losses are inversely proportional to the mass of insulation (and directly proportional to the storage period). Thus, although an increase of insulation mass is directly reflected as an increase in total mass transported, it indirectly tends to decrease the total mass transported by reducing the boil off losses. The result of these two opposing trends is a minimum in the total mass transported. This minimum occurs when the insulation mass is equal to the sum of the boil off mass and an associated incremental tank mass. The incremental tank mass constitutes a small refinement in the analysis to take into account the fact that, if a specified mass of liquid is to be supplied at the end of the storage period, the tank storage capacity must exceed this specified mass by the mass of the boil off losses. The incremental tank mass is assumed to be directly proportional to the mass of boil off losses.

In the case of the storage system with a reliquefier, the total mass transported is minimized with respect to the mass of insulation and with respect to the mass of the boil off which is reliquefied. The mass of the reliquefier is assumed to be directly proportional to the reliquefaction mass flow rate. The constant of proportionality is termed the reliquefier specific mass and has typical units of lb/(lb/hr) or simply hr. By writing the total mass transported as the algebraic sum of the various contributions, by introducing the proportionalities indicated previously, and then by comparing the result with the similar expression for a system without a reliquefier, the following general criteria are rigorously derived in Appendix B: If the specific mass of the reliquefier is less than the time period of storage then the use of a reliquefier will result in a reduction in the total mass transported and the reliquefaction mass flow rate should be made

as large as possible in order to minimize the total mass transported. The largest possible reliquefaction mass flow rate is that corresponding to reliquefaction of all the boil off. That these results are reasonable can be demonstrated as follows: The first portion of the results may be restated as: If the product of the reliquefier specific mass and the reliquefaction mass flow rate is less than the product of the time period of storage and the reliquefaction mass flow rate, then the use of a reliquefier will result in a reduction in the total mass transported. These two products are equal to the mass of the reliquefier and the mass of liquid recovered by the use of the reliquefier, respectively. Clearly, if the former is less than the latter, use of a reliquefier will result in a reduction of the total mass transported.

The minimization of the total mass transported with respect to the insulation now becomes a trade between the insulation mass and the reliquefier mass. As the insulation mass is decreased, the boil off rate and hence the reliquefaction rate and the reliquefier mass increase. A minimum is found to occur when the insulation mass and the reliquefier mass are equal. The value of the insulation mass at this minimum is less than the corresponding value for the storage system without a reliquefier.

2. Application to Lunar Hydrogen Storage

The results of the analysis described above are applied herein to the storage of liquid hydrogen at a lunar equatorial site. A storage period of twelve lunar days, 8505 hours, or approximately one earth year, is considered. A liquefier specific mass of 1000 lb/(lb/hr) is estimated for this application. (Based on the cycle studies and component design studies reported in later sections of this report, it is believed that this estimate of specific mass is conservative, that is, that lower values can be achieved.) This specific mass is considerably less than the duration of storage and hence, from the preceding discussion, application of a reliquefier is indicated.

Two comparisons are made between storage systems with and without a reliquefier: One for a 20-foot diameter spherical storage tank and the other for a 10-foot diameter tank. Data for the systems without reliquefiers are taken from the comprehensive study of cryogenic propellant lunar storage reported in Reference 1. These data are the masses of hydrogen stored, the hydrogen lost by boil off, the tank structure, and the tank insulation. These are presented in the first and third columns of Table I for the 20-foot diameter tank and the 10-foot diameter tank, respectively. In both cases, the condition required to minimize the total mass transported (per unit mass of hydrogen available at the end of the storage period) is satisfied. That is, the mass of hydrogen boiled off is equal to the insulation mass. The data for the systems with reliquefiers are derived from those without reliquefiers as follows: The tank structure mass is the same. The insulation mass is obtained from the expressions derived in Appendix B for the insulation masses which minimize the total mass transported with and without a reliquefier. Combining these expressions indicates that the ratio of these two insulation masses is equal to the square root of the ratio of reliquefier specific mass to the storage duration. In obtaining this result, the incremental tank mass

MAC A673

term included in the Appendix B analysis is deleted because this effect is taken into account herein by deducting the hydrogen boil off losses from the tank storage capacity to yield the mass of liquid hydrogen available at the end of the storage period. The reliquefier mass should, as noted previously, be made equal to the insulation mass.

The total mass transported per unit mass of hydrogen available at the end of the storage period is presented in the next to the last row of Table I. For the 20-foot diameter tank, the use of a reliquefier reduces the total mass which must be transported by 14 percent and for the 10-foot diameter tank by 28 percent. (The fact that the second reduction is just twice the first is coincidental.) The use of a reliquefier becomes more attractive as the tank diameter is reduced because the percentage boil off tends to be greater for smaller tanks. As the tank diameter is reduced, the storage capacity decreases in proportion to the diameter cubed, whereas, the surface area and therefore the heat transfer rate and the boil off losses, are reduced only in proportion to the diameter squared.

B. Night Only Operation of Reliquefier

The waste heat associated with the operation of the reliquefier must be dissipated. Due to the absence of a lunar atmosphere, it appears that the most probable technique for this dissipation is radiation to space. For a lunar equatorial site, this is much easier to accomplish during the lunar night when the radiator need not be shielded from solar radiation and when the lunar surface is cooler. Accordingly, the possibility of shutting down the operation of the reliquefier during the lunar day and allowing an unvented hydrogen storage tank to rise in pressure and temperature is considered.

A general study of liquid hydrogen storage tank thermal transients is described in Appendix C. It is concluded from this study that the only significant contribution to the change of energy storage during the transient is the change of the hydrogen internal thermal energy. The changes of tank shell internal thermal energy and strain energy were investigated and found to be negligible. These results are applied here to the two tanks with reliquefiers discussed in the previous section. The changes of hydrogen internal thermal energy are evaluated from Figure C-1 which is based on the assumption there is no significant temperature stratification within the stored liquid. This assumption is probably valid only if specific provisions for minimizing the effects of stratification are incorporated in the system design. One possibility is circulating vapor from the top of the tank up through the liquid (which tends to become subcooled during the daytime transient due to the rise in tank pressure). This might be accomplished using one of the reliquefier compressors and suitable valving.

TABLE I

HYDROGEN RELIQUEFIER APPLICATION STUDY

Storage period = 12 lunar days (Approximately one earth year)
Minimum total mass systems at a lunar equatorial site

	20-ft Diameter Tank		10-ft Diameter Tank	
	Without Reliquefier	With Reliquefier	Without Reliquefier	With Reliquefier
Tank structure	1,860 lbs	1,860 lbs	232 lbs	232 lbs
Tank insulation	2,200 lbs	753 lbs	550 lbs	188 lbs
Reliquefier*	--	753 lbs	--	188 lbs
Initial hydrogen mass	18,610 lbs	18,610 lbs	2,324 lbs	2,324 lbs
Total mass transported	22,670 lbs	21,976 lbs	3,106 lbs	2,932 lbs
Hydrogen boil off	2,200 lbs	--	550 lbs	--
Hydrogen available	16,410 lbs	18,610 lbs	1,774 lbs	2,324 lbs
$\frac{\text{Mass transported}}{\text{Hydrogen available}}$	1.381	1.181 (14% reduction)	1.751	1.262 (28% reduction)
Reliquefaction rate	--	0.753 lb/hr	--	0.188 lb/hr

* Includes all mass chargeable to reliquefier (e.g., nuclear electrical power source).

MAC A-653

Multiplying the hydrogen boil off masses of Table I by the latent heat of vaporization (190 Btu/lb at the 15 psia storage pressure of the Reference 1 studies) yields for the total amounts of heat transferred through the tank insulation during 12 lunar cycles 418,000 Btu and 104,500 Btu for the 20-foot diameter and 10-foot diameter tanks, respectively. The amounts of heat transferred per lunar cycle are one-twelfth these or 34,800 and 8,700 Btu, respectively. The amounts of heat transferred are inversely proportional to the insulation mass (for a fixed tank surface area). Thus, for the tanks with reliquefiers, the total amounts of heat transferred per lunar cycle are 101,600 and 25,400 Btu, respectively. The vast majority of these amounts of heat are transferred during the daylight hours (Reference 1). Assuming the total amounts are transferred during the daylight hours will, therefore, only slightly overestimate the rise in tank temperature and pressure. Using this assumption and dividing the amounts of heat transferred by the respective masses of stored hydrogen yields the changes in hydrogen internal thermal energy, namely, 5.46 Btu/lb and 10.92 Btu/lb for the 20-foot diameter and 10-foot diameter tanks, respectively. Assuming a 10 psia tank pressure at the dawn of the lunar day, the pressures at sunset are (from Figure C-1 of Appendix C) only 15 psia and 22 psia. It is concluded, therefore, that operation of the reliquefiers only during the lunar night is feasible. It should be noted that, under these conditions, the reliquefaction flow rates of Table I should be interpreted as average values over a complete lunar day. Since the reliquefiers are operated only approximately half the time, the design reliquefaction rates must be made twice these average values.

IV. CYCLE ANALYSES

A. Hydrogen Cycles Without Expanders

Hydrogen cycles that do not use expanders or other means to remove energy from the fluid in the form of mechanical work are dependent entirely upon the Joule-Thomson effect for cooling. The Joule-Thomson effect is a reduction of temperature resulting from an adiabatic reduction of pressure. This effect is described with the aid of the temperature-entropy diagram of Figure 1 and the schematic of the Hampson cycle shown in Figure 2. The Hampson cycle is the simplest of all cycles which rely upon the Joule-Thomson effect. Its operation is as follows: Low pressure saturated hydrogen vapor from the tank, Point 1 in Figure 2, is heated in a counterflow heat exchanger and then compressed to a high pressure. A substantial hydrogen temperature rise occurs through the compressor. However, this is offset by the cooling in the waste heat radiator through which the hydrogen next passes. The high pressure gas stream is then cooled by counter flow heat transfer to the low pressure stream and finally expanded through a valve into the storage tank. The Joule-Thomson cooling resulting from the pressure drop through the valve produces a partial liquefaction of the gas.

Paradoxically, while the only Joule-Thomson cooling occurs in the expansion valve, the application of the Hampson cycle is limited by the existence of the Joule-Thomson effect for the conditions at the top of the heat exchanger. Consider an energy balance for a control volume containing the heat exchanger, the expansion valve, and the hydrogen tank of Figure 2. A hydrogen stream leaves this control volume at Point 2, and an equal flow rate hydrogen stream enters the control volume at Point 4. Now if there is to be any net removal of energy from this control volume and hence any liquefaction of hydrogen vapor, the energy leaving the

MAC A-63

control volume must exceed the energy entering the control volume. These energies are the respective products of mass flow rate and enthalpy. Thus, since the flow rates are the same, the enthalpy at point 2 must exceed that at point 4. Now for heat transfer to take place, the high pressure flow temperature must be greater than the low pressure flow temperature at every point in the heat exchanger. In particular, the temperature at point 4 must exceed that at point 2. These two inequalities are noted on the temperature-entropy diagram of Figure 1. For the particular radiator exit state indicated (point 4) the inequalities can only be simultaneously satisfied if the compressor inlet state (point 2) lies in the shaded area. Further, unless the temperature decreases as the pressure is reduced at constant enthalpy as shown for the region between the pressures of points 4 and 2, the inequalities cannot be simultaneously satisfied. Stated in other words, there must be a positive Joule-Thomson effect.

The preceding arguments could be applied to any location in the heat exchanger. It is applied to the top of the heat exchanger of Figure 2 because the highest temperatures occur there and the Joule-Thomson effect decreases with increasing temperature. For parahydrogen, the (positive) Joule-Thomson effect vanishes at temperatures above 360°R. Theoretically, temperatures approaching this value could be employed. However, on a practical basis, substantially lower temperatures must be employed. A 200°R radiator exit temperature was employed in all of the cycle analyses described herein. A number of other somewhat arbitrary selections of cycle operating conditions were used. The general philosophy was to employ the same reasonable, although not necessarily optimum, conditions throughout the cycle studies. For example, the 4°R temperature difference at the top end of the heat exchanger was a compromise between the temperature and enthalpy inequalities which must be satisfied.

Another important consideration is the pressure drop through the low density side of the heat exchanger. This pressure drop affects the heat transfer rate and, therefore, the size of the heat exchanger. However, it also affects the compressor and radiator requirements. Joule-Thomson cooling is negligible below pressures of 100 to 200 psia at the heat exchanger exit temperature (196°R). Although compressor work is added in the low pressure range, it adds no cooling value and enlarges both the compressor and radiator. Therefore, the pressure drop through the low density side of the heat exchanger should be held to relatively small values. A value of 2 psia was selected. The high density side pressure drop was regulated to provide the maximum temperature differential at the cold end of the heat exchanger.

A summary of the conditions employed in the analysis of all cycles, with or without expanders, is as follows:

1. Hydrogen reliquefied per hour = 1 lb
2. Hydrogen storage tank pressure = 10 psia
3. Radiator exit temperature = 200°R
4. Heat exchanger pinch temperature = 4°R

5. Minimum allowable pressure drop through low density side of heat exchanger system = 2 psia

6. Pressure drop through high density side of heat exchanger system regulated to provide maximum temperature differential at cold end

7. Rotating machinery isentropic efficiency = 65%

8. Pressure drop through radiator system = 5%

Figure 3 shows the effect of varying the radiator exit pressure on the compressor power required for the Hampson cycle. The minimum power occurs at a pressure of approximately 1500 psia. Above this pressure, the increase in the Joule-Thomson cooling is slight and the recirculating mass flow rate does not decrease sufficiently to overweigh the additional enthalpy rise across the compressor. Below 1500 psia the converse is true. The mass flow rate increases so rapidly that although the compressor enthalpy rise is decreasing the net result is an increase in power.

Figures 4, 5, and 6 are schematics of Hampson cycles with one, two, and three stages of intercooling. These systems were studied to determine the desirability of using a series arrangement of compressors and radiators as a means of reducing power and radiation requirements. The final radiator exit pressure was held at 1500 psia and the compressor pressure ratios were held constant in each series. Constant pressure ratio compressors provide the minimum total compressor power using a perfect gas, which hydrogen nearly is at these conditions. The results show a large decrease in compressor power with one stage of intercooling and smaller decreases with each additional stage. The first stage drops the horsepower from 10.75 to 7.88, a 26 percent reduction. The second and third stages show much smaller successive drops. With two and three stages, the horsepower is 7.42 horsepower and 7.02 horsepower, respectively. This is a drop of approximately 5 percent per stage.

Further reductions in compressor power requirement were made with dual pressure cycles. In dual pressure cycles, the flow is divided into a high pressure refrigeration loop and a low pressure loop in which the flow out of the tank is compressed to replenish the refrigeration loop. The power is reduced by circulating only a small portion of the total mass flow in the low pressure loop where the Joule-Thomson cooling is negligible and recirculating the majority of the flow in the high pressure refrigeration loop.

Figure 7 shows a dual pressure cycle with one stage of low pressure loop intercooling integral with the intermediate pressure loop. The minimum compressor power (3.60 HP) was found by varying both the high pressure loop radiator exit pressure and the amount of expansion into the mixed phase region in the recirculation loop (See Figure 8). The pressure drop through the recirculation leg of the heat exchanger was kept small (2 psia) to reduce the enthalpy rise through the compressor. Minimum power occurs at a radiator exit pressure of 1500 psia, the same value as that in the Hampson cycle study. The graph shows that expanding to a pressure of 150 psia results in minimum power. Additional expansion results in an enthalpy rise in the high pressure loop that overweighs the accompanying reduced flow rates.

A schematic of a dual pressure cycle with one stage of primary loop intercooling is presented in Figure 9. This cycle differs from the previous dual pressure cycle in that the primary (low mass flow) loop mixes with the high pressure recirculating loop after it has been compressed to a high rather than to an intermediate pressure level. The minimum power of 4.772 HP is considerably higher than in the previous cycle. It was found by varying the amount of expansion in the recirculation loop (See Figure 10). A radiator exit pressure for both loops of 1500 psia was assumed to provide the minimum power as in previous cycles. Figure 11 shows that the power requirement in the primary loop can be reduced by 3 percent if the compressor pressure ratios are varied to take advantage of the imperfect gas characteristics.

In Figure 12, cooling of the saturated liquid between expansions has been added to the dual pressure cycle with one stage of primary loop intercooling. The variation of compressor power with the recirculation loop expansion pressure (shown in Figure 13) was based upon holding the 4° pinch temperature ground rule for both heat exchangers and splitting the 2 psia pressure drop between the heat exchangers in the tank outflow leg between Stations 1 and 3. The minimum of 4.50 HP is a slight improvement over cycles without cooling in the low temperature regime and it occurs with somewhat less expansion in the recirculation loop.

B. Hydrogen Cycles with Expanders

Hydrogen cycles with expanders are not limited to Joule-Thomson cooling alone. The energy removed from the fluid by the expander adds to the Joule-Thomson cooling and thereby results in lower flow rates and reduced power requirements.

Figure 14 shows a schematic of a cycle employing one stage of intercooling and an integral high temperature refrigeration loop with one expander. Although doing a bigger percentage of the cooling, the flow rate in the recirculation loop has been reduced to less than one-tenth the flow rates in the recirculation loops without expanders.

The variation of compressor power with expander exit pressure is shown in Figure 15. A power requirement of 2.40 HP was selected rather than the actual minimum (2.16 HP) on the basis of a much lower expander pressure ratio. The small increment in power did not appear to warrant an increase in expander pressure ratio of a factor of 4.

In Figure 14, the majority of the cooling was done in the high temperature refrigeration loop. This loop consumed only a fraction of the total compressor power. A cycle was designed that would separate the loops and eliminate the need for high compression in the primary loop, thereby, reducing the compressor enthalpy rise. If the primary loop flow rates remain low enough, the result would be a lowering of the compressor power in this loop. The cycle is shown in Figure 16. The interaction between the mass flows and compressor pressure ratios of both loops were simultaneously investigated to determine the amount of primary loop compression and refrigeration loop expansion that would result in the minimum total compressor power. Figure 17 shows the effect of changing either of the variables while holding the other constant. The 1.58 HP shown for the expander exit pressure of 10 psia and radiator exit pressure of 1500 psia represents the minimum power for this cycle.

A Claude-Heylandt cycle is shown in Figure 18. In Claude-Heylandt cycles, the fluid is expanded from the high pressure side of the cycle to the low pressure side. The compressor power is found by varying the expander inlet pressure and temperature. The expander exit pressure is fixed by the storage tank pressure and the pressure drop through the low density side of the heat exchanger between the tank and expander.

The data shown in Figure 19 indicate that the pressure drop through the heat exchanger between the radiator and expander should be held to a minimum. This plot is based upon the 1500 psia radiator exit pressure previously found to provide maximum cooling per unit compressor power in nearly all cycles, and not limiting all radiator to a pinch temperature of 4°R. The minimum power was found to be 1.84 HP at an expander exit temperature of 176.5°R.

The results of Figure 20 indicate that by lowering the radiator exit pressure to 720 psia and holding the pressure drop to 2 psia through the heat exchanger between the radiator and expander, the compressor power requirement can be lowered to 1.54 HP.

Figure 21 represents the first approach to solving a Claude-Heylandt cycle with two expanders and two stages of intercooling. The compressor power shown does not represent a minimum for the cycle. The compressor power is found by varying the top expander inlet temperature at a constant expander inlet pressure. The pressure selected corresponds to a radiator exit pressure of 1500 psia with a minimum pressure drop through the top heat exchanger. The variation of compressor power with expander inlet temperature is shown in Figure 22. The minimum power of 2.07 HP occurs when the top heat exchanger is removed. A schematic of this cycle with the top and bottom heat exchangers removed is presented in Figure 23.

Table II is a summary of the results of all the hydrogen cycles, with and without expanders, that were analyzed.

C. Cascade Cycles

As noted previously, cycles without expanders are wholly dependent upon the Joule-Thomson cooling effect and the highest temperature at which these cycles may reject heat is limited by the inversion of the Joule-Thomson effect for parahydrogen. This occurs at approximately 360°R. However, maintaining sufficiently large heat exchanger temperatue differences and reasonable overall cycle performance limits the maximum temperature to values of the order of 200°R. Cycles with expanders circumvent this limitation by removing energy (in part) in the form of the shaft work of the expanders.

An alternate way to circumvent this limitation is to transfer heat from the hydrogen to another substance whose Joule-Thomson inversion temperature is higher. This is the principle of the cascade cycle. A schematic diagram of a hydrogen-neon cascade cycle is shown in Figure 24.

TABLE II

SUMMARY OF HYDROGEN RELIQUEFACTION CYCLES STUDIED

Cycle Description	Reference Figure Number	Maximum Pressure (psia)		Maximum Temperature (°R)		Flow Rate (lbs/hr)		Total Compressor Power		Expander Power
		Refrig.	Primary	Refrig.	Primary	Refrig.	Primary	Btu/hr	HP	Btu/hr
Hampson cycle	2	1575	--	1168	--	7.85	--	27350	10.75	--
Hampson cycle with one-stage intercooling	4	1537.5	--	544	--	7.85	--	20040	7.88	--
Hampson cycle with two-stage intercooling	5	1523	--	414	--	7.85	--	18900	7.42	--
Hampson cycle with three-stage intercooling	6	1521	--	358	--	7.85	--	17800	7.02	--
Dual pressure - one stage of low pressure loop intercooling integral with intermediate pressure loop	7	1537.5	185.5	491	585	6.64	1.708	9160	3.60	--
Dual pressure - one stage of primary loop intercooling	9	1537.5	1537.5	453	544	7.87	1.727	12150	4.772	--
	11	1537.5	1537.5	453	590	7.87	1.727	12030	4.772	--
Dual pressure - one stage of primary loop intercooling cooling between expansions	12	1537.5	1537.5	429	590	8.95	1.337	11460	4.50	--
Dual pressure - one stage of intercooling and integral high temperature refrigeration loop with expanders	14	1537.5	1537.5	522	590	0.58	2.17	6100	2.40	127.5

TABLE II (Continued)

Cycle Description	Reference Figure Number	Maximum Pressure (psia)		Maximum Temperature (°R)		Flow Rate (lbs/hr)		Total Compressor Power		Expander Power
		Refrig.	Primary	Refrig.	Primary	Refrig.	Primary	Btu/hr	HP	Btu/hr
Dual pressure - one stage of intercooling per loop-separate high temperature refrigeration loop with expander	16	1537.5	615	590	447	0.518	1.45	4025	1.58	171
Claude-Heylandt - one stage intercooling with one expander	18	1537.5	1498	590	176.5	1.89	1.325	4690	1.84	130
	20	740	718	457	135.5	2.05	1.083	3920	1.541	173
Claude Heylandt - with two expanders - two series of intercooling	21	1525	1498	533	186	2.58	1.037	5929	2.34	130
	23	1525	1500	533	200	2.28	1.049	5279	2.07	135

It is worth noting that this is not a cascade cycle in the usual sense, in that cascade usually implies a cascade of vapor compression refrigeration cycles (for example, Keesom's nitrogen-methane-ethylene-ammonia cascade air liquefier). Such a system is dependent upon a sequence of substances whose liquid temperature ranges overlap. In the present instance neon may be employed after hydrogen since the triple point temperature of neon (44.0°R) is between the triple point and critical point temperatures (25.1°R and 59.4°R) of hydrogen and the critical point temperature of neon (79.5°R) is somewhat greater than that of hydrogen.

However, there is no pure substance suitable for the next higher temperature range in a vapor compression loop. This is illustrated by the triple point temperature list of Table III.

TABLE III

SUBSTANCES CONSIDERED FOR CASCADE RELIQUEFIERS

Substance	Triple Point Temperature (°R)	Critical Point Temperature (°R)
Parahydrogen	25.1	59.4
Neon	44.0	79.5
Florine	96.4	--
Nitrogen	113.9	226.9
Oxygen	98.6	--
Argon	151.0	--
Carbon monoxide	122.6	239.2

There is some possibility that a mixture might prove satisfactory. However, efforts to find a suitable mixture have thus far proven fruitless. A mixture of argon and neon was thought to be a likely one. From the data of Table III, the temperature range would appear to be correct. Additionally, it is known that helium and neon are mutually soluble. Thus, it might be expected that neon and argon would be mutually soluble since all three of these substances are of the same chemical family. However, a search of the literature reveals that recent experimental studies have shown that neon and argon are not soluble.

Use of the hydrogen-neon cycle shown in Figure 24 probably cannot be justified on the basis of the relatively small difference between the Joule-Thomson inversion temperatures of neon and hydrogen. However, it might be justified on the basis of a redundant radiator design to offset meteoroid damage. The general radiator redundancy design approach involved is discussed in Reference 2. As applied here, a single hydrogen loop would transfer heat to a number of small neon

loops operating in parallel with one another. Meteoroid puncture of the radiator tubes in one of these neon loops would then leave the remainder of the system in operation. Note that if hydrogen is circulated through a radiator, punctures must be detected and then isolated by closing valves. The authors of Reference 2 point out the strong influence of the reliability of the detection devices and valves on the overall system reliability.

V. RELIQUEFIER COMPONENT DESIGN STUDIES

A. Cycle Selection

It is not possible to make a proper reliquefier cycle selection without quantitative analyses of such factors as radiator meteoroid damage. Such analyses are beyond the scope of the studies reported herein. Hence, beyond indicating the several applicable classes of cycles and analyzing cycles within these classes, no selection is attempted. As a consequence, the component studies of this section are for the most part presented in such a fashion as to make them broadly applicable to all the cycles of interest. In the case of the compressor design studies, however, a single cycle was employed as the basis of the design.

B. Reliquefier Power Source

Investigations of nuclear power sources and the combustion of hydrogen as the sources of the energy required to power the reliquefier compressors may be summarized as follows. Nuclear power sources presently under development, such as SNAP 2, result in a mass chargeable to the reliquefaction system which is a small fraction of the mass of hydrogen recovered by reliquefaction. Next generation nuclear power sources will result in an almost negligible mass chargeable to the reliquefaction system. By contrast, the combustion of hydrogen with oxygen requires approximately 10 pounds of mixture per pound of hydrogen reliquefied. Hence, this approach would make sense only if there were a requirement for the by-product water which is formed.

1. Nuclear Power Sources

From the preceding cycle analyses, it is seen that of the order of 10,000 Btu of compressor power must be supplied for each pound of hydrogen reliquefied. Data for the evaluation of nuclear electrical power sources are included in Table IV. The electrical power, system mass, and system design life for nine systems ranging from those currently under development to those in preliminary study phases are presented.

These data were taken from Reference 3. The electrical energy per unit system mass computed from the other data of Table IV are presented in the last column. For the SNAP 2 system currently under development, electrical power equivalent to 69,200 Btu is supplied per lb of system mass. Comparing this with the 10,000 Btu/lb of hydrogen requirement indicates that 0.14 lb of the SNAP 2 system is required to recover one pound of hydrogen boil off. In the cases of the more advanced systems, this value becomes much smaller. For the START system, 0.00557 lb is chargeable to the recovery of one pound of hydrogen boil off. This can, by

multiplying by the system life of 8755 hrs (one year), be converted to the contribution of this power source to the specific mass of the reliquefier. The result is 49 lbs/(lb/hr) which is almost negligible compared to the total reliquefier specific mass estimate of 1000 lbs/(lb/hr) employed in the preceding application studies. It is concluded, therefore, that the use of nuclear power sources constitutes a feasible approach to driving the reliquefier compressors.

TABLE IV

SUMMARY OF NUCLEAR ELECTRICAL POWER SOURCES CONSIDERED

System	Electrical Power (kw)	Mass (lbs)	Time	Electrical Energy per Unit System Mass (Btu/lb)
SNAP 10A	0.5	525	1 yr	2.85×10^4
SNAP 2	2	865	1 yr	6.92×10^4
SNAP 8	30	1700	10,000 hr	60.2×10^4
SNAP 8*	60	2700	10,000 hr	75.8×10^4
STAR-R	70	1400	1 yr	149.5×10^4
START	60	1000	1 yr	179.4×10^4
SPUR	300	2800	10,000 hr	365.6×10^4
T/I REACTOR	300	1200	1 yr	747.7×10^4
DCR-300	300	1900	1 yr	472.2×10^4

* High temperature system

2. Hydrogen-Oxygen Reaction

The combustion of hydrogen to supply the energy input for a heat engine could conceivably supply the reliquefier compressor power input. However, this is a totally impractical approach unless there is a requirement for the by-product water which is produced. Assuming lunar night operation, a maximum working fluid temperature of 2500°R, a sink temperature of 500°R, and a 20 percent engine efficiency (compared to a thermodynamically reversible cycle), 16 percent of the heat of combustion of approximately 60,000 Btu/lb could be converted to 9,600 Btu/lb of hydrogen as mechanical energy. For each 2.016 lb of hydrogen burned, 16.0 lbs of oxygen are required. Hence, 1,070 Btu of mechanical work is developed per pound of fuel mixture. Note, however, approximately 10,000 Btu of mechanical energy are required to reliquefy one pound of hydrogen. Clearly, this is a losing proposition unless there is a requirement for the water which is produced.

C. Radiator

1. Equivalent Thermal Environment

A radiator located on the moon will radiate to and be irradiated by deep space and the lunar surface. The temperature of the lunar surface will to some degree be affected by the presence of the radiator. These interactions are considered herein in determining a simpler yet entirely equivalent radiator thermal environment for a horizontal radiator. The equivalent thermal environment consists of a surface of uniform temperature which completely surrounds the radiator. (This surface is hereafter referred to as the heat sink or simply as the sink.) This equivalent radiation environment is quantitatively described by the equivalent sink temperature and the equivalent net radiation conductance from the radiator to the sink. It is possible to derive values of these two quantities such that, irrespective of the radiator temperature (provided only that it is the same in both cases), the radiator will exchange the same amount of heat with the equivalent environment as with the actual environment.

Knowledge of the equivalent sink temperature provides a direct insight into the selection of reliquefier cycle operating conditions in that the fluid temperature at the exit of the radiator must be greater than the equivalent sink temperature. This equivalent environment approach also results in a considerable simplification of radiator area computations. (However, perhaps the most important implications are those associated with radiator testing.)

The first step in the analysis is the determination of the heat transfer characteristics of the lunar crust from measurements of lunar surface temperatures. Shortly after the lunar sunset, the lunar surface temperature approaches a value of approximately 216°R (Reference 1) which persists through the remainder of the lunar night. The generally accepted explanation for this is as follows: At a sufficient depth below the lunar surface, the effects of variations of surface heat transfer conditions during the complete lunar day are damped out and the substrate temperature becomes constant. This constant substrate temperature has been inferred from surface temperature measurements to be approximately 420°R. Quasi-steady state heat transfer from the lunar surface to deep space by radiation is supplied by and equal to the quasi-steady heat transfer from the constant temperature substrate to the lunar surface. The former heat transfer rate is calculated from the lunar surface temperature, the temperature of deep space, and the emissivity of the lunar surface. The heat transfer conductance for the latter is then calculated assuming the heat transfer in the lunar crust is preponderantly by gray body radiation. A lunar surface emissivity of 1.0 is employed. This results in a very slight conservatism in the overall radiator analysis. A deep space temperature of 20°R is used. However, the results of the analysis are virtually independent of this assumption. (This temperature raised to the fourth power is entirely negligible compared to the lunar surface temperature raised to the fourth power.)

For a unit lunar surface area, the resulting lunar crust radiation conductance is 0.0752. This number is dimensionless inasmuch as the details of the analysis are carried out using the gray body radiation network method of Oppenheim (Reference 4). (With this method, the potential for radiant heat transfer is taken

to be the product of the temperature raised to the fourth power and the Stefan-Boltzmann constant.) The Oppenheim radiation network for this portion of the analysis is shown in Figure 25-A.

The analysis of the horizontal radiator now proceeds as follows. Radiant heat transfer from the lunar substrate through the lunar crust to the lower surface of the radiator or to the lower surface of one or more radiation shields placed under the radiator is considered. This radiant heat transfer is assumed to be one-dimensional. An emissivity of 0.05 (typical of clean aluminum) is employed for the lower surface of the radiator and for the aluminized Mylar radiation shields. (A sketch of a radiator design concept is presented in Figure 26). The upper surface of the radiator is assumed to be coated in such a manner that an emissivity of 0.9 is obtained.

The Oppenheim type network employed in analyzing this case is shown in Figure 25-B for (n) radiation shields where (n) may be zero or a positive integer. Combining all the radiation resistances in series between the node T_{ss} representing the lunar substrate and the node T_R representing an element of the radiator surface in Figure 25-B yields the simpler network of Figure 25-C. The analysis up through Figure 25-C may be accomplished by the method of Oppenheim or any of several entirely equivalent techniques described in standard heat transfer texts.

However, the step from Figure 25-C to Figure 25-D is not covered in these sources and hence is described in some detail here. The values of the equivalent radiation conductance (G) and equivalent sink temperature (T_e) of Figure 25-D are chosen such that, in combination with the radiator temperature (T_R), the same radiator heat transfer rate is predicted as with the radiation conductances and temperatures of Figure 25-C. Now, equating the radiator heat transfer rates yields one equation in two unknowns: The equivalent conductance and the equivalent temperature. There are, of course, any number of combinations of these two unknowns which will satisfy this equation. However, there is only one combination which is independent of the radiator temperature, namely,

$$G = G_{r_\infty} + G_{rss}$$

$$T_e^4 = \frac{G_{r_\infty} T_\infty^4 + G_{rss} T_{ss}^4}{G}$$

This combination has the greatest utility and hence is employed in the computations reported herein.

MAC A 653

Values of the equivalent radiation conductance and the equivalent sink temperature are plotted in Figures 27 and 28, respectively, as functions of the number of radiation shields employed under the radiator. The equivalent conductance is little affected by the number of radiation shields. It drops only from 0.930 in the case of no shields to 0.904 in the case of five shields. (As the number of shields is increased it asymptotically approaches the 0.900 value of the radiator to deep space conductance (G_r)). This is a consequence of the fact that, even with no radiation shield, the radiator to lunar substrate conductance (G_{rss}) is small compared to the radiator to deep space conductance (G_r). By contrast, the equivalent sink temperature is significantly affected by the number of radiator shields employed. This temperature drops from 178°R in the case of no radiation shield to 111°R in the case of five shields. The reason for this is as follows. The deep space temperature (T_∞) is so much smaller than the lunar substrate temperature (T_{ss}) that the first term in the numerator in the above equation is negligible in spite of the fact that the conductance in this term is many times that in the second term. This also leads to the somewhat paradoxical result that the equivalent sink temperature is virtually independent of the deep space temperature and almost directly proportional to the lunar substrate temperature.

In the cycle analyses reported herein, a radiator exit fluid temperature of 200°R is employed. From the results of Figure 28, temperatures this low are possible since even in the absence of radiation shields the equivalent sink temperature is only 178°R. Use of radiation shields will of course reduce the sink temperature and thereby provide a greater potential for radiant heat transfer.

Only the horizontal radiator is analyzed herein. However, it appears that a vertical radiator may have considerable merit. Considering both surfaces of both types of radiators, they both have the same radiation view factor with respect to deep space and with respect to the lunar surface. However, the horizontal radiator completely shields from deep space the portion of the lunar surface which it views, whereas the vertical radiator only partially shields the lunar surface. Consequently, the vertical radiator on the average views a cooler lunar surface and hence is able to radiate a greater amount of energy for otherwise identical design conditions. For a lunar equatorial site a vertical radiator may also be superior from the standpoint of meteoroid damage. Reference 2 indicates the majority of meteoroids travel in paths near the ecliptic plane. Since the lunar axis is on the average normal to the ecliptic plane, a vertical radiator at an equatorial site would provide the minimum projected area in the direction of greatest meteoroid incidence.

2. Surface Area

As a fluid is cooled in passing through a radiator, the reduction in fluid temperature results in a reduction in the radiant heat transfer rate per unit surface area. This effect is considered in a general analysis of radiator area requirements presented in Appendix D. This analysis is used here to size a typical total radiator package, that is, all the radiators employed in a reliquefier cycle. Three radiation shields are considered and hence, from Figures 28 and 27, the equivalent sink temperature and equivalent radiation conduction are 123°R and 0.907, respectively. From the cycle analysis studies, of the order of 10,000 Btu/hr must be dissipated by the radiators for a 1 lb/hr hydrogen reliquefaction rate and the typical radiator inlet and exit temperatures are 340°R and 200°R, respectively.

MAC A673

One other piece of data is required in order to apply the analysis of Appendix D, namely, the surface heat transfer effectiveness. This is defined as the actual local radiant heat transfer rate divided by the radiant heat transfer rate that would prevail if the local radiator fin surface temperatures were equal to the local fluid (hydrogen) temperature. As such, the surface heat transfer effectiveness includes the effects of the temperature differences associated with both the convection within the fluid passage and the conduction from the walls of the fluid passage to the radiation surfaces. The term "surface heat transfer effectiveness" is used herein since only the effect of the latter is included in the usual definition of fin heat transfer effectiveness.

Ironically, in the radiator applications considered herein, the temperature difference between the hydrogen and the tube wall is negligible insofar as the determination of radiator surface area requirements are concerned and the surface heat transfer effectiveness is essentially equal to the fin effectiveness. (This is in part due to the comparatively low radiator temperatures involved. These tend to make the thermal resistance to radiation large and therefore controlling as compared to the convective thermal resistance within the tube.) The fin dimensions which maximize the heat transfer rate per unit fin mass (for a constant fin width) are presented in Reference 5 for the case of a constant thickness rectangular fin. The results are somewhat dependent upon the ratio of fin base temperature to the sink temperature. However, combination of these results with the more general results of Reference 5 reveals that designing for a fin effectiveness of 60 percent comes very close to maximizing the heat transfer rate per unit fin mass for all conditions. Accordingly, this value is used herein.

Following the simple calculation procedure outlined in Appendix D a total radiator surface area of 1488 sq ft is obtained. Analyses of the fin indicates that for an aluminum fin thickness of 0.010 in. the fin length should be 9.0 in. to attain a fin effectiveness of 60 percent (The coolant tubes would be spaced 18 in. on centers.) The resulting total fin mass is 214 lbs.

D. COMPRESSORS

The preliminary design study of the hydrogen compressor system shown in Figure 29 was based on the thermodynamic cycle shown in Figure 9. The purpose of this design was to evolve a typical configuration that could be used to establish compressor system weights and to evaluate its feasibility from a technical and manufacturing viewpoint. The weight of this assembly is estimated to be 200 pounds.

For this initial investigation, the system design point was assumed to be the pressure and temperature conditions existent in the storage system at the end of lunar night, i.e., hydrogen gas is at its lowest pressure. Other criteria used in the design were as follows:

a. Life (one earth year - lunar night operation): 4383 hrs

b. Pumps: Diaphragm type for a contamination and leak free system

c. Diaphragm materials: 17-7 PH stainless steel

d. Diaphragm stress: not to exceed 80 percent endurance limit. Figure 30 shows endurance limits for 17-7 PH stainless steel.

e. Construction: Composite honeycomb where applicable. Used for stiffness and low weight.

The cycle shown in Figure 9 requires three compressors. The primary circuit, which processes 1.727 lbs per hr of hydrogen, has two compressors each with a pressure ratio of 16.4. The secondary recirculating circuit has a 10.4 pressure ratio compressor. Figure 31 is a schematic of the designed compressor system which shows the first and second stages of each of the above compressors, their inlet and exit temperatures and pressures, radiators where needed, operating speed, and the number of compressor cylinders in each stage.

The mechanical assembly shown in Figure 29 is an arrangement of ten compressor cylinders (six low pressure and four high pressure; those units that have a discharge pressure of 1537.5 psia are identified as high pressure units). The compressors are located around cam shafts and they are stacked in three tiers on a centrally mounted base plate. An electric motor mounted on the other side of this base plate drives through reduction gearing a hydraulic pump and two different speed cam shafts. Also mounted on this side of the base plate is a 3-gallon hydraulic tank with space available for an accumulator if necessary. The complete assembly is installed within a double walled, sealed and insulated container whose top closure incorporates all of the external piping, electric power, and control system connections. It is assumed that the two container sections would have tailored environments, e.g., low temperature-low pressure hydrogen gas in the compressor section and higher pressure hydrogen for convective cooling or heating of the motor-pump section.

The low pressure compressors are actuated at a rate of 300 times a minute--a life cycle of 7.9×10^7 cycles. The diaphragm thickness and deflection is based upon the following relationships presented in Reference 6.

Diaphragm Deflection:

$$w_o = 0.802 \sqrt[3]{\frac{q\, a^4}{E\, h}}$$

Diaphragm Stress:

$$\sigma = 0.616 \frac{E\, w_o^2}{a^2} = 0.396 \sqrt[3]{\frac{E\, q^2 a^2}{h^2}}$$

Where

a = Diaphragm radius, ins.

q = Uniform pressure, psi

E = Young's modulus, psi

h = Diaphragm thickness, ins.

MAC A-68

Parametric curves of the above relationships are given in Figures 32 and 33. A plot of the volume displaced by diaphragms in the range of interest for this study is given in Figure 34.

Volumetric flow rate based upon perfect gas laws, inlet pressure, and the deflection volume of a spherical sector establishes a relationship of diaphragm diameter to thickness. Table V summarizes the pertinent data used in the compressor design.

When the diaphragm, due to inlet pressure, attains full deflection, a ram piston actuated by a cam controlled hydraulic cylinder starts the compression stroke. Mechanical deflection of the diaphragm is used because of the low temperature of the inlet gas. The hydraulic piston is sized for the maximum pressure-area force in the compressor cylinder.

The high pressure compressors (the second stages of the primary and secondary circuit compressors) are actuated 900 times a minute--a life cycle of 2.37×10^8 cycles. The diaphragm is actuated and supported in the units by an intermediate fluid (acetone or toluene). This concept is used because of the high intake and discharge pressures specified in this cycle and (by the omission of a radiator between stages) permits the compressor to operate at an average temperature of about 400°R. A membrane bellows separates the hydraulic fluid from the intermediate fluid. Hydraulic pressure relief valves in the discharge piping prevent over-deflection of the diaphragm by inlet hydrogen pressure.

The electric motor is an 11,000 rpm, 15 HP unit typical of special designs available from several electric motor manufacturers. By means of a three-to-one planetary gear set, a typical hydraulic pump with a 3000 psi and 10 gpm rated capacity is shown. The gear housing incorporates an integral lubrication system. The opposite end of the motor powers a reduction gear set that drives the 300 and 900 rpm cam shafts.

This preliminary design study shows that a hydrogen compressor system that uses membrane diaphragms is feasible and that through the use of high strength materials and existing state-of-the-art fabricating techniques, the component we weights listed in Table VI can be achieved. Diaphragms are utilized at the present time in commercial and experimental liquid and gaseous compressors, but their application in the configurations presented should have further analysis, design optimization, and structural evaluation in order to achieve the life, performance, and weight goals of this system.

TABLE V

SUMMARY OF COMPRESSOR DESIGN DATA

Unit			Number Required	Maximum Pressure (psi)	Compressor Area (sq in.)	Maximum Force (lbs)	Diaphragm			Hydraulic Cylinder	
Item	Compressor	Stage					Total Deflection (in.)	Thickness (in.)	Maximum Stress (psi)	Area (sq ins.)	Displacement (cu in.)
a	1	1	2	32.4	50.2	1625	0.440	0.004	53,000	0.744	0.327
b	1	2	1	131.2	28.2	3800	0.400	0.006	76,000	1.695	0.680
c	2	1	1	379.5	14.2	5400	0.260	0.015	60,000	2.460	0.640
d	2	2	1	1537.5	5.8	8900	0.140	0.004	50,000	5.800	0.270
e	3	1	2	477.0	17.65	8430	0.320	0.019	80,000	3.800	1.215
f	3	2	3	1537.5	5.8	8900	0.150	0.004	57,000	5.800	0.287

TABLE VI

SUMMARY OF COMPONENT WEIGHTS OF THE COMPRESSOR SYSTEM

Item	Description	Weight (lbs)
1.	Electric motor	30
2.	Hydraulic pump	13
3.	Pump reduction gear unit	12
4.	Compressor cam reduction gear unit (Incl. cams, shafts, etc.)	5
5.	Main mounting plate and mounting ring	7
6.	Container	51
7.	Compressor mounting plates and support tubes	5
8.	End plate (Cover)	8
9.	Piping, fittings, and miscellaneous items	5
10.	Compressors:	
	a. Primary 1st comp.-1st stage, 2 at 5.25 lbs = 10.50	
	b. Primary 1st comp.-2nd stage, 1 at 4.25 lbs = 4.25	
	c. Primary 2nd comp.-1st stage, 1 at 4.75 lbs = 4.75	
	d. Primary 2nd comp.-2nd stage, 1 at 3.25 lbs = 3.25	
	e. Secondary comp.-1st stage, 2 at 4.75 lbs = 9.50	
	f. Secondary comp.-2nd stage, 3 at 3.25 lbs = 9.75	
	42.00 lbs	42
	DRY WEIGHT:	178 lbs
11.	Hydraulic fluid - 3 gals at approx. 7.35 lb/gal	22
	SYSTEM WET WEIGHT:	200 lbs

MAC A 673

VI. CONCLUSIONS

The following conclusions are based on the studies reported herein:

1. For storage periods of the order of one earth year, the total mass which must be transported in order to supply a given quantity of liquid hydrogen can be substantially reduced by the use of hydrogen reliquefiers.

2. Night only operation of a hydrogen reliquefier for a lunar equatorial site is both desirable and feasible and permits the use of comparatively simple reliquefier cycles.

3. Nuclear electrical power systems (SNAP systems) constitute feasible power sources for hydrogen reliquefiers.

4. The combustion of hydrogen should not be employed as a reliquefier power source unless it can be justified solely on the basis of need for the water produced.

5. Final selection of a reliquefier cycle should reflect detailed consideration of component design requirements which are beyond the scope of the studies reported herein. In particular, the meteroid protection requirements for the radiator should be investigated in detail.

VII. RECOMMENDATIONS

Based on the results of the studies reported herein, the following recommendations are made:

1. A complete detailed design of a full scale reliquefier for lunar applications should be prepared to firmly establish the feasibility of the reliquefier concept and to form the basis for the next item below.

2. A reliquefier development plan should be prepared considering such items as reliquefier test facilities and scheduling of key component subelement tests (e.g., compressor diaphragm tests).

3. Consideration should be given to extending reliquefier investigations to

   a. Other propellants, in particular oxygen

   b. Deep space missions

   c. The preparation at a lunar or orbital base of partially solidified propellants to be employed in subsequent deep space missions.

MAC A678

VIII. REFERENCES

1. Martin-Marietta Corporation Report ER 12387-I, "Earth Lunar Transportation System--Lunar Propellant Storage, December 1961 to May 1962", Contract NAS 8-1531, Task No. 2. UNCLASSIFIED.

2. NASA Lewis Research Center, Cleveland, Ohio Report 2543-62, "Meteoroid Protection for Space Radiators", (I. J. Loeffter, S. Lieblein, and N. Clough), 25 September 1962. UNCLASSIFIED.

3. "SNAP-Systems for Nuclear Auxiliary Power", Atomics, Vol. 16, No. 3, May-June 1963.

4. Oppenheim, A. K., "Radiation Analysis by the Network Method", Transactions of the ASME, May 1956.

5. NASA Report TN D-196, "Analysis of Temperature Distribution and Radiant Heat Transfer Along a Rectangular Fin of Constant Thickness", (S. Lieblein), November 1959. UNCLASSIFIED.

6. Timoshenko, S, "Theory of Plates and Shells, Article 101", McGraw-Hill Co., New York, N.Y. 1959.

7. National Bureau of Standards Technical Note TN 130 (PB 161631), "Provisional Thermodynamic Functions for Parahydrogen", (H. M. Roder and R. G. Goodwin), December 1961. UNCLASSIFIED.

8. Engineering Experiment Station of the Georgia Institute of Technology Technical Report No. 1, Project No. A-593, "The Thermodynamic Properties of Parahydrogen from 1° to 22°K", (J. C. Mullens, W. T. Ziegler, and B. S. Kirk), National Bureau of Standards, Boulder, Colorado Contract No. CST-7339, 1 November 1961. UNCLASSIFIED.

9. ASD-TDR-61-360, "Thermodynamic Properties of 20.4°K Equilibrium Hydrogen", (A. Shaffer and J. Rousseau, AiResearch Manufacturing Co.), October 1961. UNCLASSIFIED.

10. National Bureau of Standards Monograph No. 21, "Specific Heats and Enthalpies of Technical Solids at Low Temperatures," (R. J. Corruccini and J. J. Griewek), 3 October 1960. UNCLASSIFIED.

MAC A673

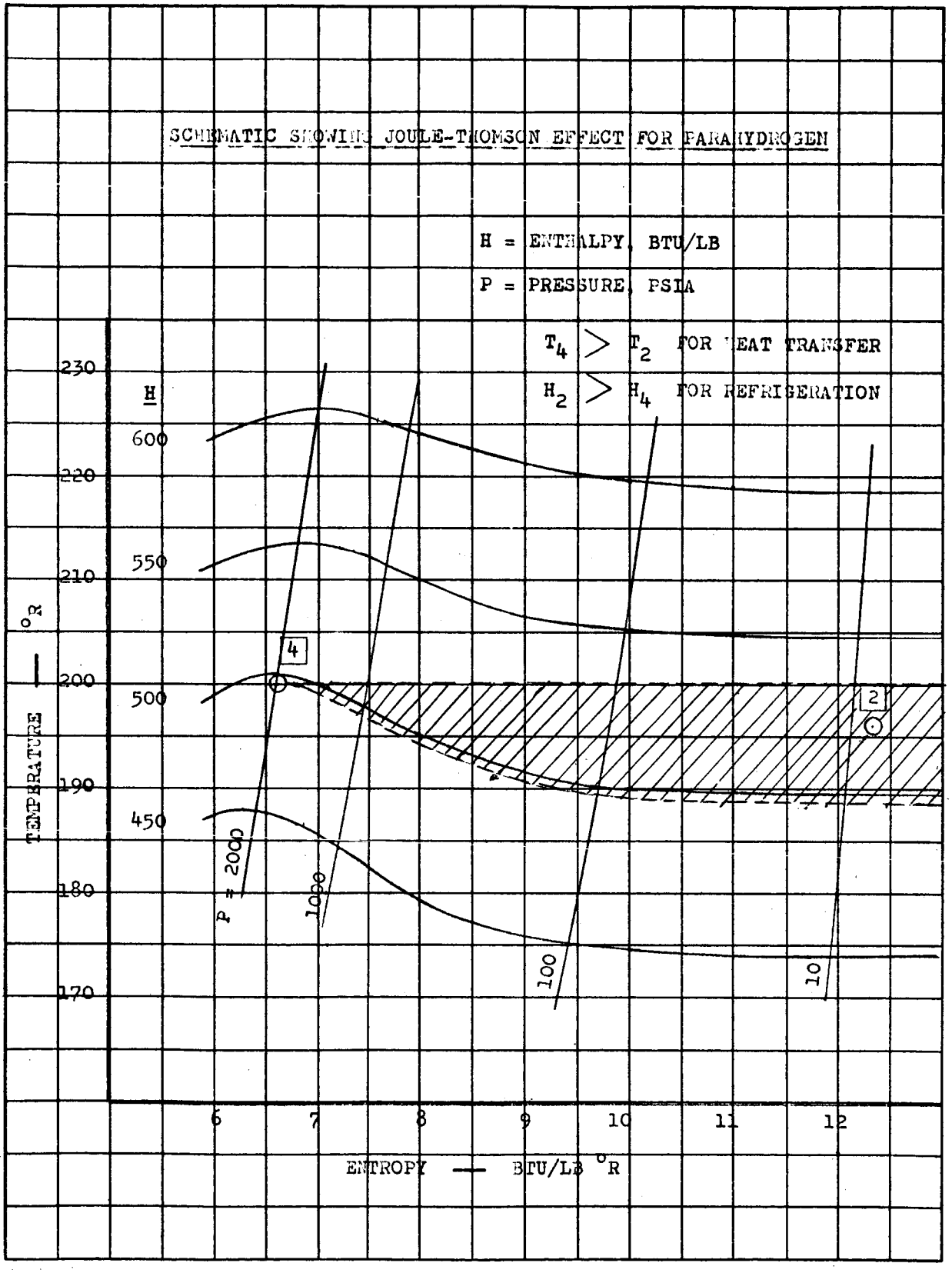

MAC A673

FIGURE 1

HAMPSON CYCLE SCHEMATIC

TOTAL COMPRESSOR POWER = 27,350 BTU/HR = 10.75 H.P.

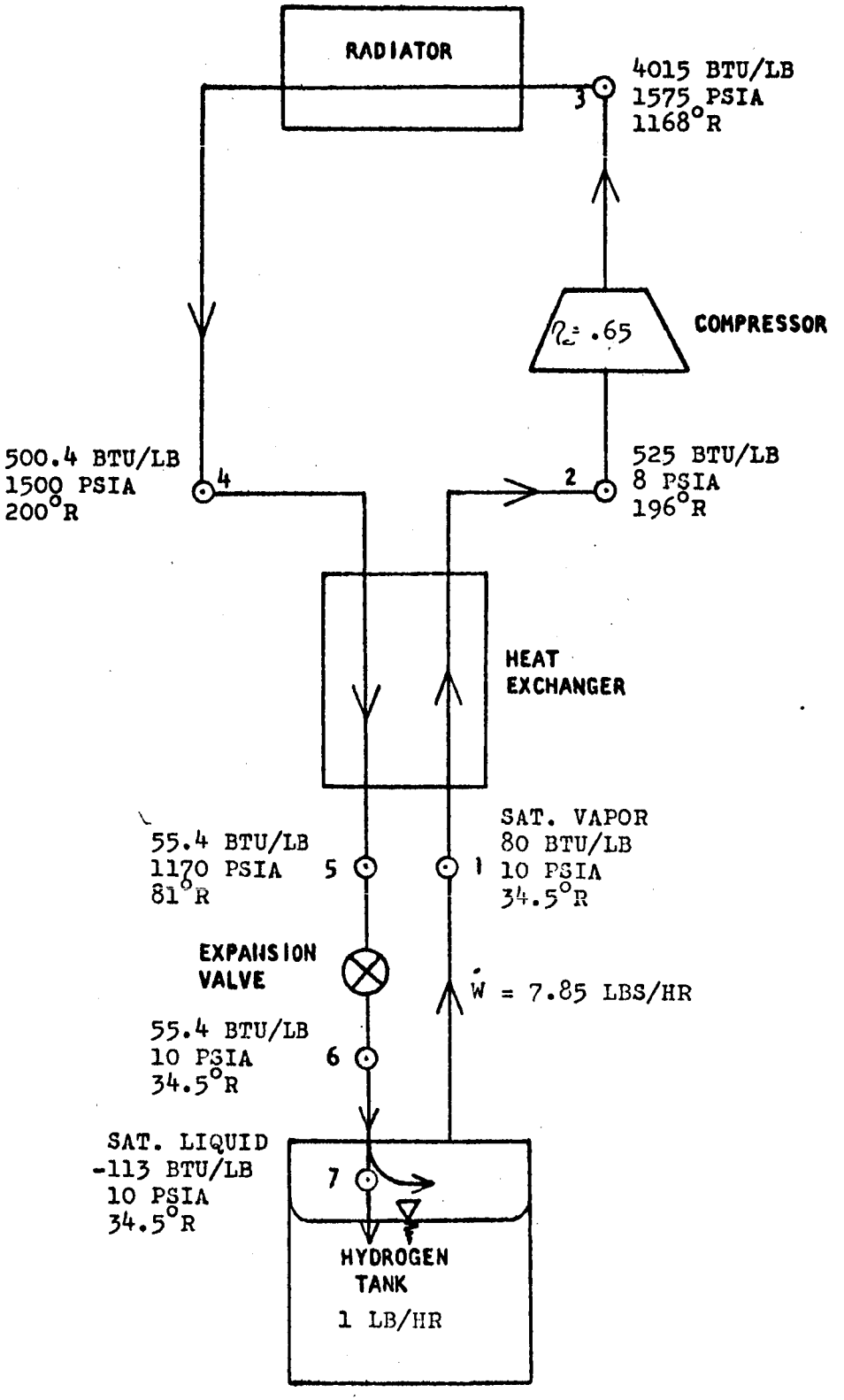

MAC A673

FIGURE 2

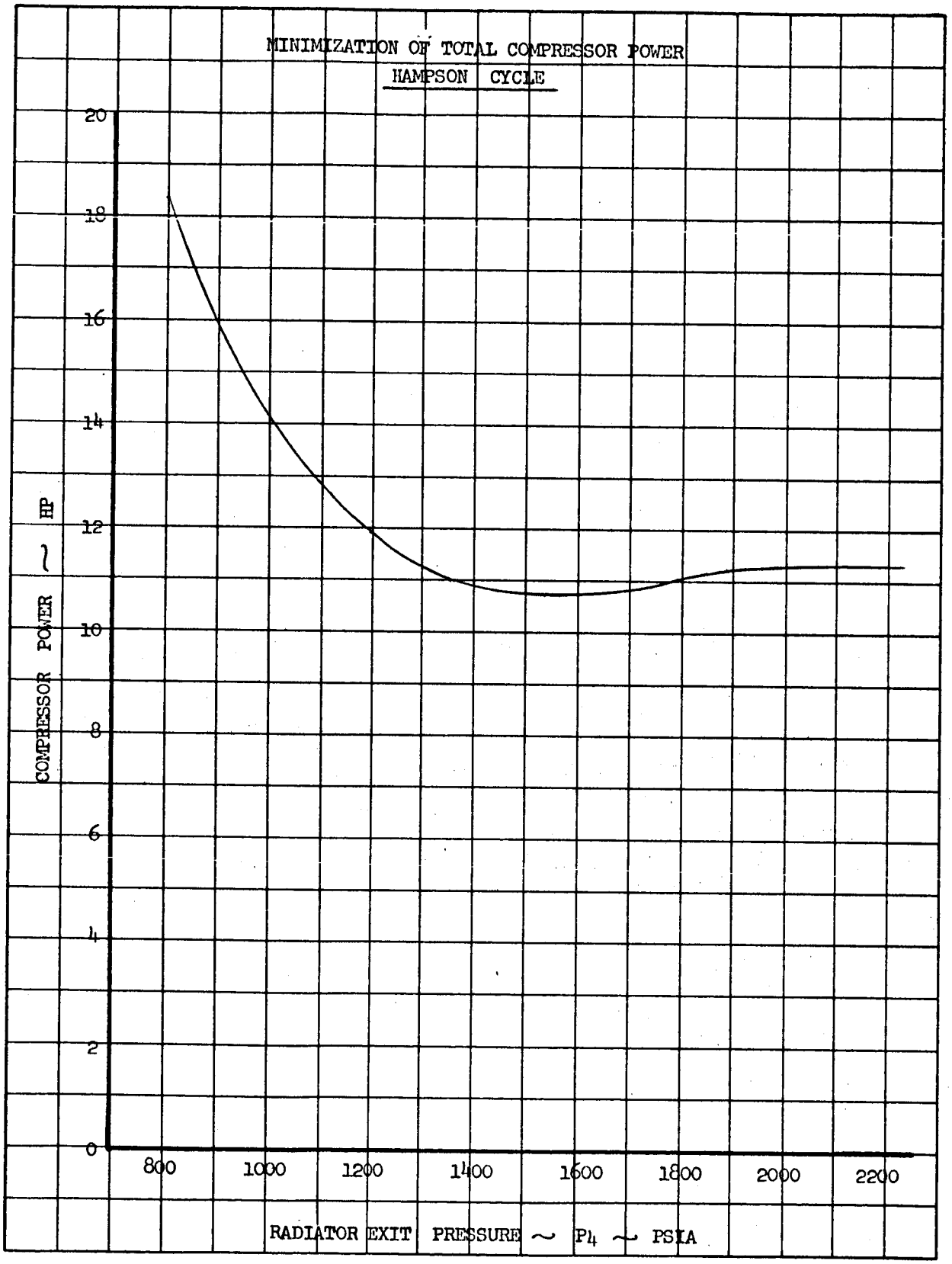

MAC A673

FIGURE 3

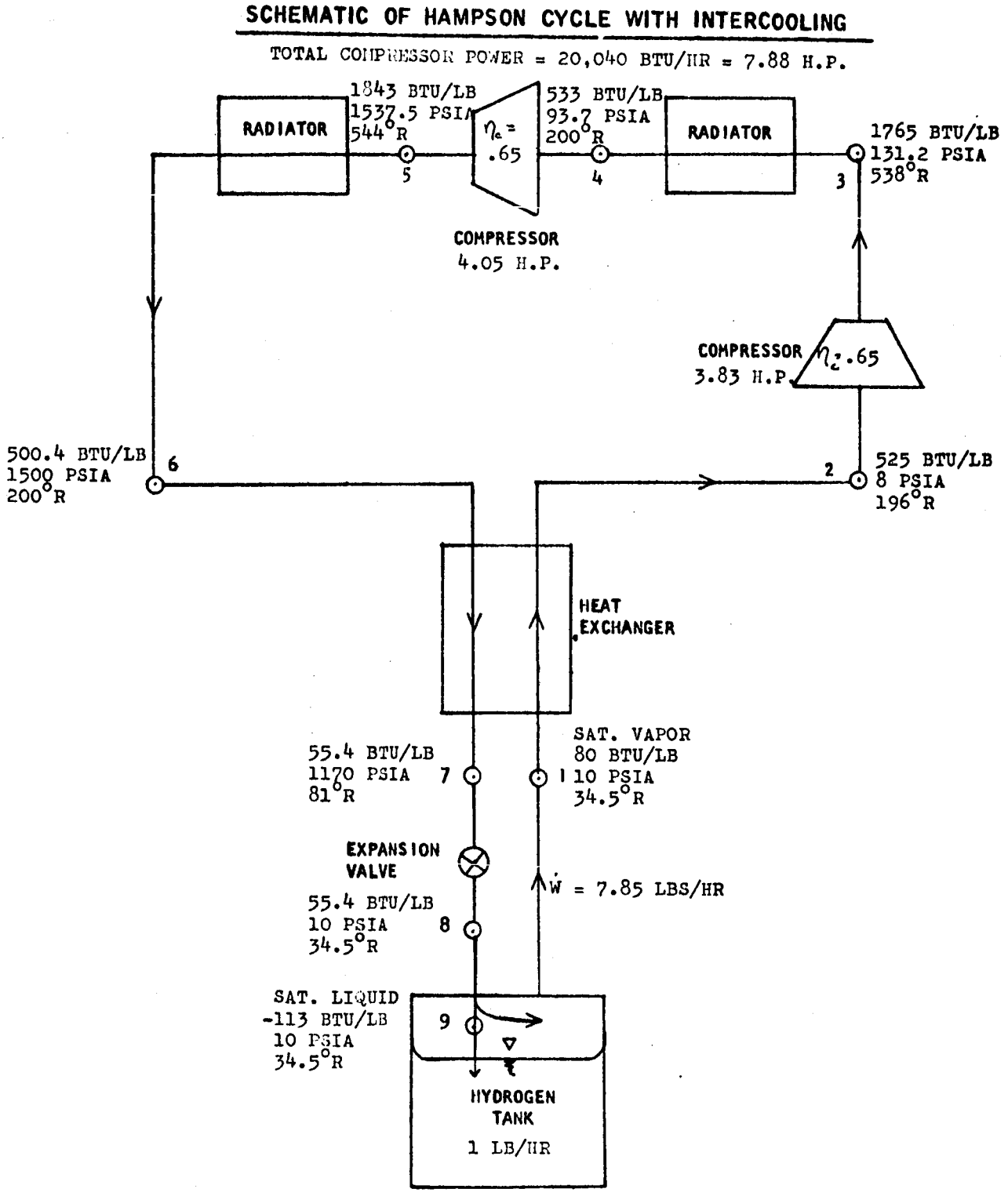

MAC A673

FIGURE 4

SCHEMATIC OF HAMPSON CYCLE WITH THREE STAGES OF INTERCOOLING

TOTAL COMPRESSOR POWER = 17,800 BTU/HR = 7.02 H.P.

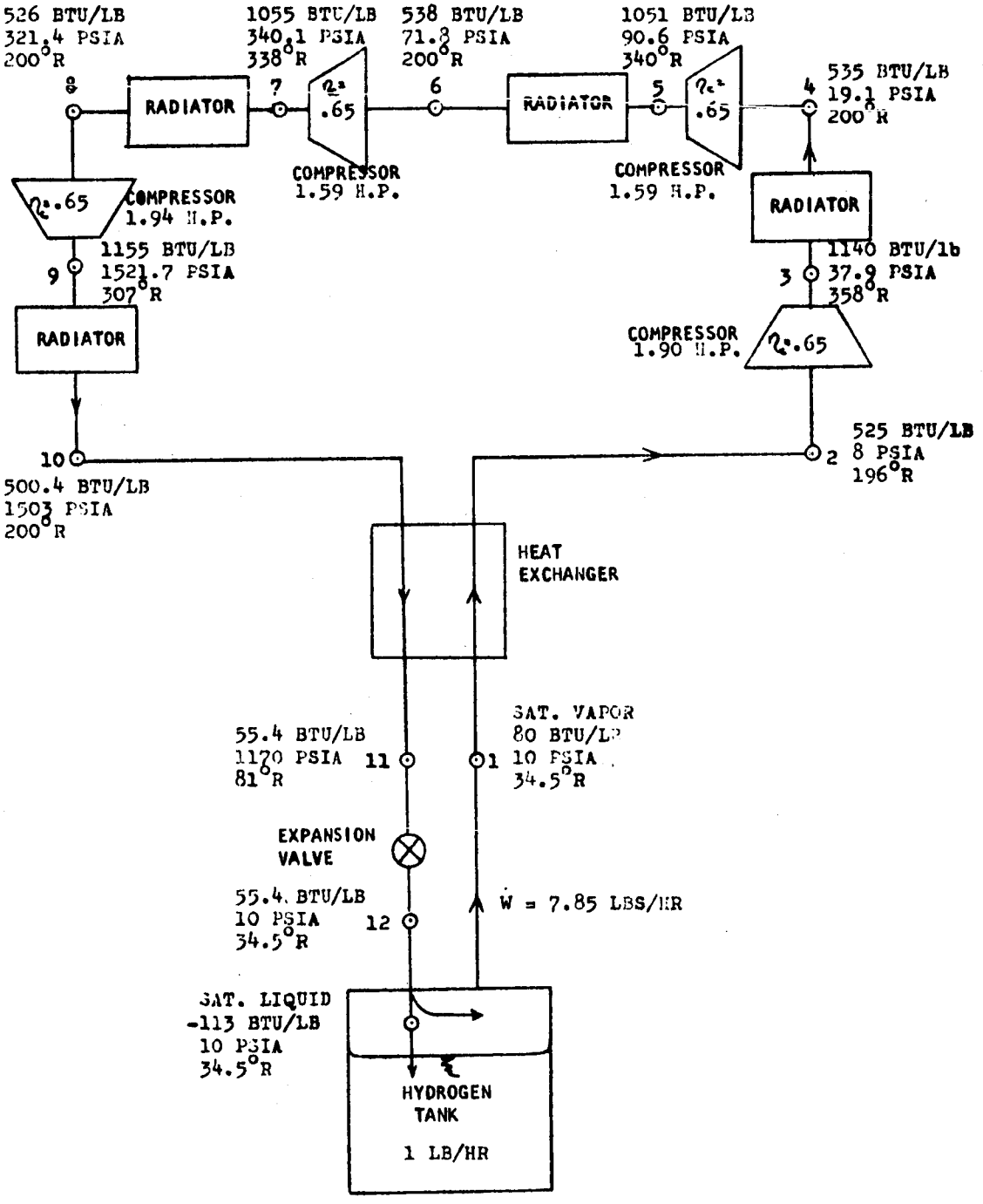

MAC A673

FIGURE 5

SCHEMATIC OF HAMPSON CYCLE WITH TWO STAGES OF INTERCOOLING

TOTAL COMPRESSOR POWER = 18,900 BTU/HR = 7.42 H.P.

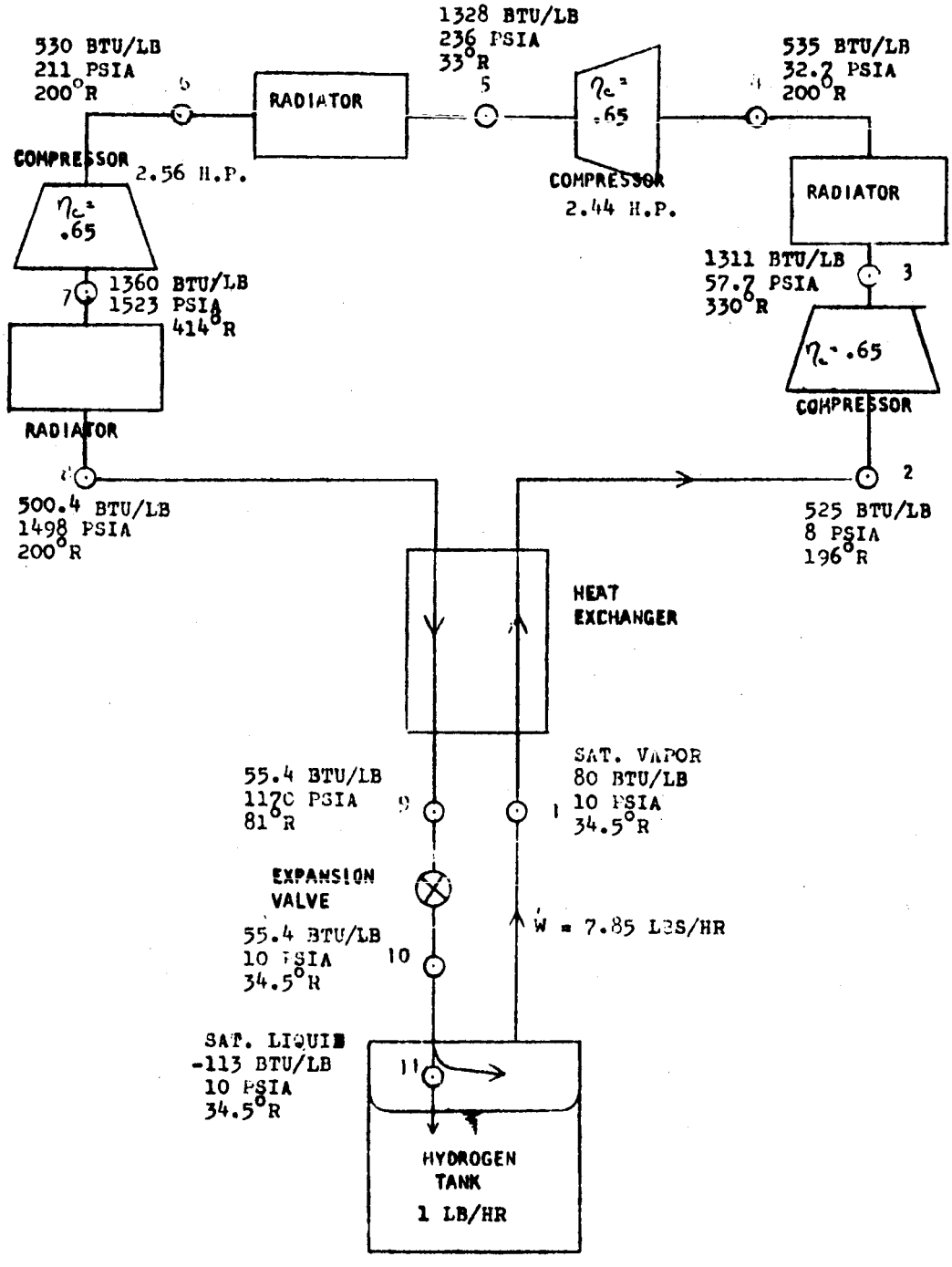

MAC A673

FIGURE 6

SCHEMATIC OF DUAL PRESSURE CYCLE - ONE STAGE OF LOW PRESSURE LOOP INTERCOOLING INTEGRAL WITH INTERMEDIATE PRESSURE LOOP

TOTAL POWER = 9160 BTU/HR = 3.60 H.P.

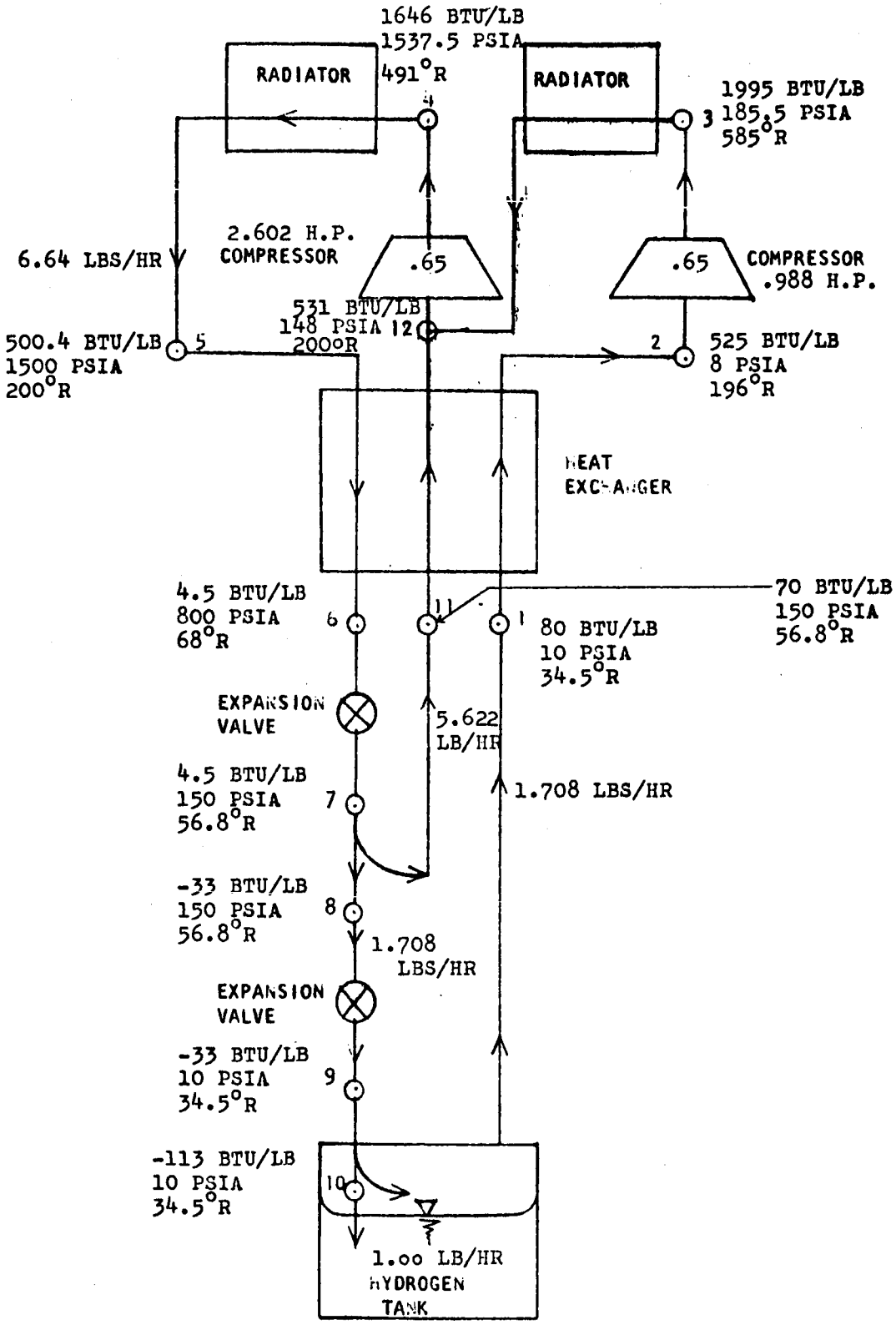

MAC A673

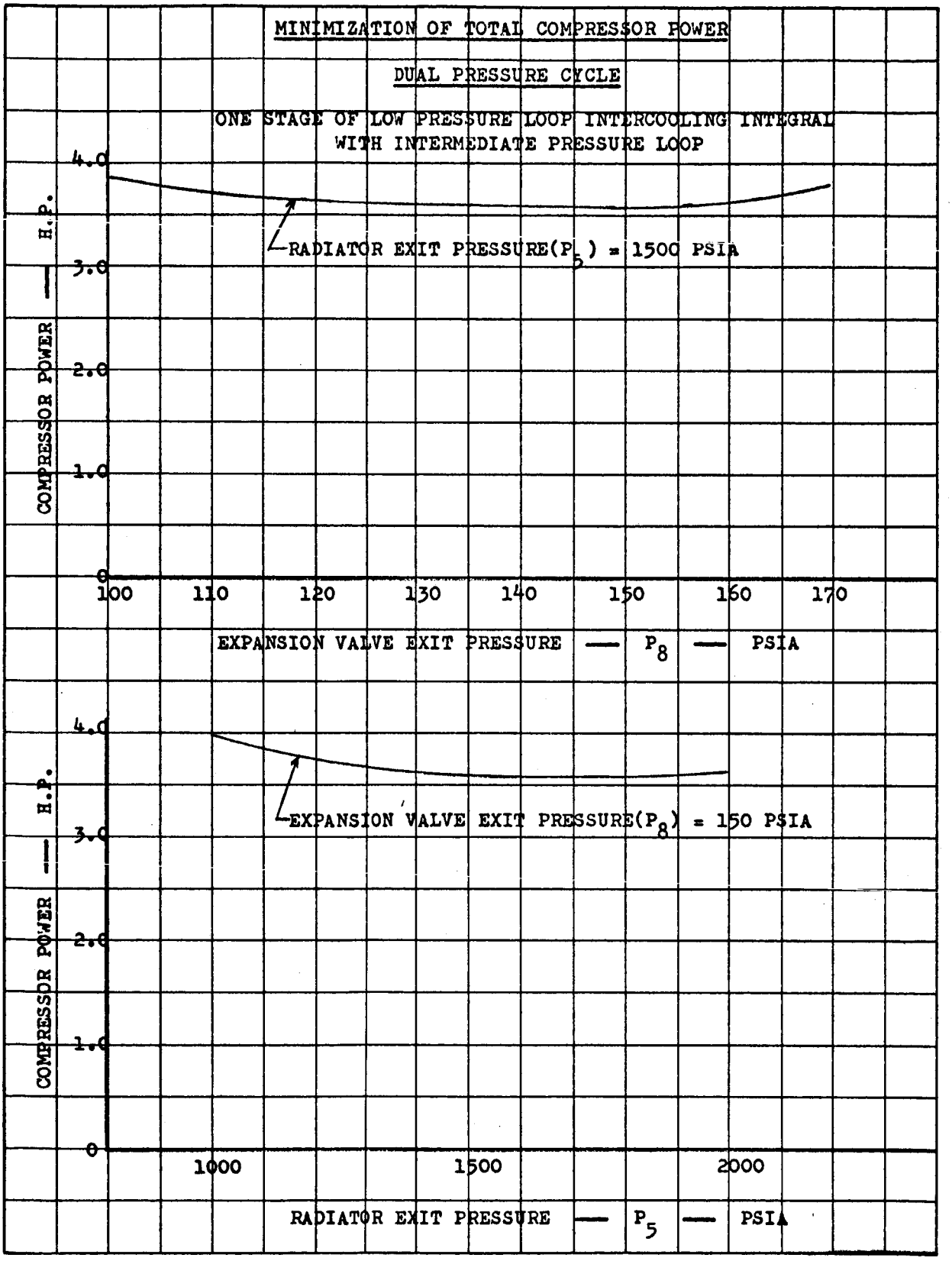

MAC A673

FIGURE 8

SCHEMATIC OF DUAL PRESSURE CYCLE

ONE STAGE OF PRIMARY LOOP INTERCOOLING

TOTAL POWER = 12150 BTU/HR
4.772 H.P.

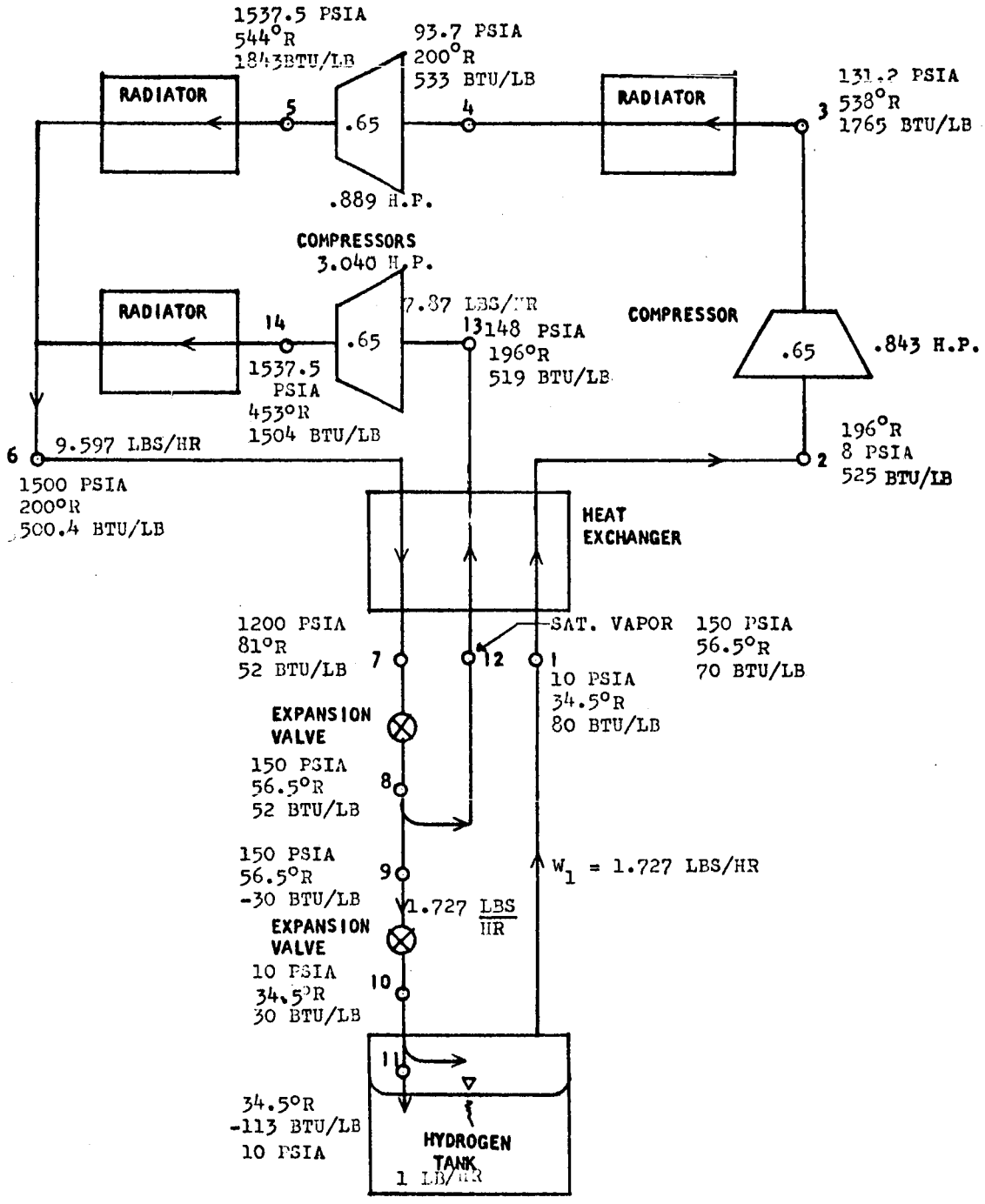

MAC A673

FIGURE 9

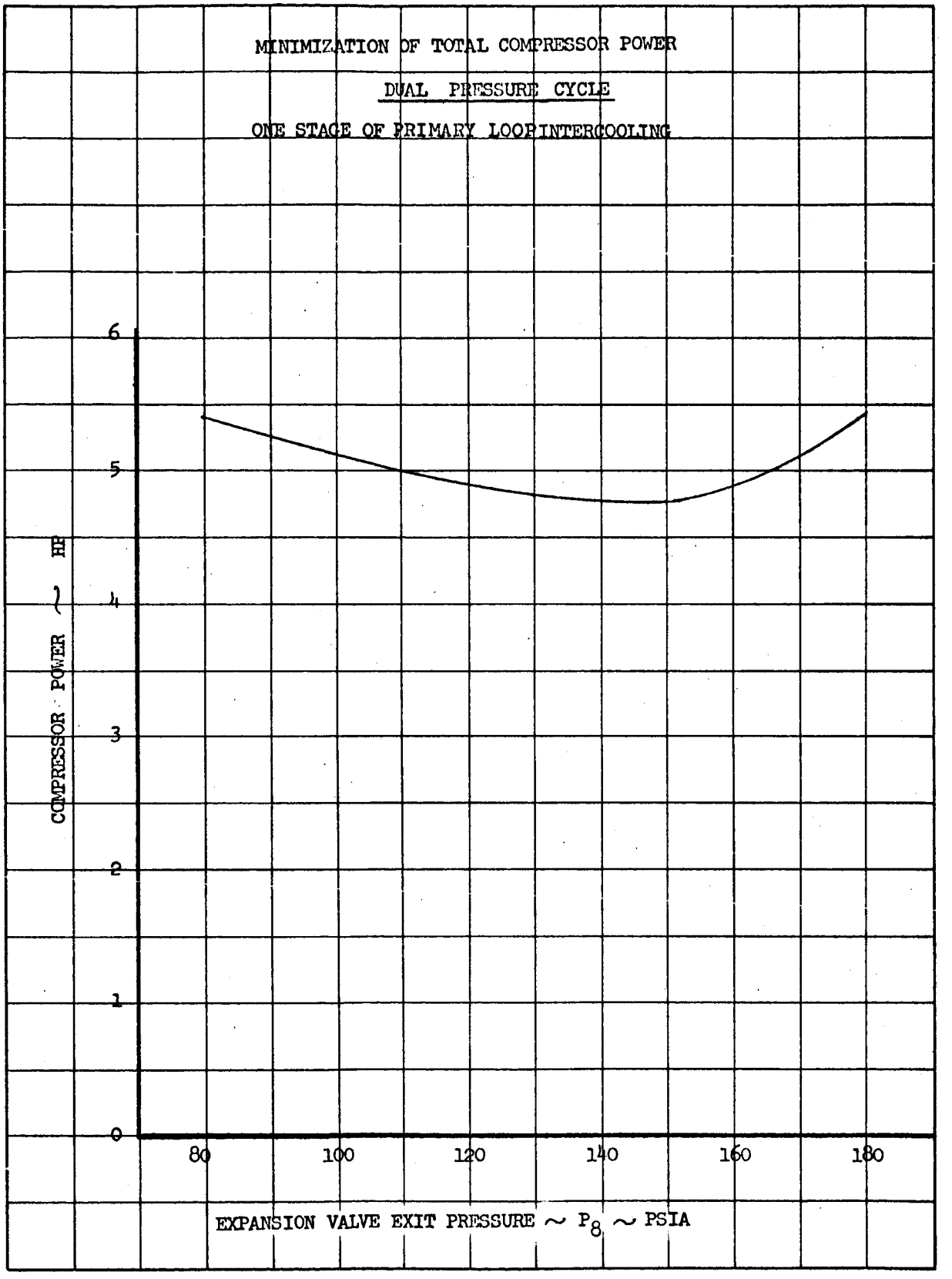

MAC A673

FIGURE 10

SCHEMATIC OF DUAL PRESSURE CYCLE WITH ONE STAGE OF PRIMARY LOOP INTERCOOLING

TOTAL POWER = 12,030 BTU/HR
= 4.722 H.P.

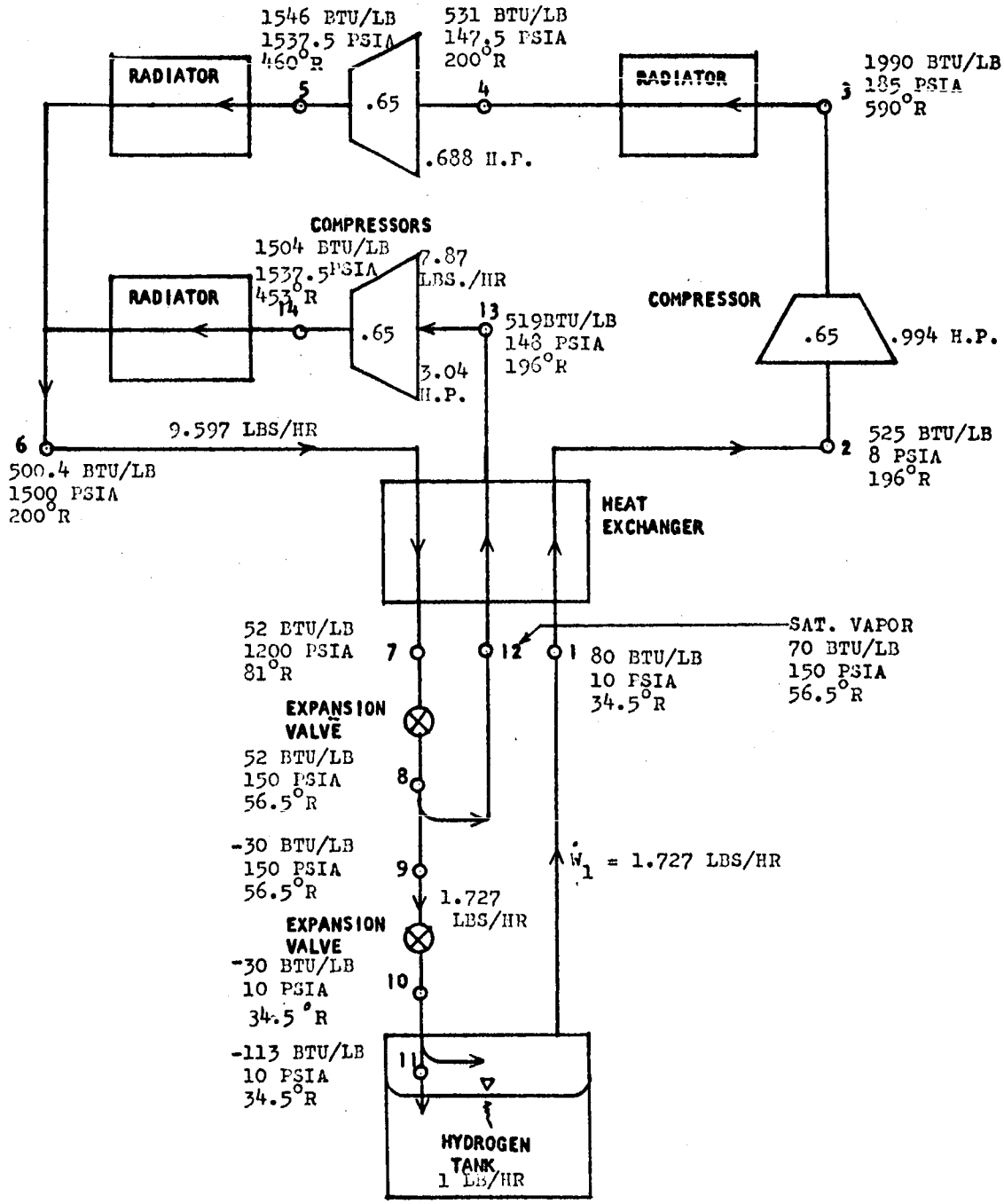

MAC A673

SCHEMATIC OF DUAL PRESSURE CYCLE WITH ONE STAGE OF PRIMARY LOOP INTERCOOLING
COOLING BETWEEN EXPANSIONS
TOTAL COMPRESSOR POWER = 11,460 BTU/HR = 4.50 H.P.

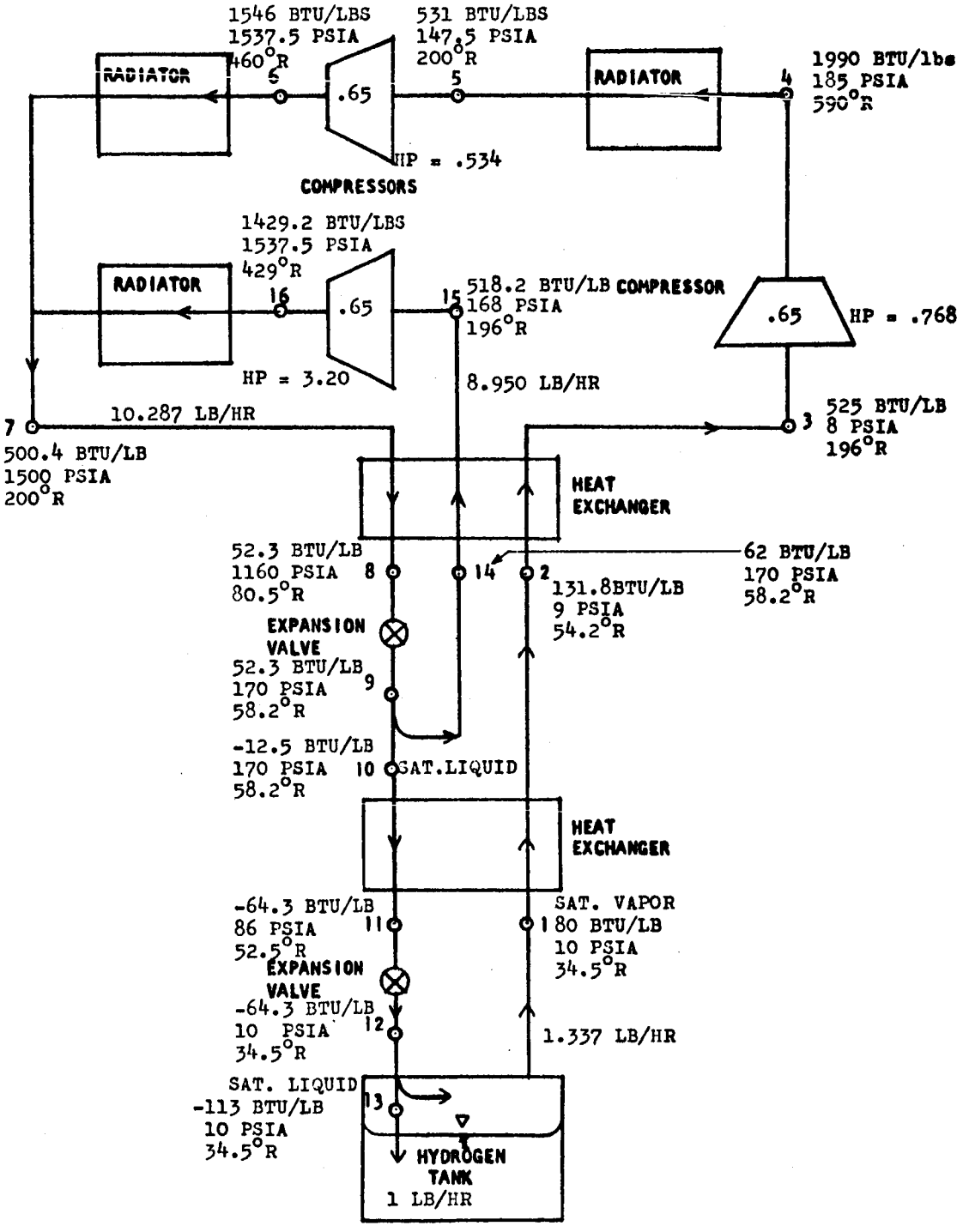

MAC A673

FIGURE 12

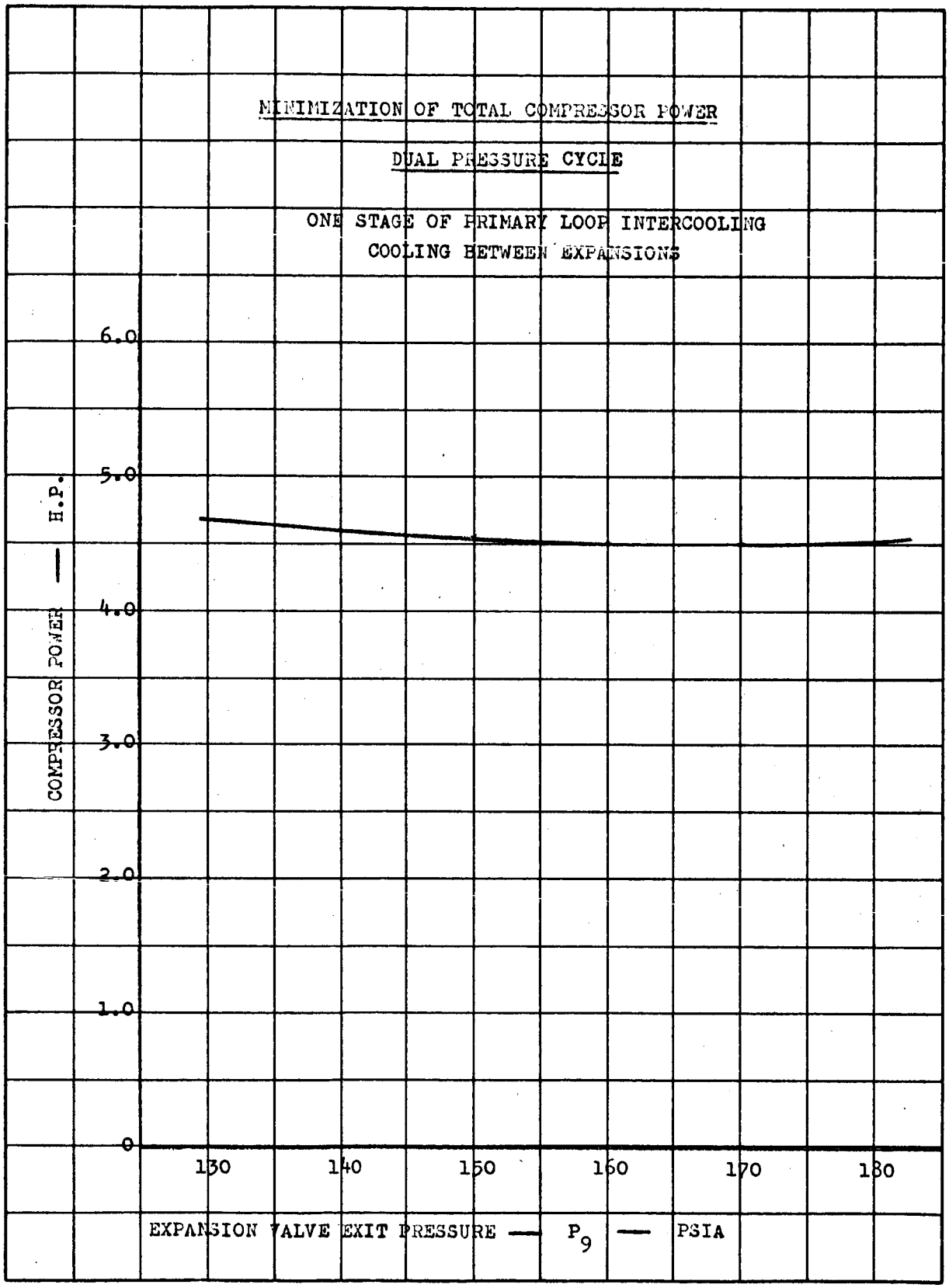

MAC A673

FIGURE 13

SCHEMATIC OF DUAL PRESSURE CYCLE WITH ONE STAGE OF INTERCOOLING AND INTEGRAL HIGH TEMPERATURE REFRIGERATION LOOP WITH EXPANDER

TOTAL COMPRESSOR POWER = 6100 BTU/HR = 2.40 H.P.

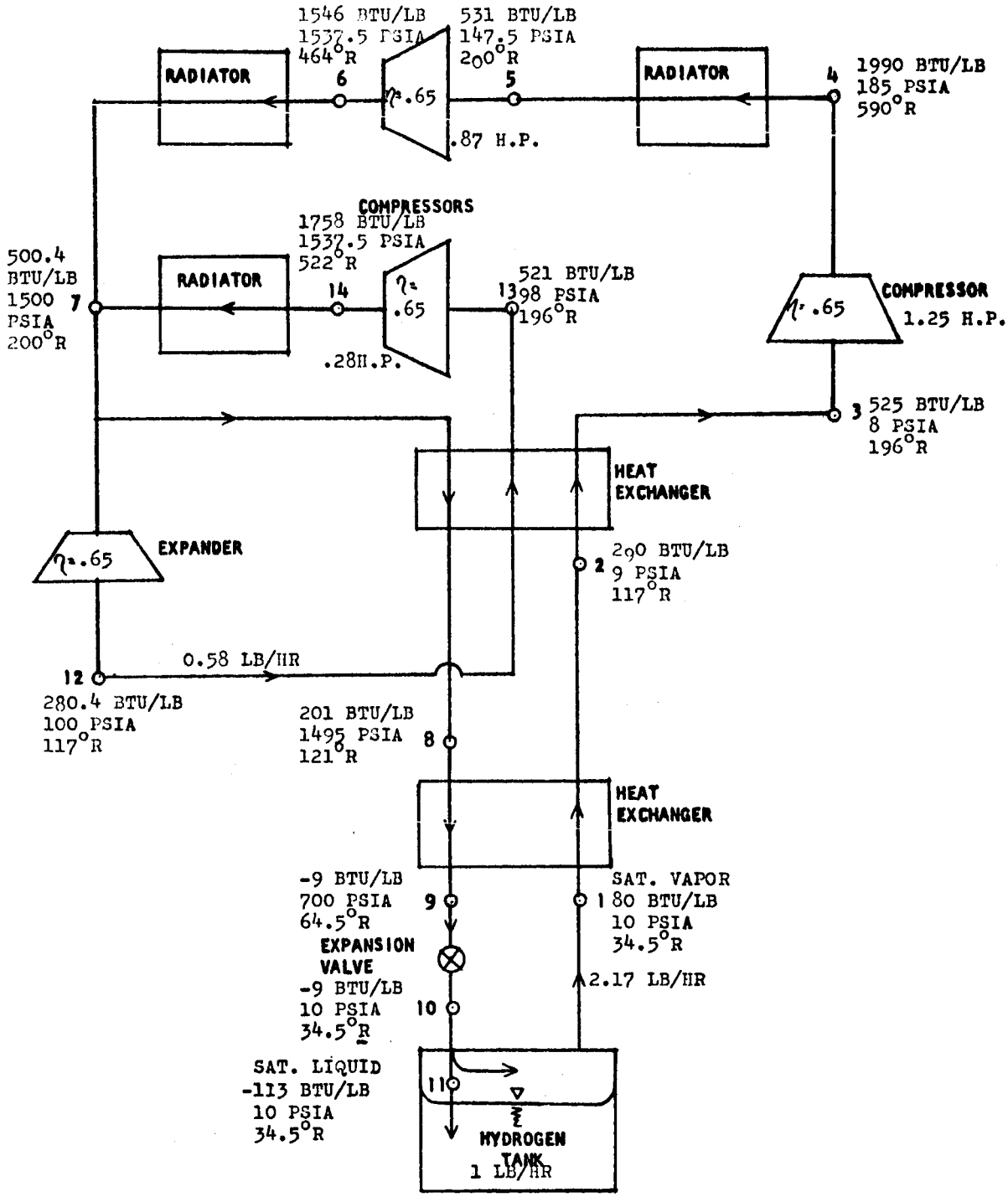

MAC A673

FIGURE 14

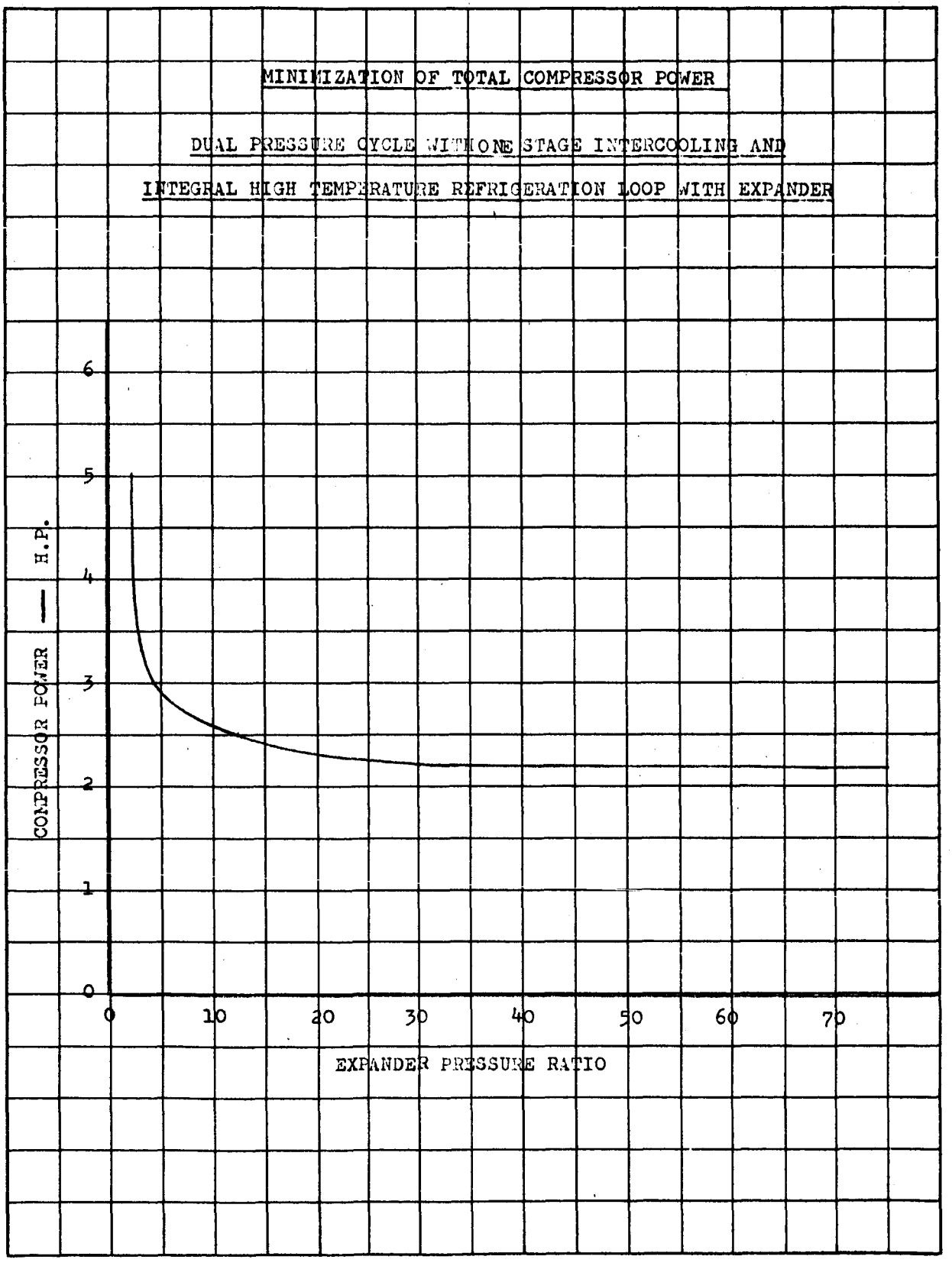

MAC A673

FIGURE 15

DUAL PRESSURE CYCLE WITH ONE STAGE OF INTERCOOLING PER LOOP - SEPARATE HIGH TEMPERATURE REFRIGERATION LOOP WITH EXPANDER

TOTAL COMPRESSOR POWER 2 4025 BTU/HR = 1.58 H.P.

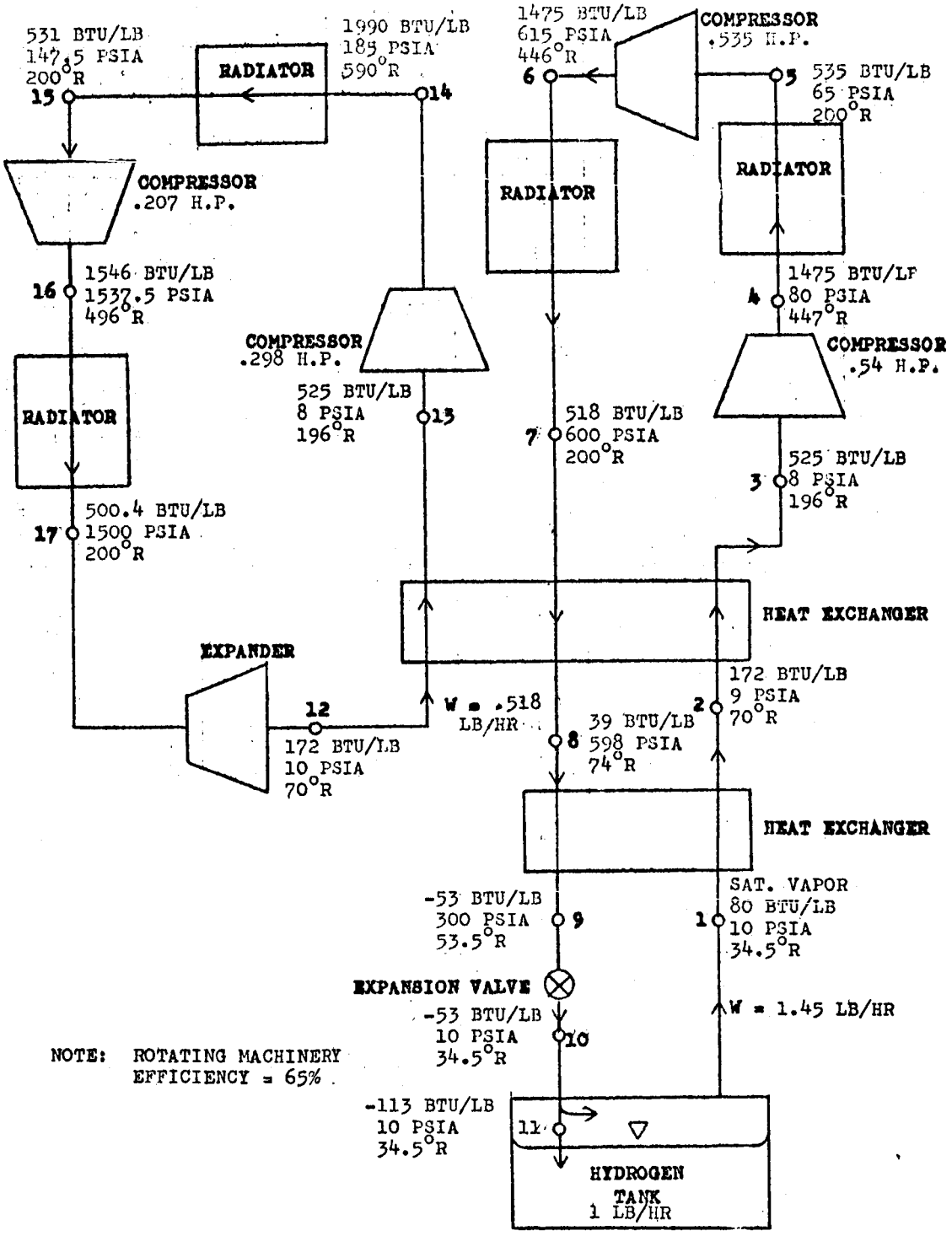

MAC A673

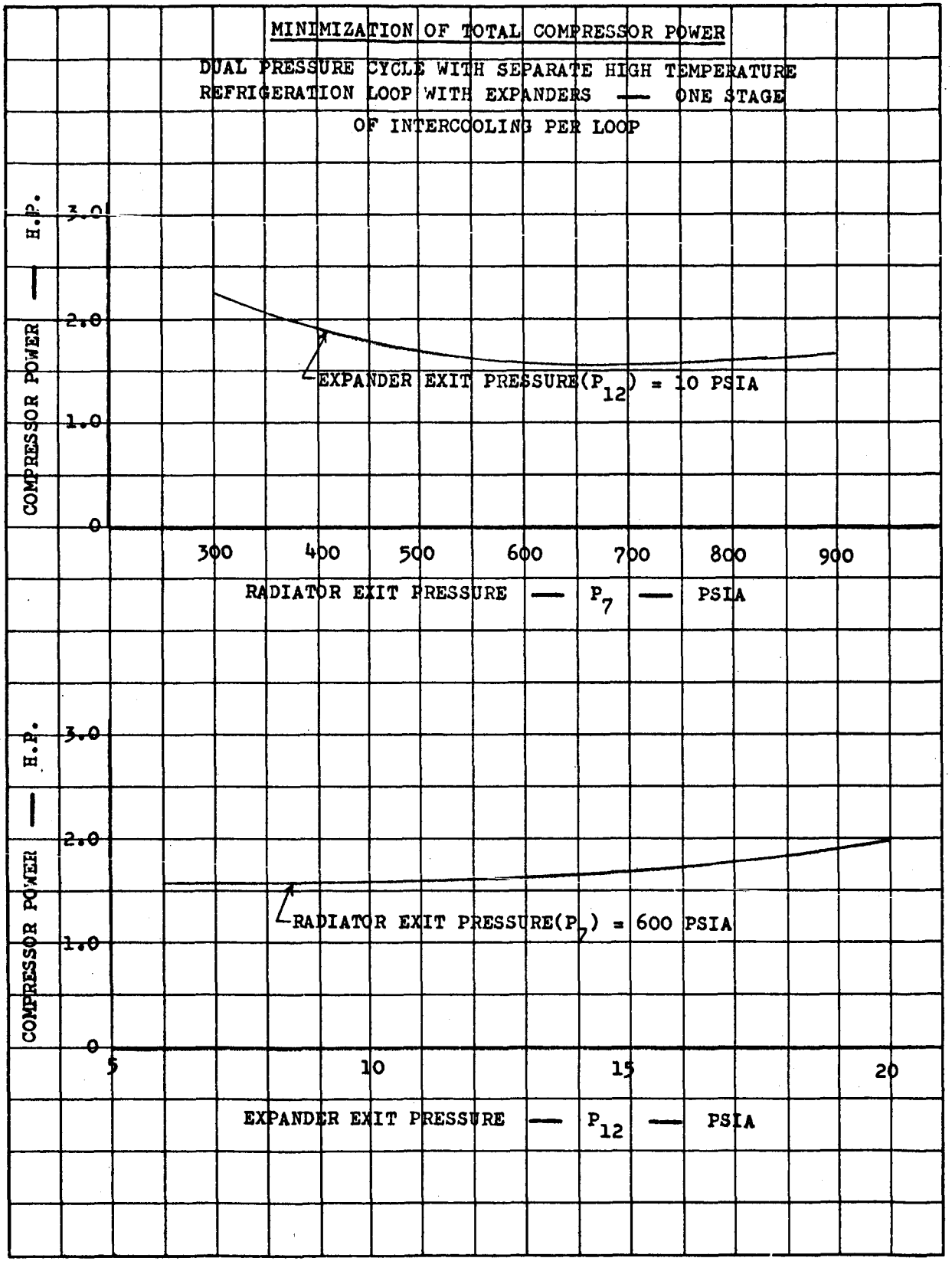

MAC A673

FIGURE 17

SCHEMATIC OF

CLAUDE HEYLANDT CYCLE - ONE STAGE OF INTERCOOLING

TOTAL POWER = 4690 BTU/HR = 1.84 H.P.

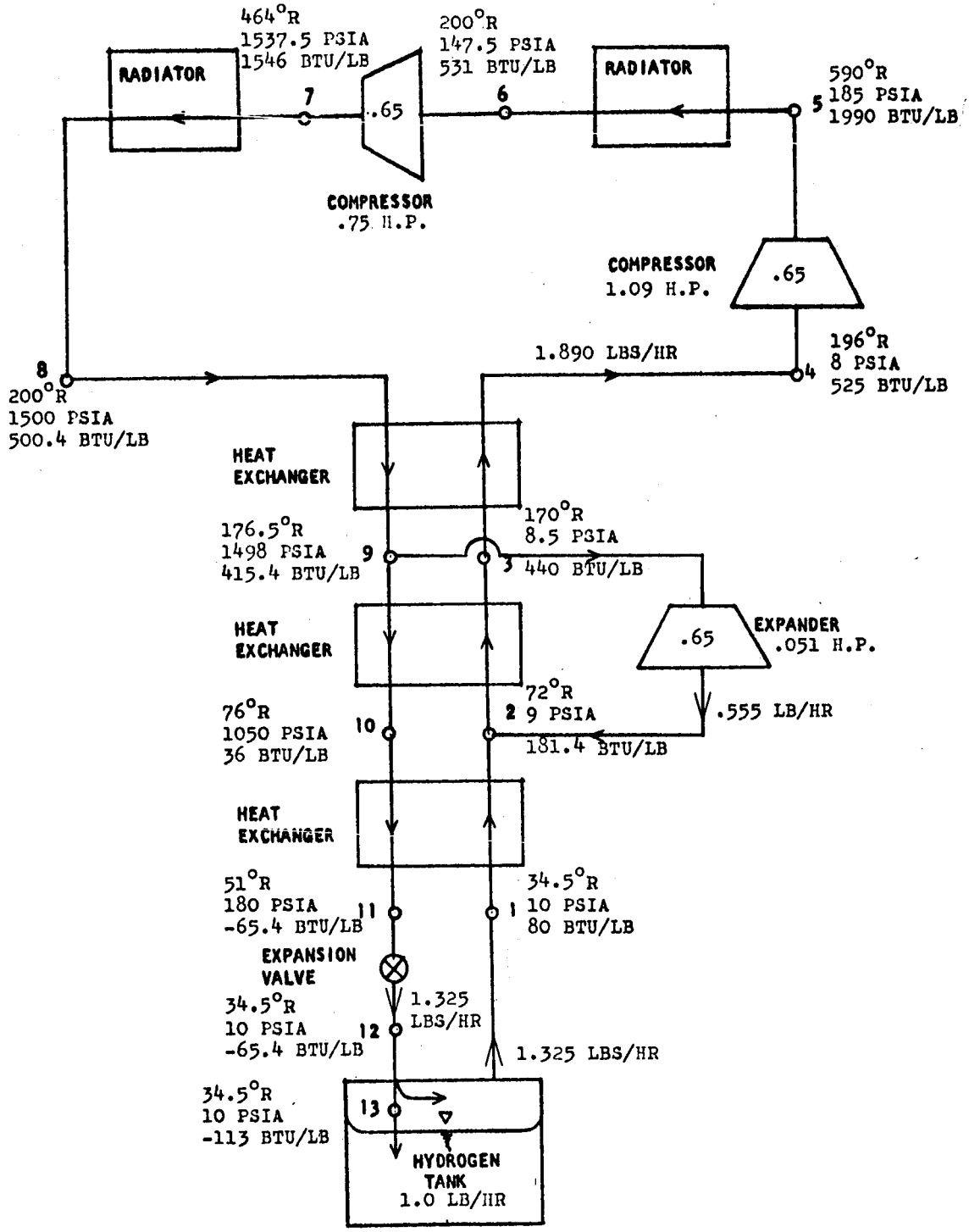

MAC A673

FIGURE 18

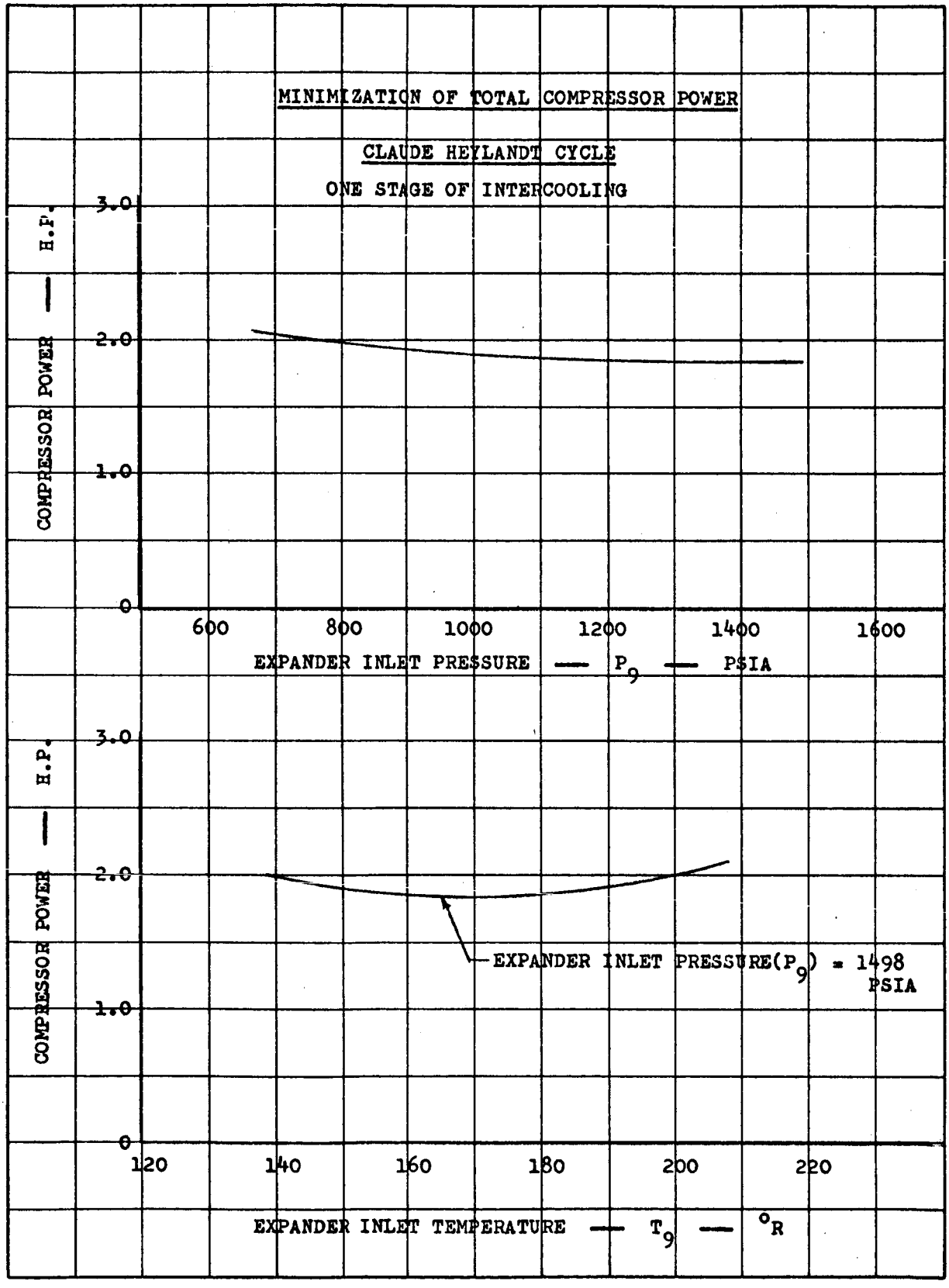

MAC A673

FIGURE 19

SCHEMATIC OF
CLAUDE HEYLANDT CYCLE - ONE STAGE INTERCOOLING
TOTAL POWER = 3920 BTU/HR = 1.541 H.P.

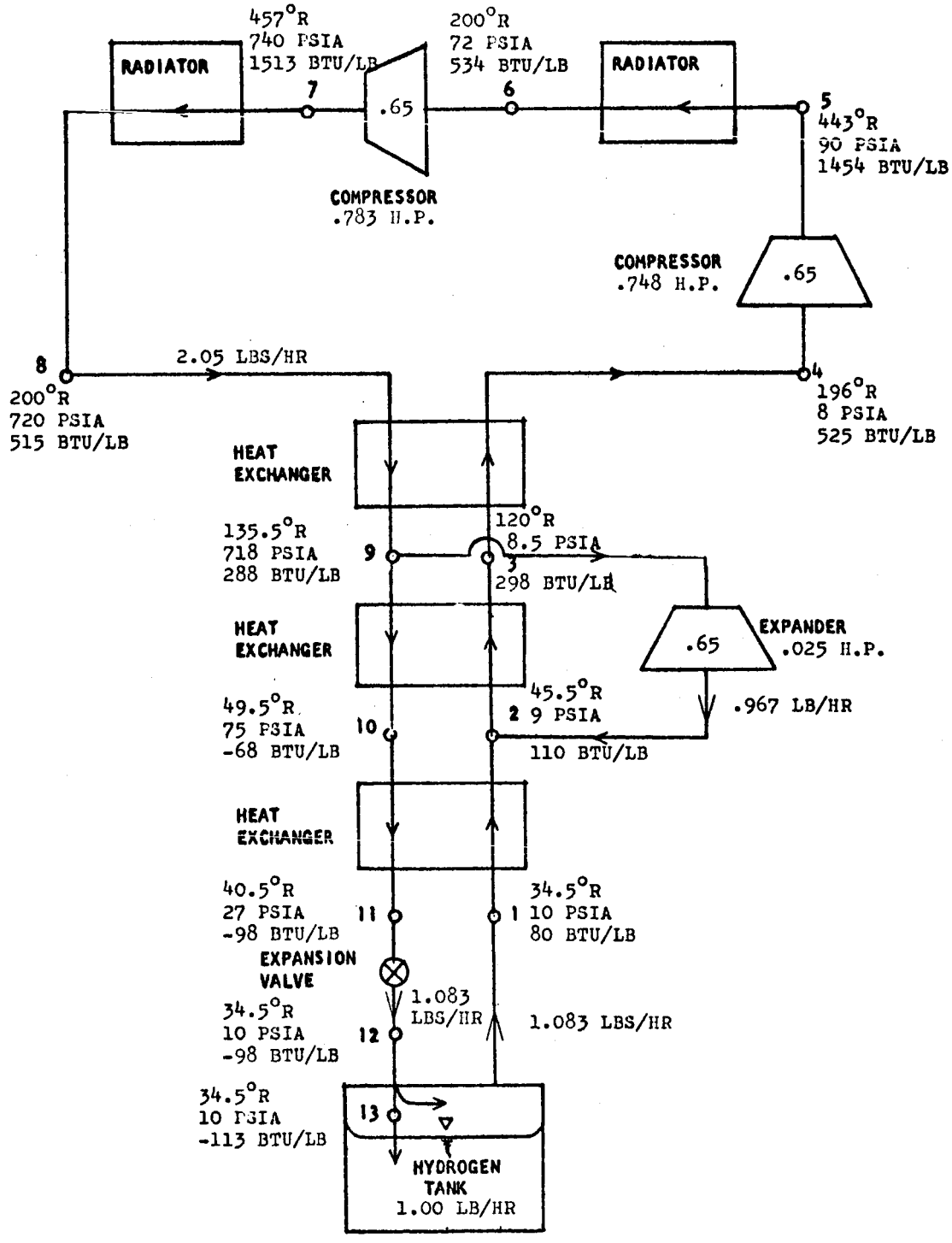

MAC A673

FIGURE 20

SCHEMATIC OF CLAUDE-HEYLANDT CYCLE WITH TWO EXPANDERS - TWO STAGE INTERCOOLING

TOTAL POWER = 5929 BTU/HR = 2.34 H.P.

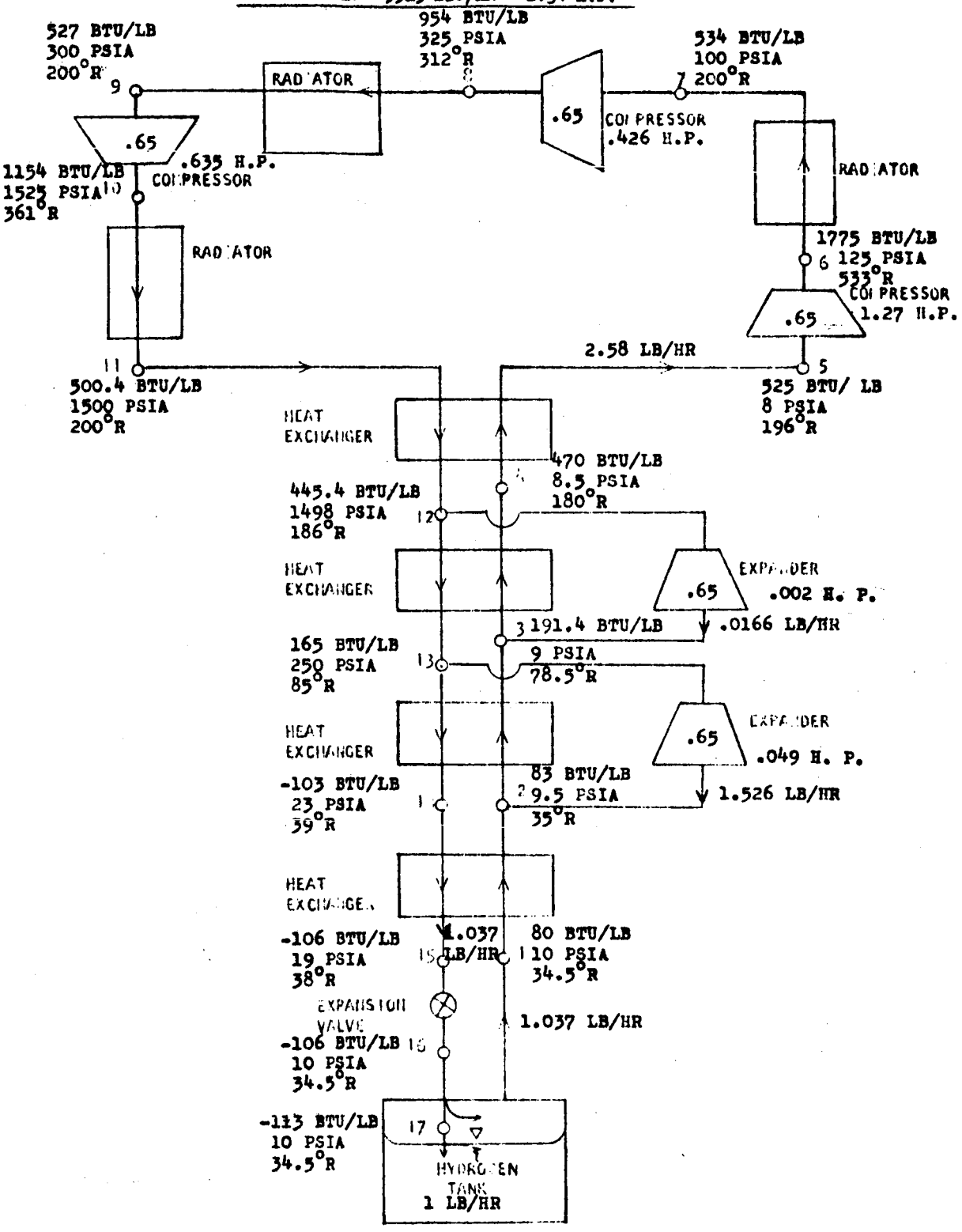

MAC A673

FIGURE 21

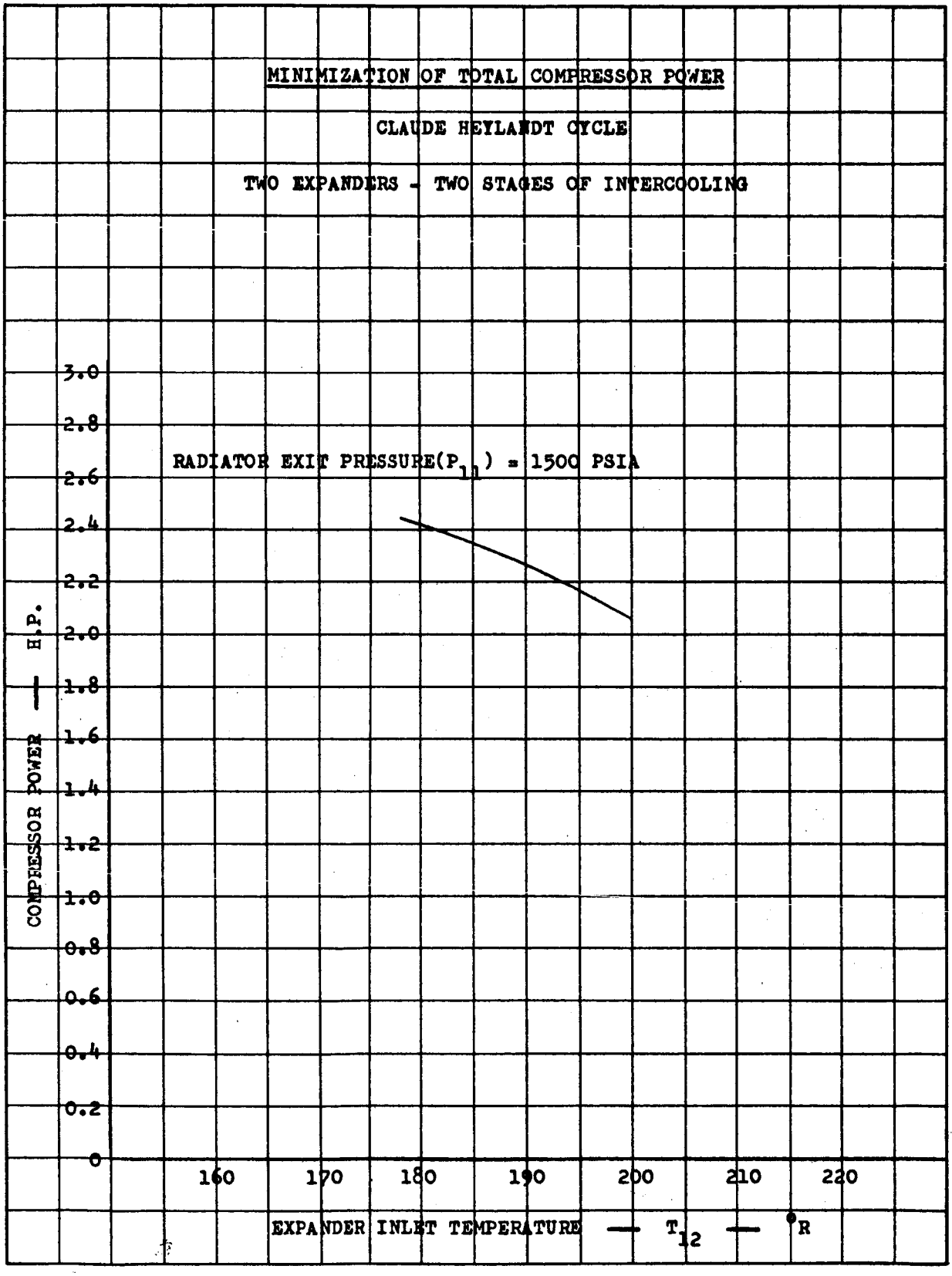

MAC A673

FIGURE 22

SCHEMATIC OF CLAUDE - HEYLANDT CYCLE WITH TWO EXPANDERS - TWO STAGES OF INTERCOOLING
TOTAL POWER = 5279 BTU/HR = 2.07 H.P.

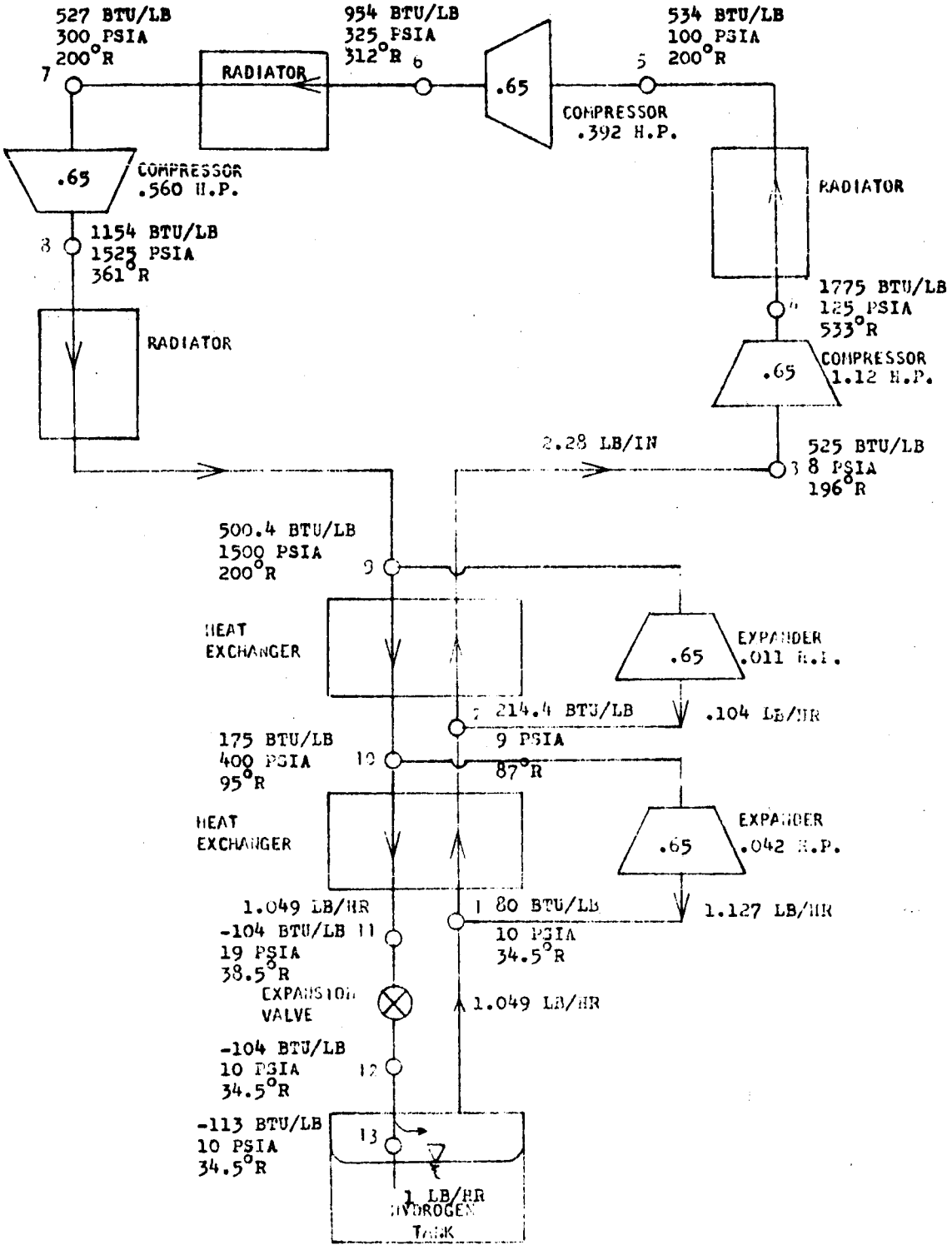

MAC A673

FIGURE 23

HYDROGEN - NEON CASCADE CYCLE SCHEMATIC

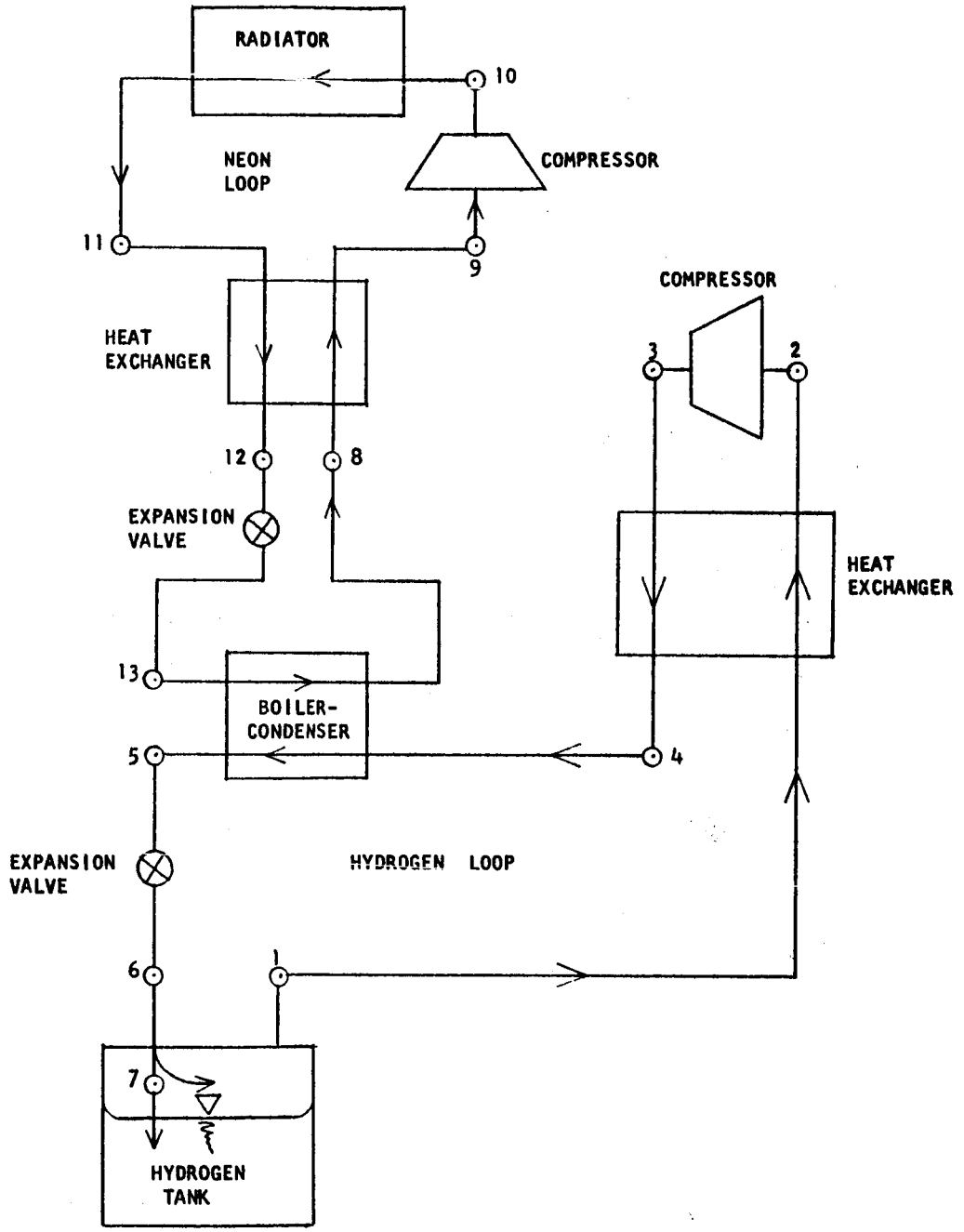

MAC A673

FIGURE 24

RADIATION ANALYSIS NETWORKS
HORIZONTAL RADIATOR

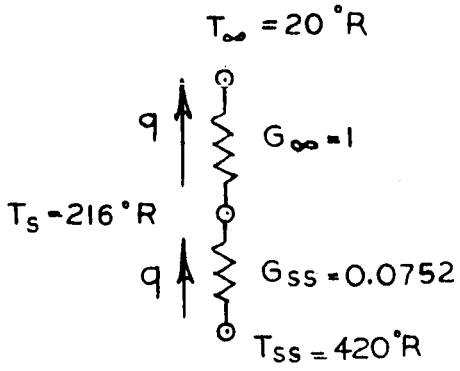

FIGURE 25A

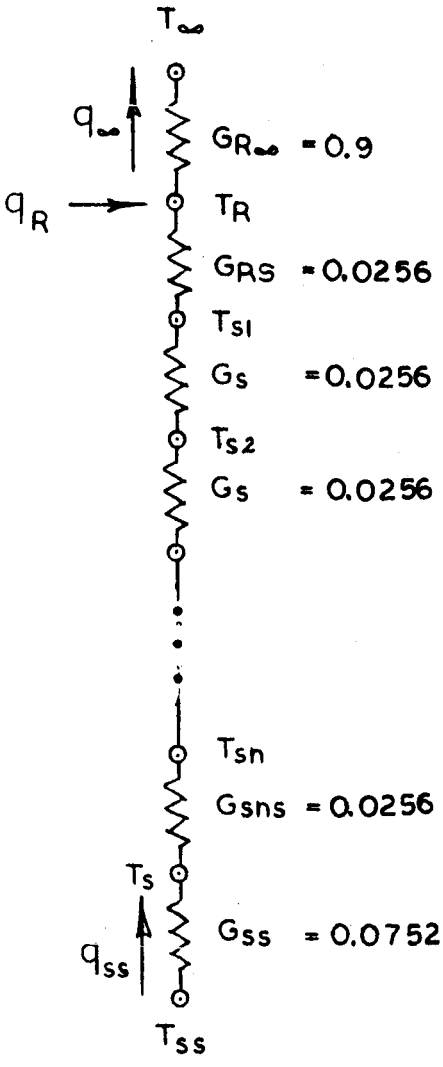

FIGURE 25B

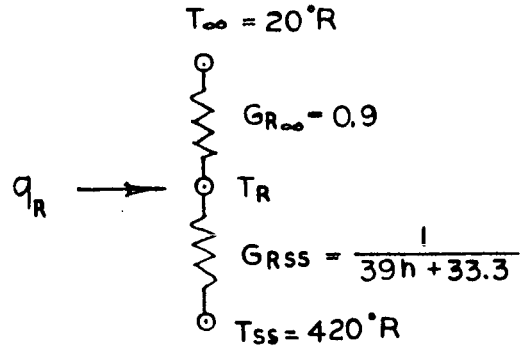

FIGURE 25C

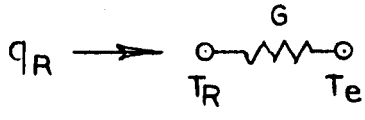

FIGURE 25D

MAC A673

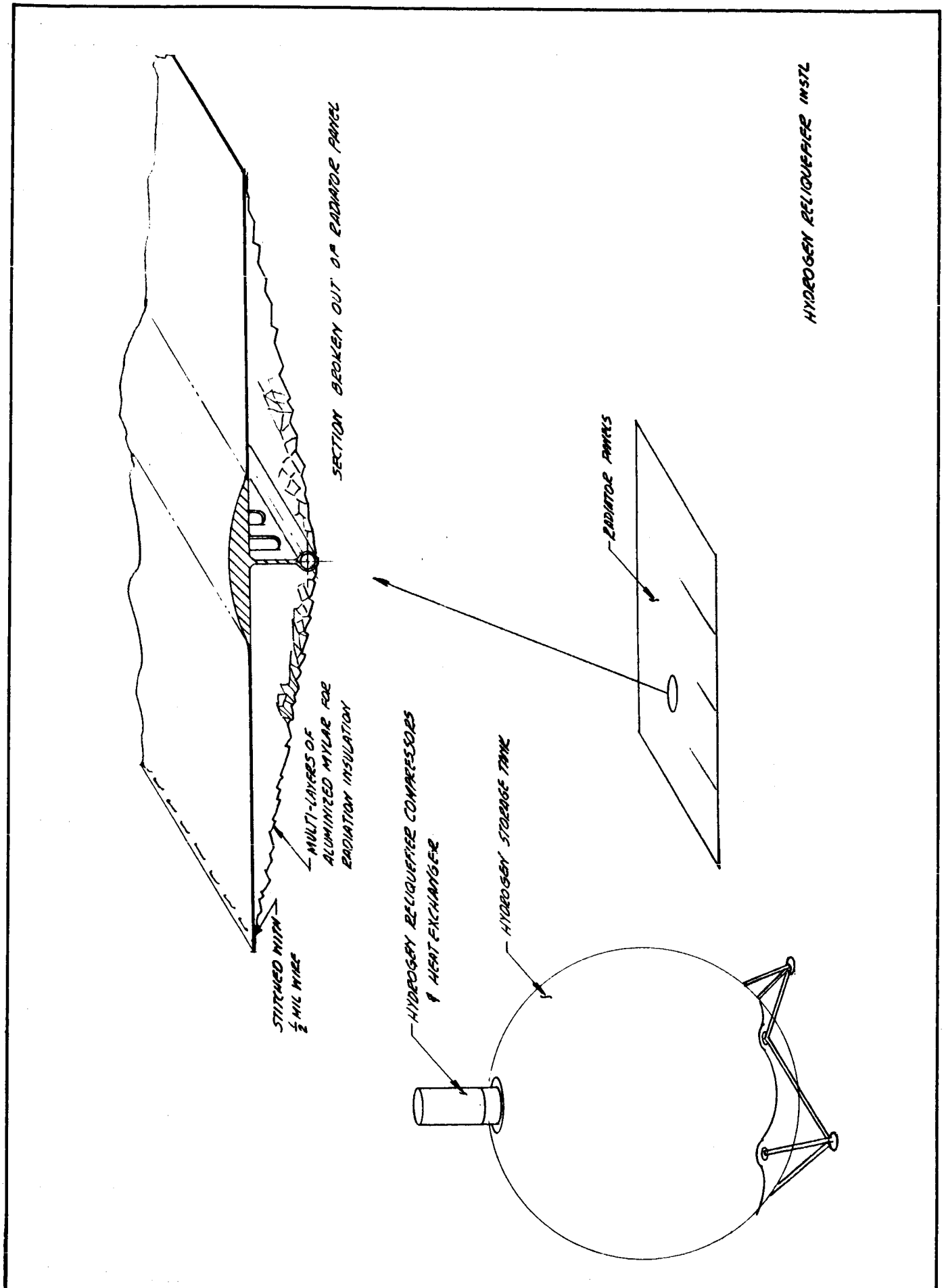

MAC A673

FIGURE 26

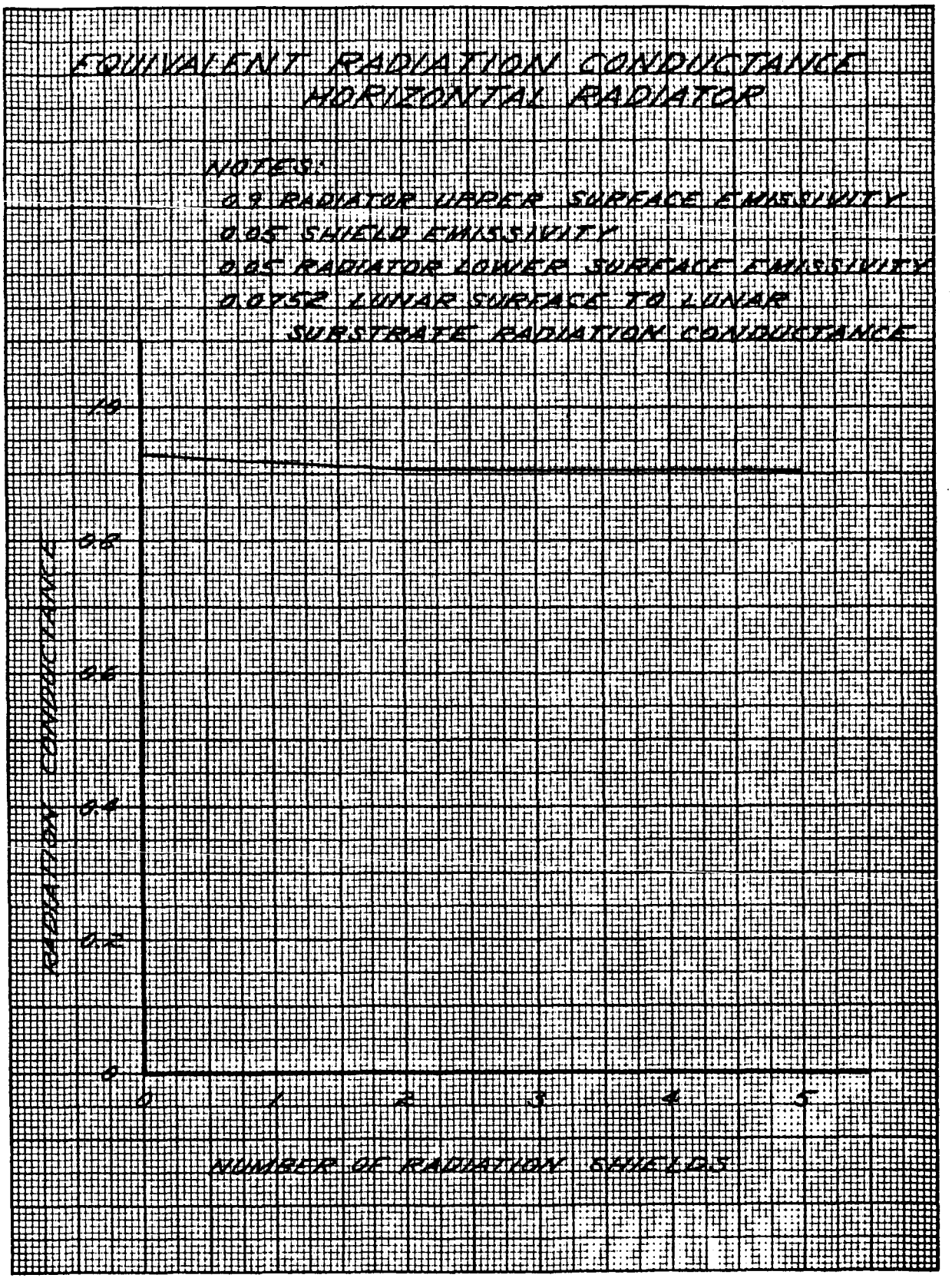

MAC A 673

FIGURE 27

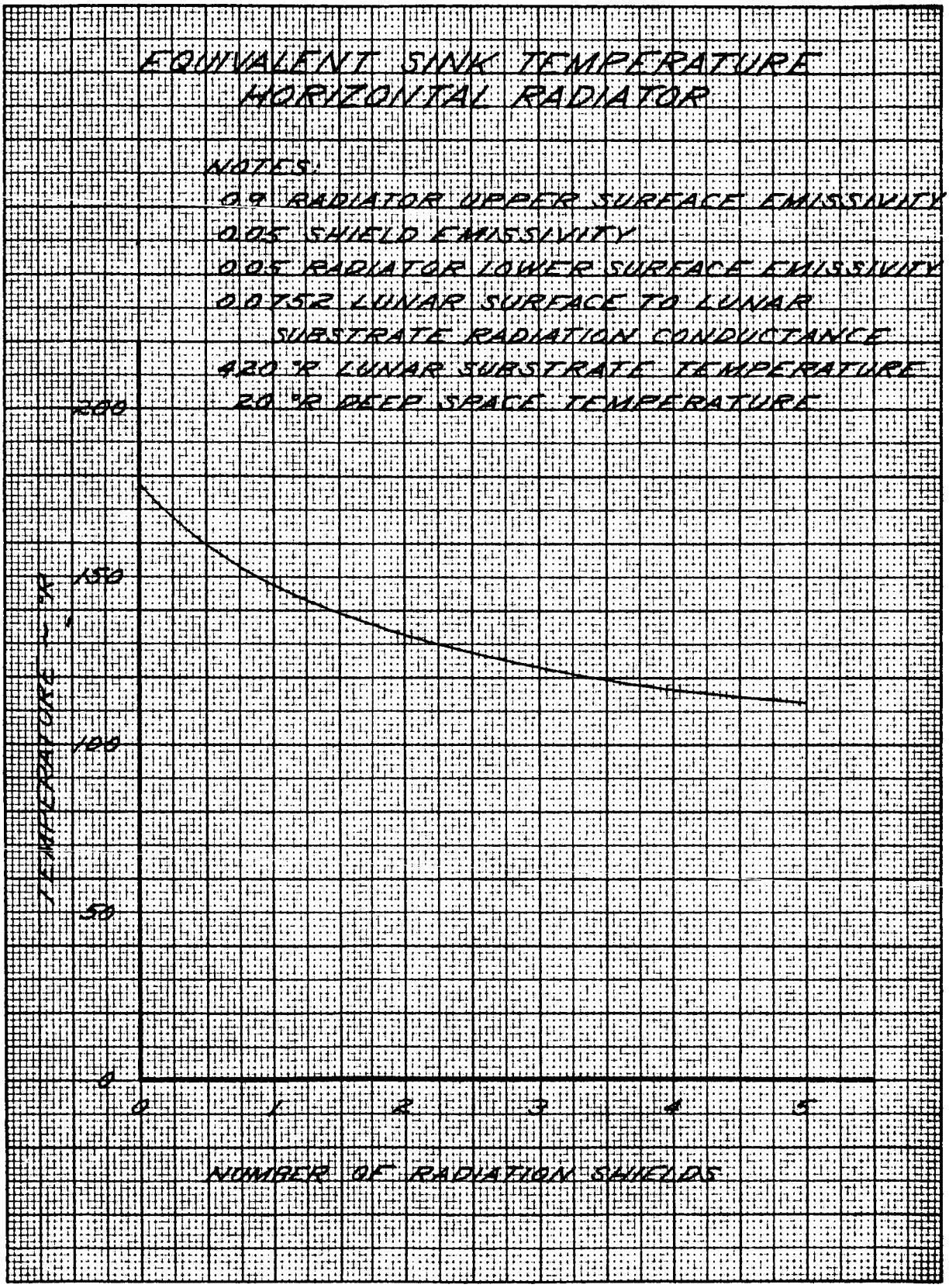

MAC A 673

FIGURE 28

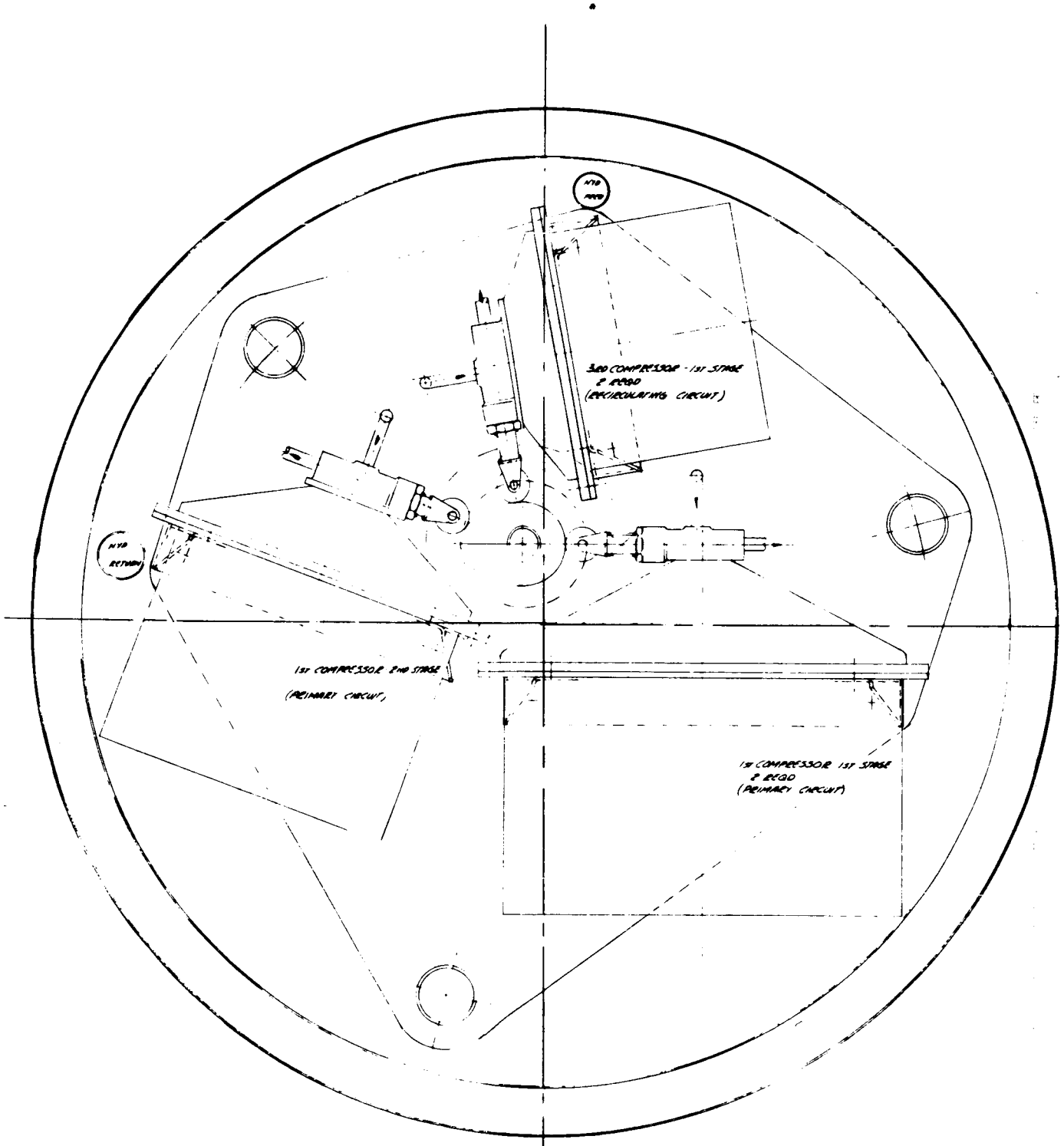

SECTION **D - D**
LOW PRESSURE DIAPHRAGM COMPRESSORS (300 CYCLE 7200 RPM)

Page 54 (1)

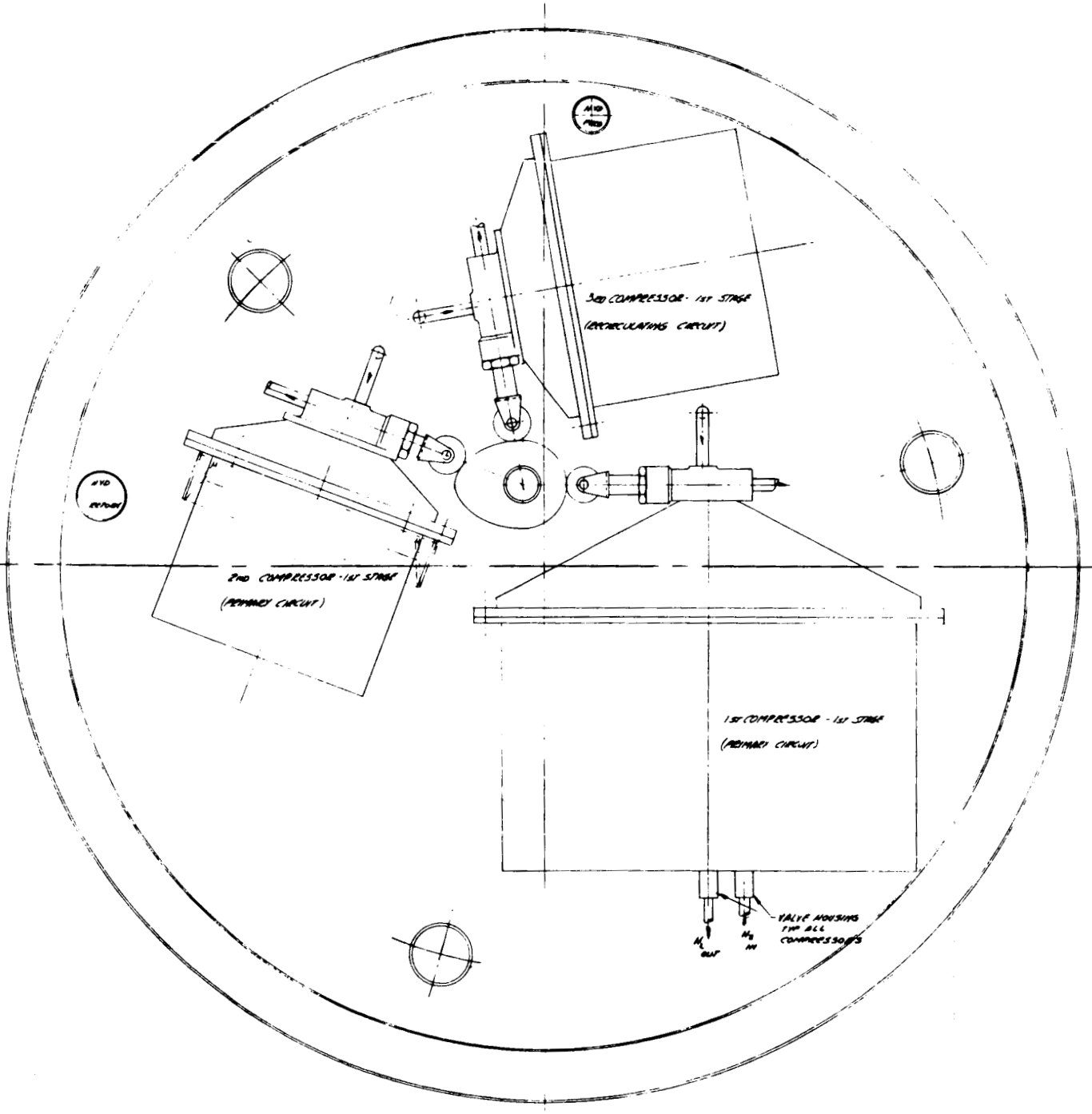

SECTION **C - C**

LOW PRESSURE DIAPHRAGM COMPRESSORS (3000 PSIG MAX)
MECHANICALLY COMPRESSED & DRIVEN BY HYDRAULIC CYL.

P.54

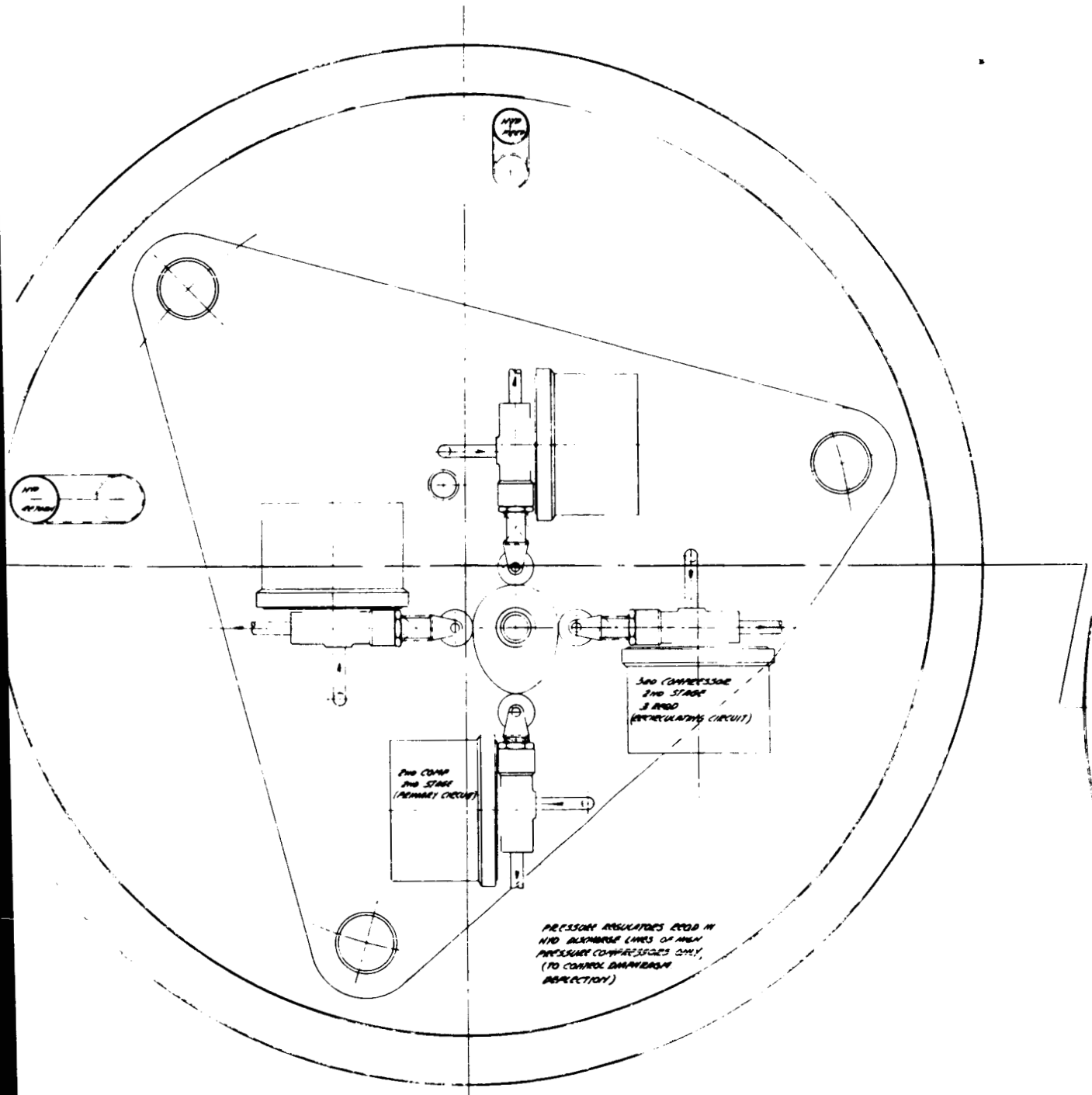

SECTION **B - B**

MAIN PRESSURE DIAPHRAGM COMPRESSORS (900 CYCLE)
HYDRAULICALLY ACTUATED

P. 54

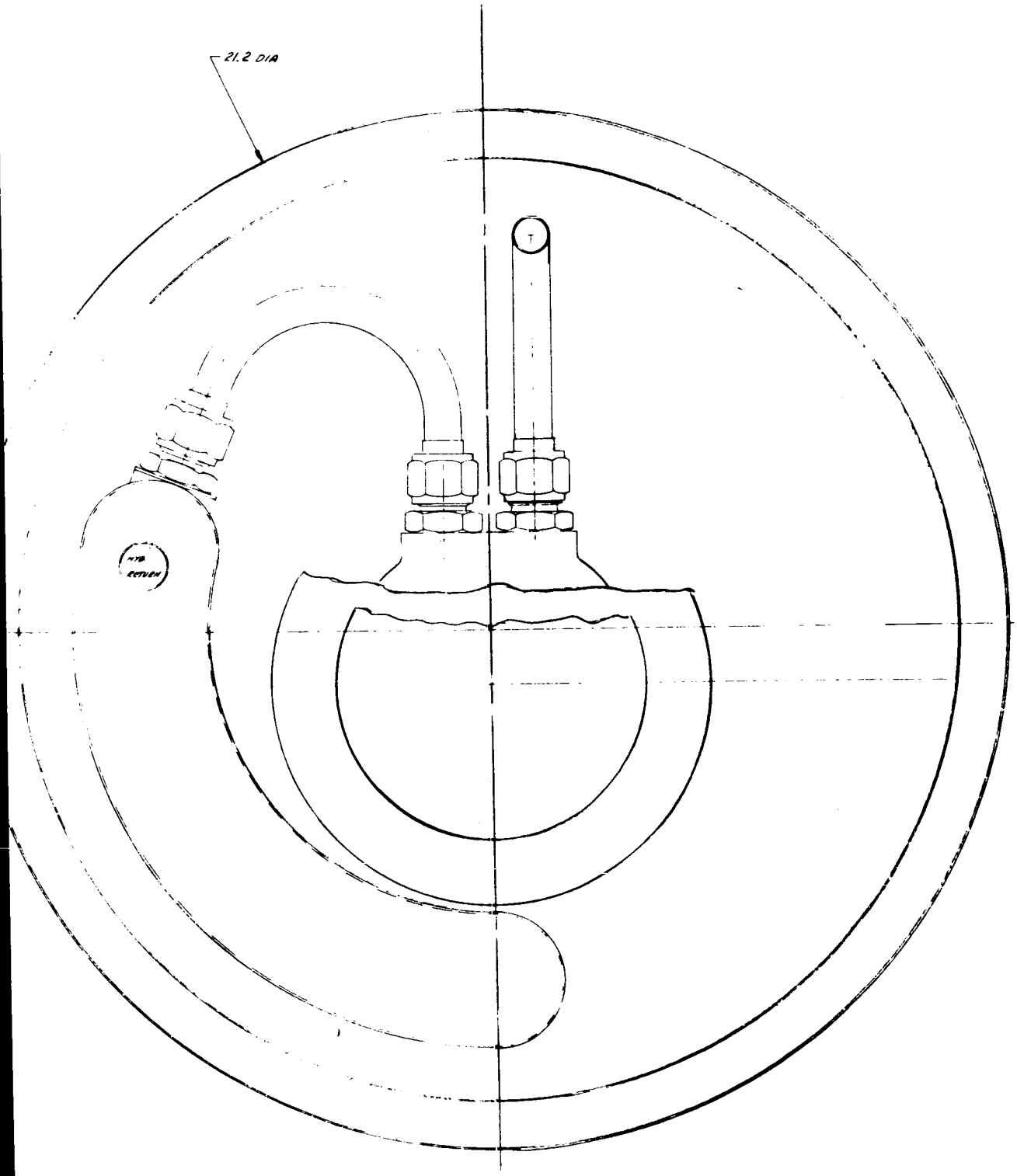

SECTION A-A

(4) P.54

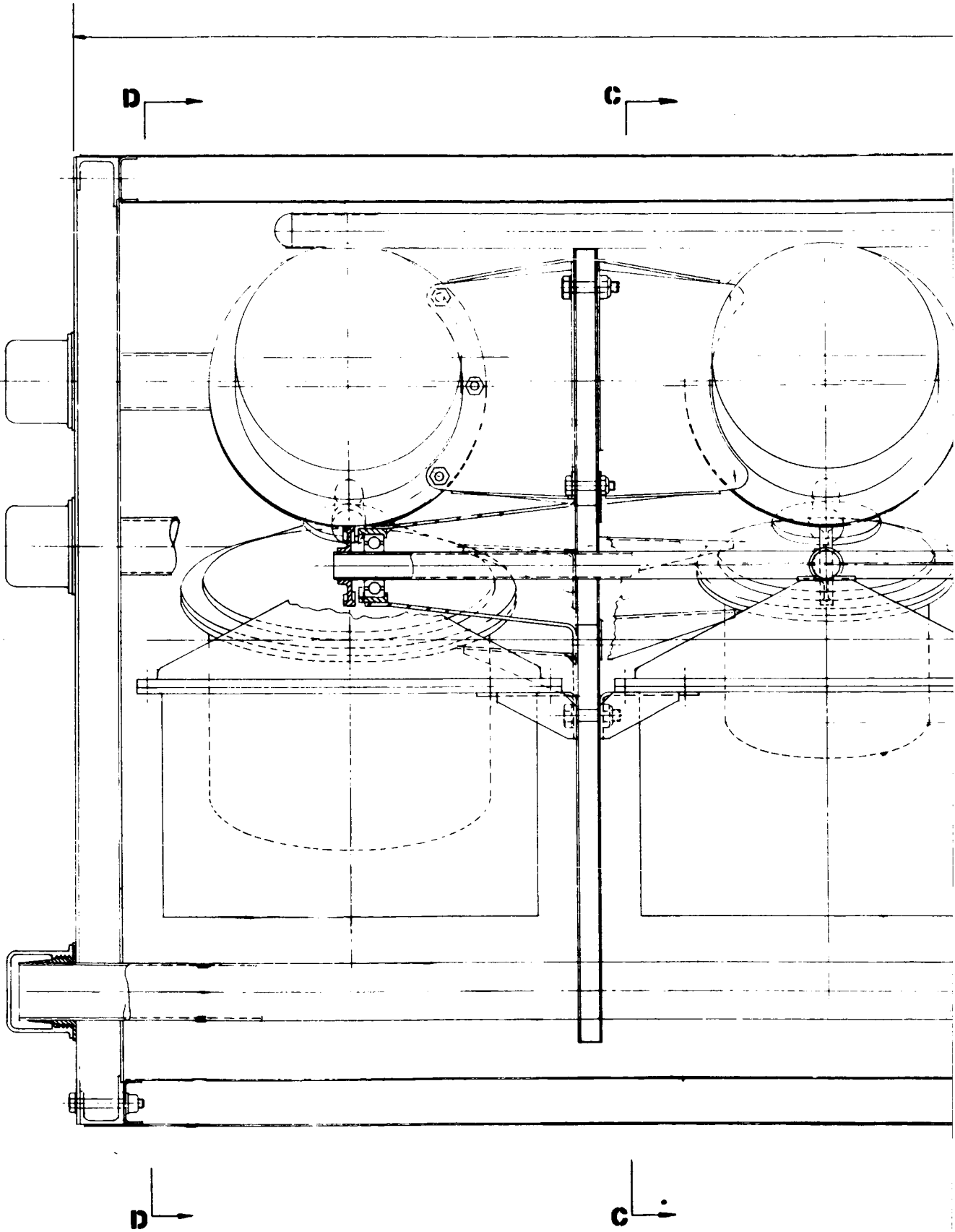

(5) p. 54

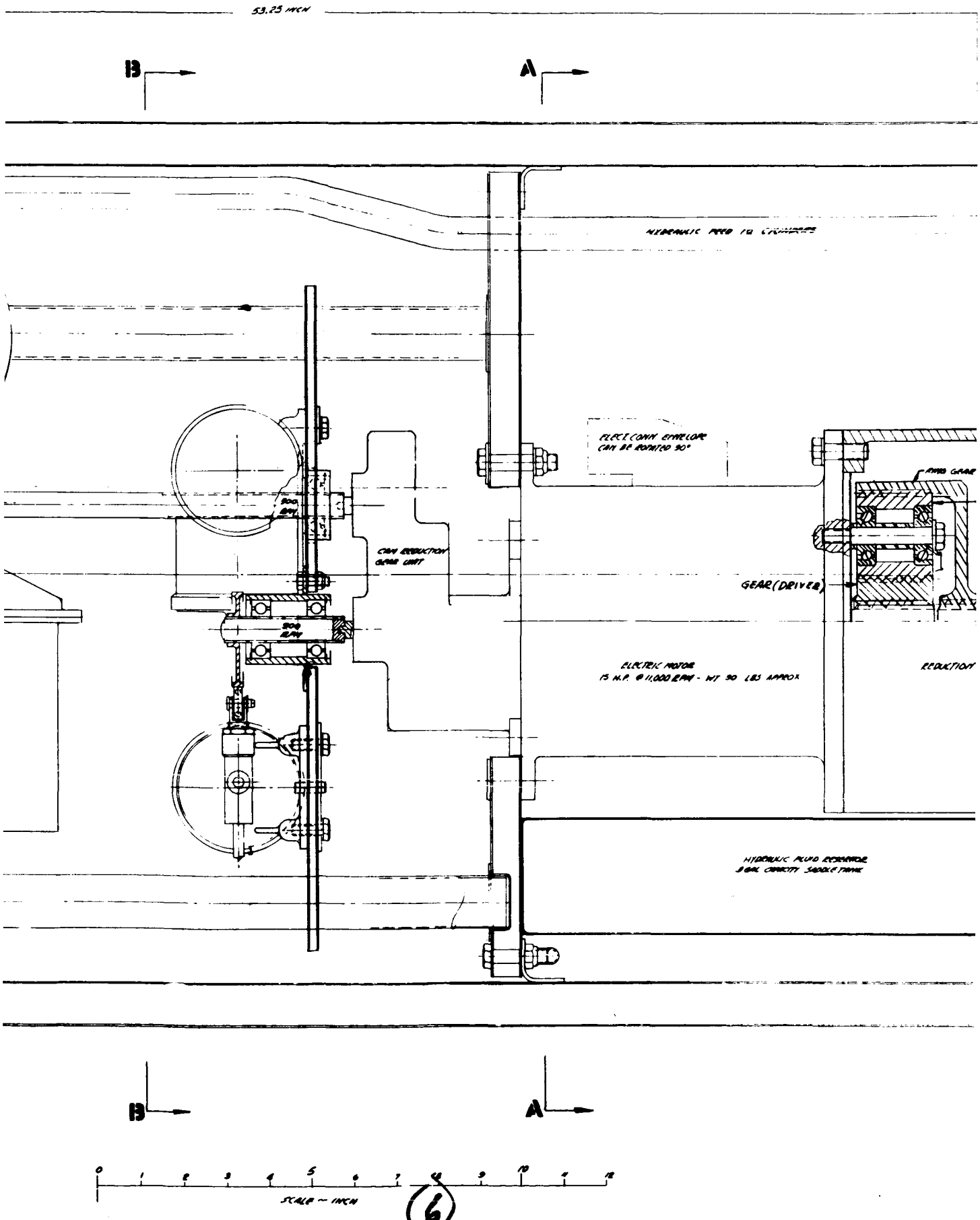
53.25 INCH
B
A
HYDRAULIC FEED TO CYLINDER
ELECT. CONN. ENVELOPE CAN BE ROTATED 90°
CAM REDUCTION GEAR UNIT
GEAR (DRIVER)
ELECTRIC MOTOR
15 H.P. @ 11,000 R.P.M. - WT 90 LBS APPROX.
REDUCTION
HYDRAULIC FLUID RESERVOIR
B
A
0 1 2 3 4 5 6 7 8 9 10 11 12
SCALE — INCH
6
4
3

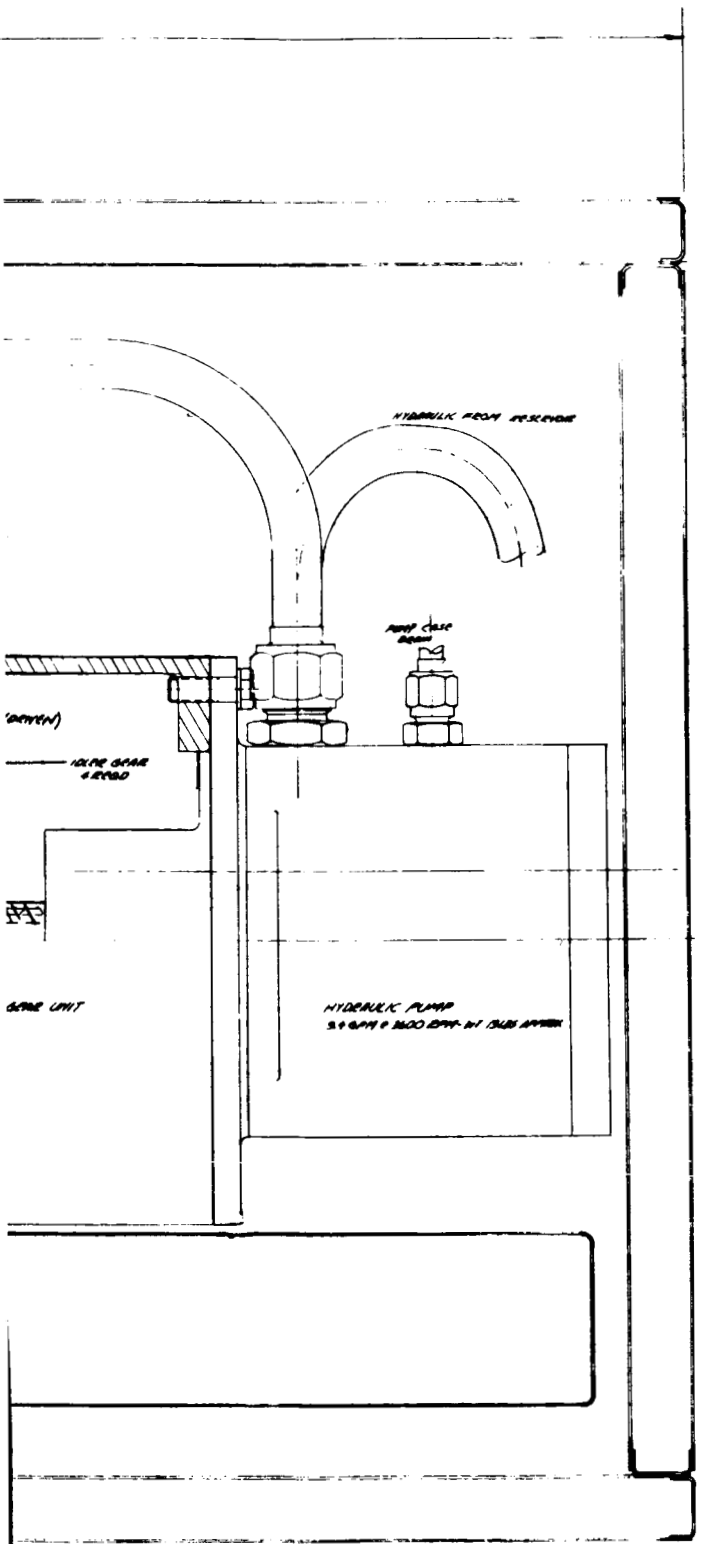

DRAWN E. YATES 2-24-64	PRELIMINARY DESIGN- HYDROGEN RELIQUEFIER COMPRESSION SYSTEM
CHECKED	
APPROVED 2-24-64	
APPROVED 2-24-64	
	CODE IDENT NO. 66845 SIZE e L 5193
	SCALE SHEET 1 OF 1

FIGURE 29

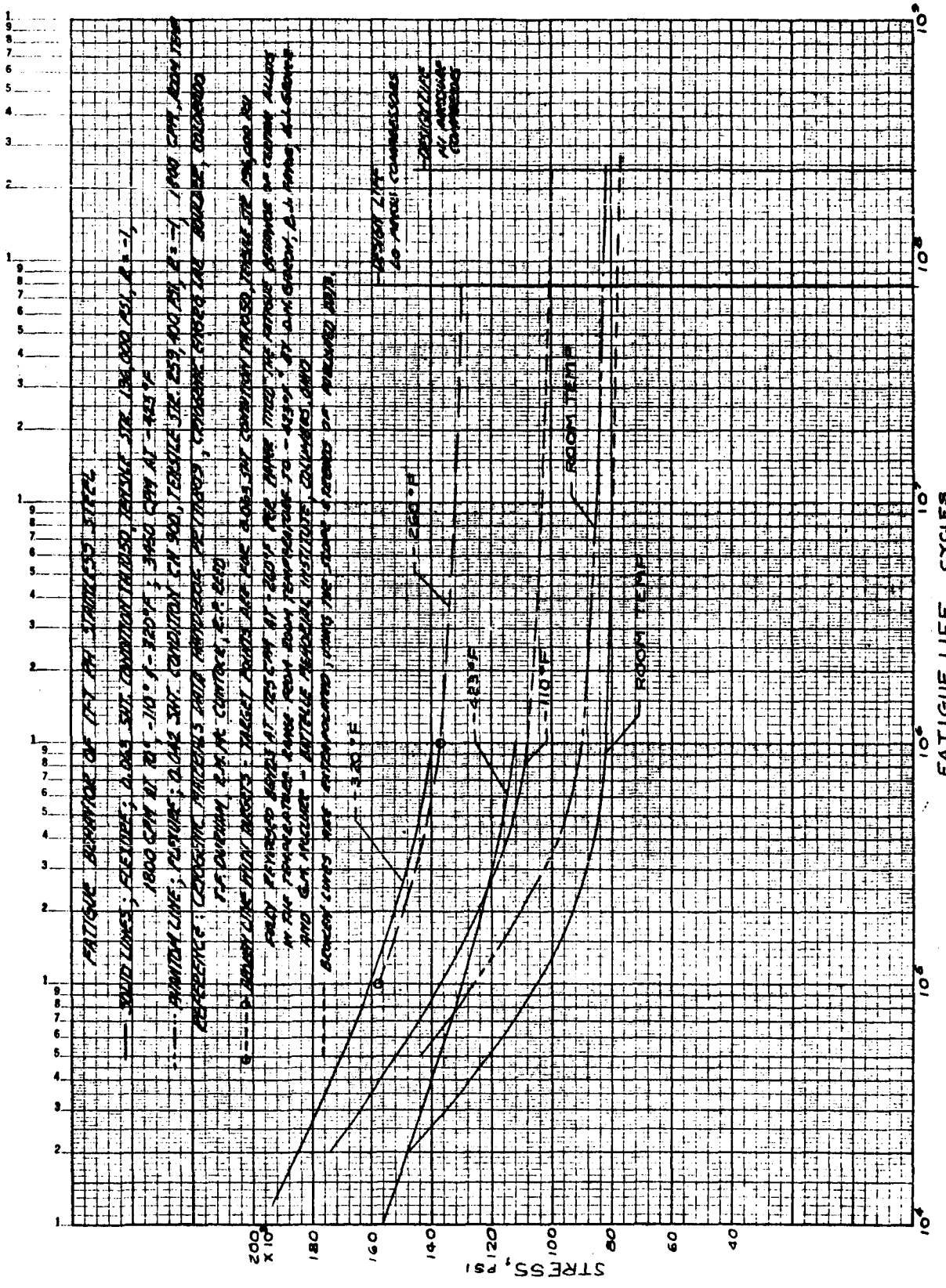
FATIGUE LIFE, CYCLES
STRESS, PSI
ROOM TEMP
-110°F
-423°F
-320°F
ROOM TEMP

FIGURE 30

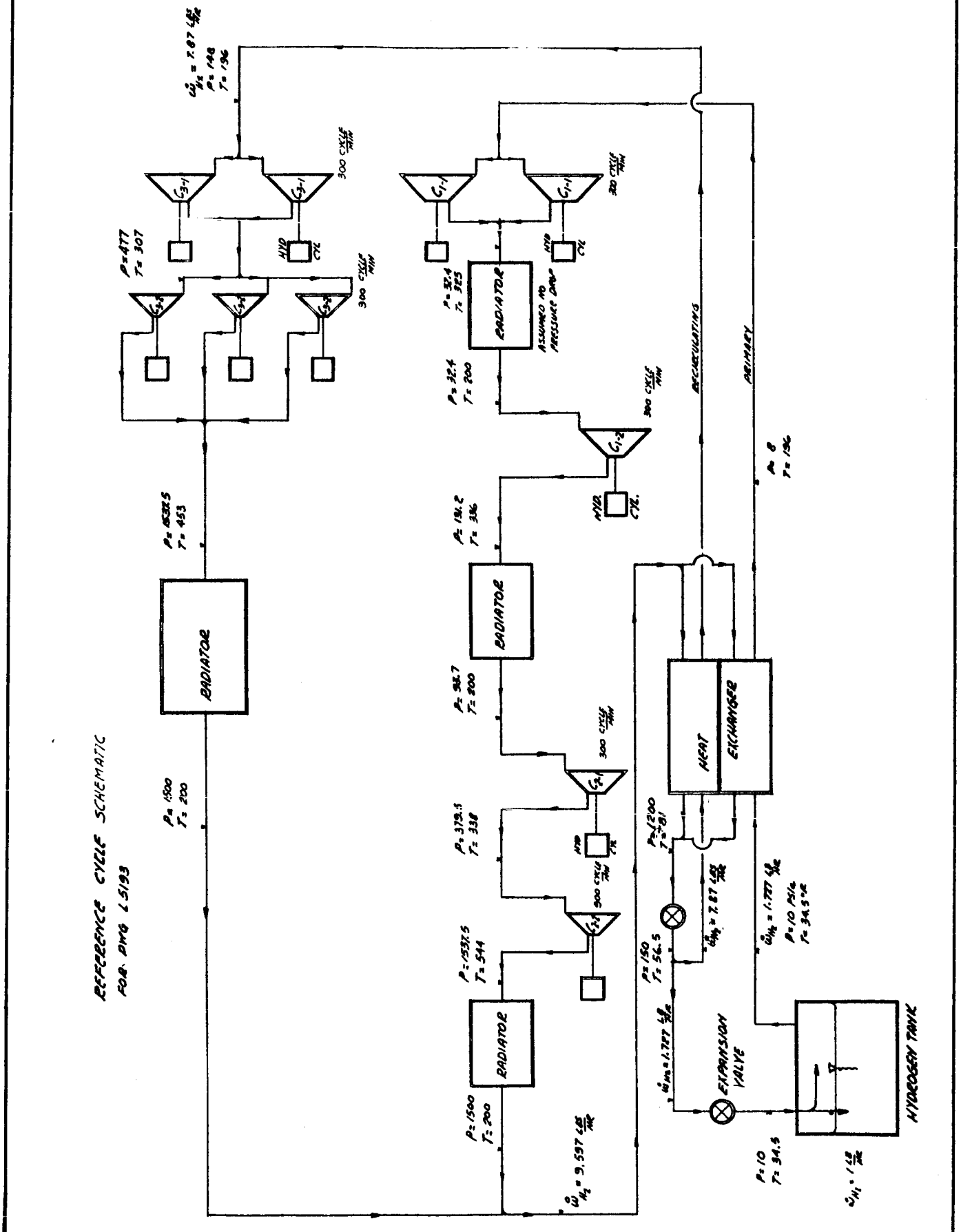
REFERENCE CYCLE SCHEMATIC
FOR DWG 1.5193
RADIATOR
RADIATOR
RADIATOR
RADIATOR
HEAT EXCHANGER
EXPANSION VALVE
HYDROGEN TANK
ACCESSORIES
PRIMARY
300 CYCLE MW
ASSUMED NO PRESSURE DROP

FIGURE 31

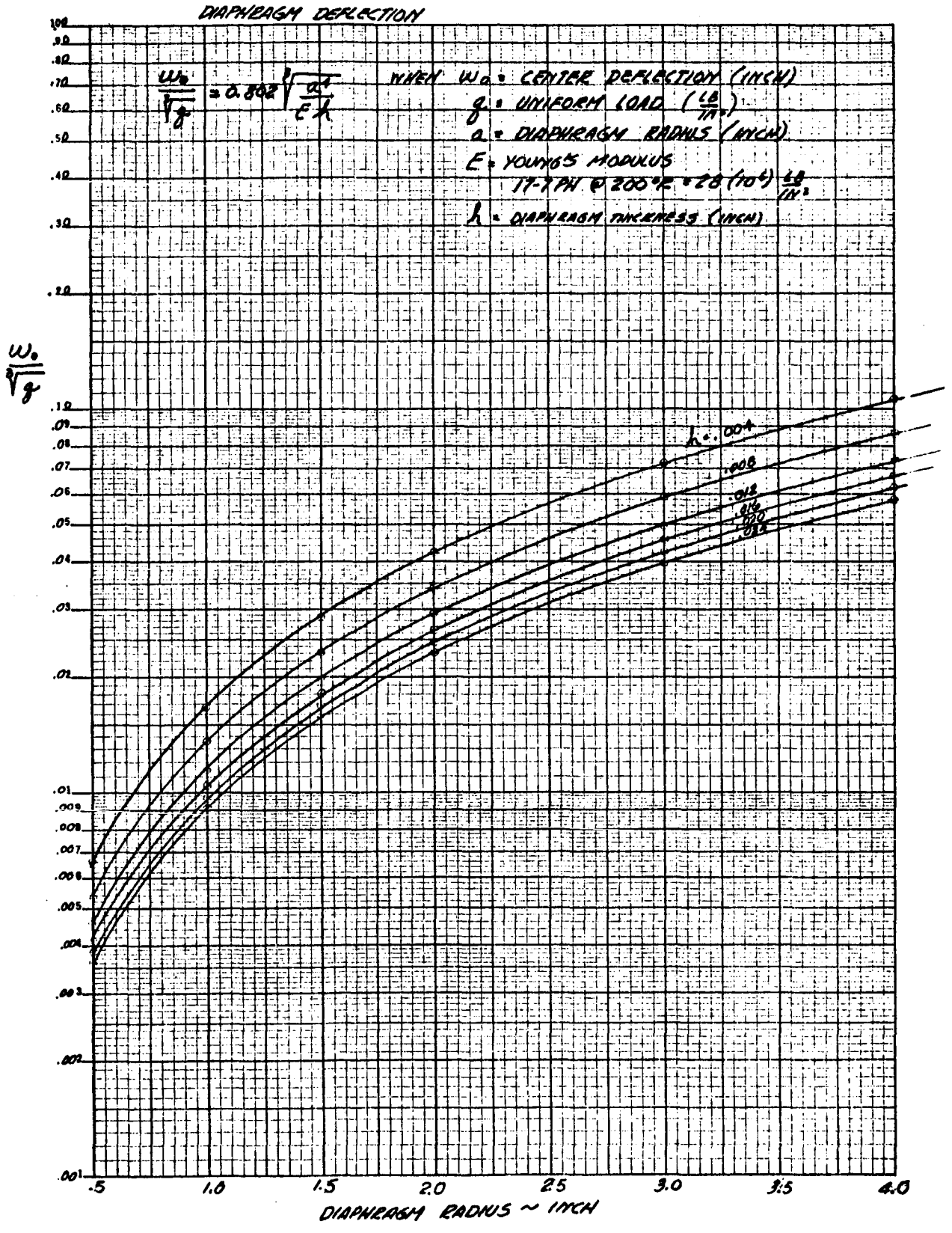

MAC A673

FIGURE 32

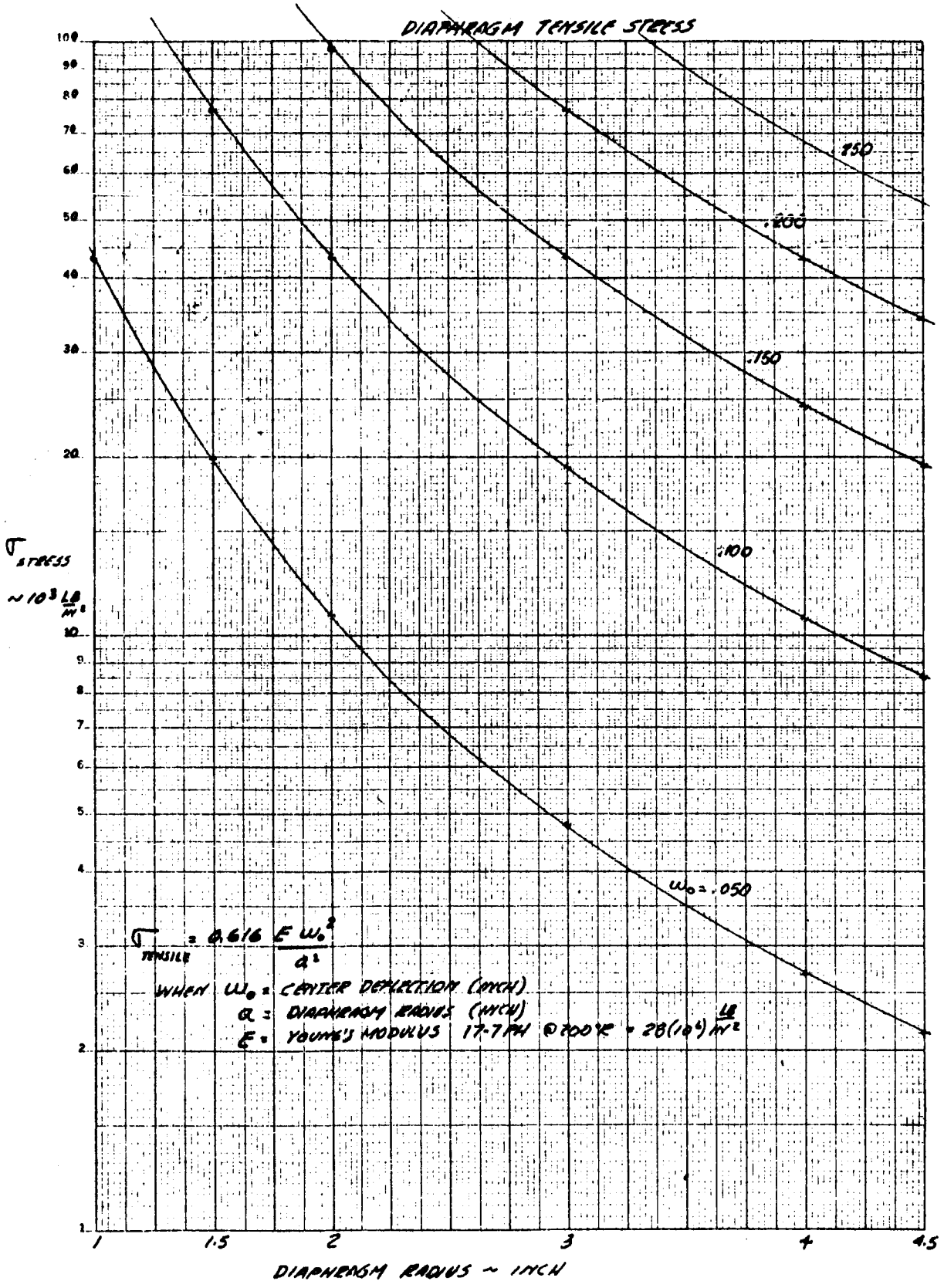

MAC A673

FIGURE 33

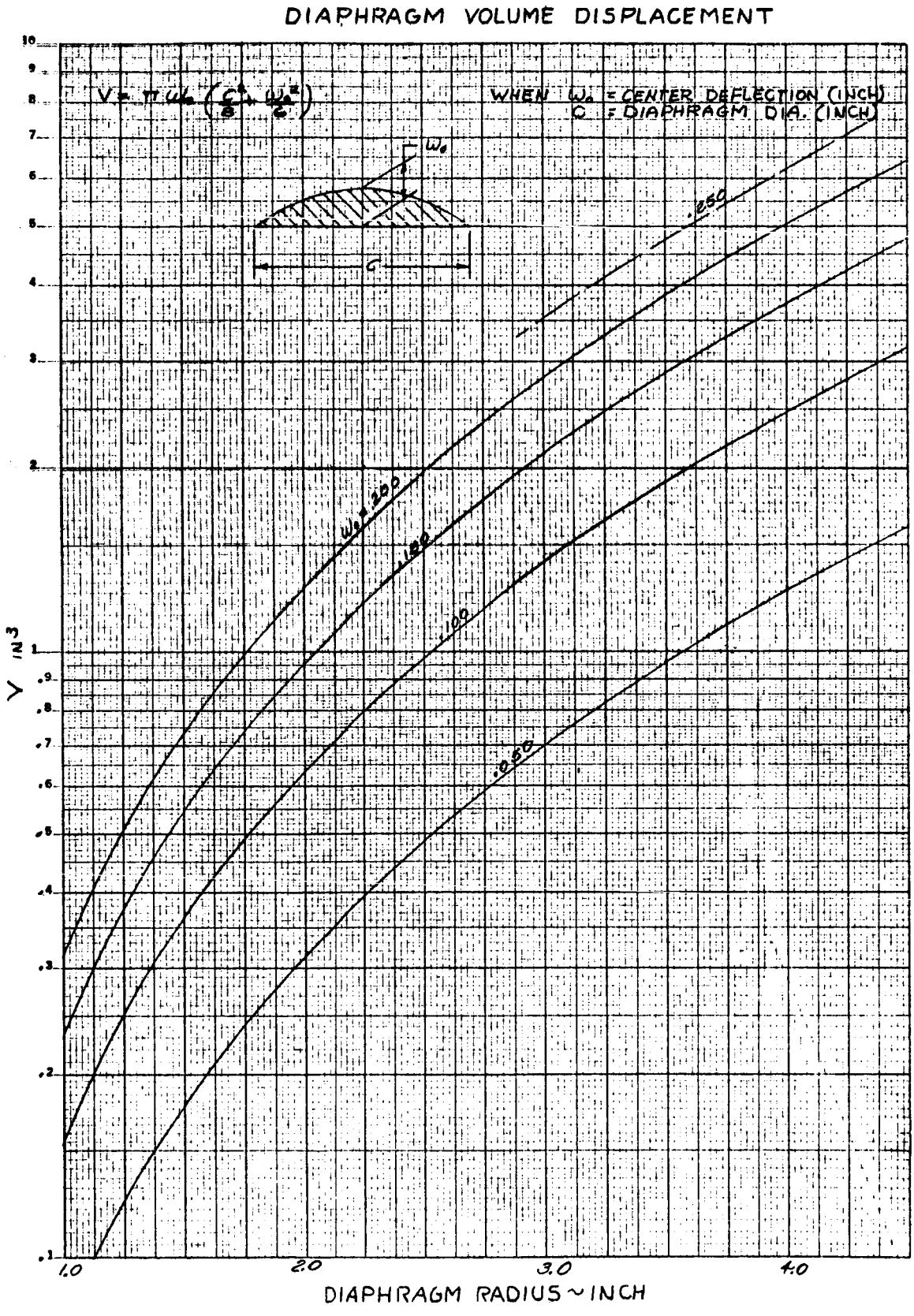

MAC A673

FIGURE 34

APPENDIX A

THERMODYNAMIC DATA FOR HYDROGEN

Hydrogen thermodynamic data from References 7, 8, and 9 are employed in the studies reported herein. References 7 and 8 are for parahydrogen, whereas Reference 9 is for 20.4°K (36.7°R) equilibrium hydrogen (99.79 percent parahydrogen and 0.21 percent orthohydrogen). However, the differences between the thermodynamic properties of these two types of hydrogen are very small, and they are entirely negligible for the studies reported herein. For example (from Figure 2 of Reference 9), the maximum difference between the enthalpies of parahydrogen and orthohydrogen is 303 Btu/lb and occurs for temperatures less than 90°R. Multiplying this enthalpy difference by the 0.21 percent mass fraction of orthohydrogen in 20.4°K equilibrium hydrogen yields a maximum enthalpy difference between parahydrogen and 20.4°K equilibrium hydrogen of 0.6 Btu/lb. (An error of 0.6 Btu/lb in the enthalpy of hydrogen results in a maximum temperature error of approximately 0.2°R.) The authors of Reference 8 estimate the accuracy of their enthalpy data to be 1 Btu/lb.

Changes in the equilibrium ortho-para composition of the hydrogen as it circulates through a cycle of a reliquefier are not considered in the studies reported herein. The use of a catalyst to speed up the conversion rates between the para and ortho forms of hydrogen could conceivably result in substantial benefits in reliquefier performance. However, this use is not considered herein. In the absence of a catalyst, the time required for an element of hydrogen to make one circuit of the reliquefier is insufficient for any significant approach to equilibrium composition to take place. The order of magnitude of this time is one second whereas a matter of hours is required for equilibrium to be approached. Of equal importance in justifying the neglect of composition changes is the fact that at any instant only a very small portion of the total hydrogen in the storage system is in the reliquefier. Over long periods of time, the composition will approach a value corresponding to equilibrium at a time averaged hydrogen temperature. Under these conditions, the time averaged temperature is essentially equal to the storage tank temperature and no significant composition change occurs.

In the case of the storage tank thermal transients, there is sufficient time for equilibrium to be approached. However, the changes in equilibrium composition are not significant.

The enthalpy datum of Reference 7 is employed. A correction of 164 Btu/lb is subtracted from the enthalpies of Reference 8 to render them consistent with those of Reference 7. The former enthalpies are first converted to units of Btu/lb by multiplying by the following conversion factor:

$$0.8929 \frac{\text{Btu/lb}}{\text{cal/gm mole}}$$

The enthalpy datum of Reference 9 is apparently consistent with that of Reference 7.

MAC A 678

APPENDIX B

ANALYSIS OF HYDROGEN RELIQUEFIER UTILIZATION

B-I. SUMMARY

This appendix describes a brief optimization study which was conducted to determine the best utilization of a hydrogen reliquefier considering the possibility of variations in hydrogen tank insulation thickness and reliquefaction of only a portion of the hydrogen boil off. The results indicate that if the specific mass of the reliquefaction system (including the mass of the power source chargeable to this system) in lb/(lb/hr) of hydrogen liquefied is less than the time period of hydrogen storage in hours, then the use of a reliquefier is advantageous and all of the boil off should be reliquefied. Further, the optimum storage tank insulation thickness with a reliquefier is less than the optimum value without a reliquefier. These results are independent of the environmental conditions and the tank construction.

B-II. NOMENCLATURE

C_1	Transport tank mass per unit hydrogen mass, lb/lb
C_2	Defined by Equation (6), lb^2/hr
M	Total variable mass (Defined by Equation (1)), lbs
M_b	Mass of hydrogen boil off, lbs
M_i	Mass of tank insulation, lbs
$\dot{m}_b$	Hydrogen boil off rate, lbs/hr
m_b*	Hydrogen boil off rate in absence of reliquefier, lbs/hr
M_r	Mass of hydrogen reliquefier, lbs
m_r	Hydrogen reliquefaction rate, lbs/hr
M_t	Incremental mass of transport tank required to carry an amount of hydrogen equal to the boil off loss, lbs
M_{min}	Minimum total variable mass without a reliquefier, lbs
M_{min-r}	Minimum total variable mass with a reliquefier, lbs
Θ	Storage period, hrs
R	Reliquefier specific mass, lbs/(lb/hr)

APPENDIX B (Continued)

variable mass is set by a constraint ($m_b \geqq 0$) rather than a minimum in the mathematical sense. It should be further noted that minimizing the total variable mass with respect to the insulation mass must (as is done above) be accomplished after the minimization with respect to the reliquefaction mass flow rate. To do so before involves the implicit assumption that the insulation mass, M_i, and the reliquefaction mass flow rate, m_r, are independent variables. They are independent only so long as the constraint, $m_b \geqq 0$, is not operative.

To obtain a standard of comparison the minimum total variable mass in the absence of a reliquefier is obtained as follows. Setting the reliquefaction mass flow rate, m_r, equal to zero in equation (9) and minimizing the total variable mass with respect to the insulation by means of the calculus -

$$\frac{dM}{dM_i} = 0 = - \frac{C_2 \theta (1 + C_1)}{M_i^2} + 1$$

whence

$$M_i = \left\{C_2 \theta (1 + C_1)\right\}^{1/2} \qquad \text{for } M = M_{min} \tag{17}$$

and

$$M_{min} = 2 \left\{C_2 \theta (1 + C_1)\right\}^{1/2} \tag{18}$$

The mass of boil-off loss for the conditions which minimize the total variable mass is obtained by setting the reliquefaction mass flow rate, m_r, in equation (5) equal to zero and combining the result with equations (4), (6), and (17) -

$$M_b = \left\{\frac{C_2 \theta}{1 + C_1}\right\}^{1/2} \qquad \text{for } M = M_{min} \tag{19}$$

Combining equations (2) and (19) yields the associated incremental transport tank mass

$$M_t = C_1 \left\{\frac{C_2 \theta}{1 + C_1}\right\}^{1/2} \tag{20}$$

Dividing equation (15) by equation (18) provides a measure of the saving in total variable mass associated with the utilization of a reliquefier -

$$\frac{M_{min - r}}{M_{min}} = \left\{\frac{R}{\theta (1 + C_1)}\right\}^{1/2} \tag{21}$$

MAC A 673

APPENDIX B (Continued)

B-III. ANALYSIS

In the following analysis the total mass of hydrogen and associated equipment which must be transported to the moon (or any other destination) to supply a given mass of hydrogen is minimized with respect to the following two variables: the mass of boil-off hydrogen vapor reliquefied and the mass of storage tank insulation employed. In this minimization only that portion of the total mass which is influenced by these two variables need be considered. This portion is hereafter referred to as the total variable mass and is equal to the sum of the mass of the boil-off hydrogen lost, the incremental mass of the transport tank required to carry a mass of hydrogen equal to the boil-off loss, the mass of the storage tank insulation, and the mass of the hydrogen reliquefier (including all mass chargeable to the reliquefier).

$$M = M_b + M_t + M_i + M_r \tag{1}$$

The incremental transport tank mass is assumed to be directly proportional to the additional mass of hydrogen which must be transported to the moon to offset the boil-off losses.

$$M_t = C_1 M_b \tag{2}$$

Substituting for the incremental transport tank mass in equation (1) by means of equation (2)

$$M = (1 + C_1)M_b + M_i + M_r \tag{3}$$

The mass of boil-off hydrogen lost is equal to the boil-off rate times the duration of hydrogen storage. (Since substantial differences in environmental conditions exist between the lunar night and the lunar day, all mass flow rates and heat transfer rates should be considered to be time averaged values.)

$$M_b = m_b \Theta \tag{4}$$

The boil-off loss rate is equal to that which would exist in the absence of a reliquefier less the rate at which hydrogen is reliquefied.

$$m_b = m_b^* - m_r \tag{5}$$

MAC A673

APPENDIX B (Continued)

In the absence of a reliquefier the boil-off loss rate is proportional to the heat transfer rate to the hydrogen. The vast majority of the thermal resistance to this heat transfer is that associated with the tank insulation. As a result the heat transfer rate and the boil-off loss rate are very nearly inversely proportional to the thickness and therefore the mass of the insulation.

$$m_b^* = \frac{C_2}{M_i} \tag{6}$$

where C_2 is dependent only upon the tank thermal environment, the tank geometry, and the type of insulation employed. Eliminating m_b^* from equation (5) by means of equation (6) and substituting for m_b in equation (4) by means of the resulting equation yields -

$$M_b = \left(\frac{C_2}{M_i} - m_r\right) \theta \tag{7}$$

Defining the reliquefier specific mass, R, as the mass of reliquefier in lb. per lb./hr. of hydrogen reliquefied -

$$R = \frac{M_r}{m_r} \tag{8}$$

Substituting in equation (3) for M_b and M_r by means of equations (7) and (8), respectively,

$$M = \frac{C_2\ \theta\ (1 + C_1)}{M_i} + M_i + m_r \left\{R - \theta\ (1 + C_1)\right\} \tag{9}$$

From inspection of equation (9) the total variable mass, M, will be reduced below that in the absence of a reliquefier ($m_r = 0$) if and only if

$$R < \theta\ (1 + C_1) \tag{10}$$

Even assuming that the transport tank incremental mass per lb. of hydrogen, C_1, is very small compared to unity, the total variable mass can be reduced by the utilization of a reliquefier provided the specific mass of the reliquefier is less than the duration of storage, i.e.

$$R < \theta \tag{11}$$

MAC A673

APPENDIX B (Continued)

From inspection of equation (9), if the employment of a reliquefier is indicated, the reliquefaction mass flow rate should be as large as possible to minimize the total variable mass, M. The maximum possible reliquefaction rate is that corresponding to zero boil-off loss. Setting the boil-off loss rate in equation (5) equal to zero and combining the result with equation (6) yields -

$$m_r = \frac{C_2}{M_i} \qquad \text{for } M = M_{min} - r \qquad (12)$$

Substituting equation (12) in equation (9) -

$$M = M_i + \frac{RC_2}{M_i} \qquad \text{for } M = M_{min} - r \qquad (13)$$

Minimizing, the total variable mass, M, with respect to the insulation mass, M_i, by means of the calculus

$$\frac{dM}{dM_i} = 0 = 1 - \frac{RC_2}{M_i^2}$$

whence

$$M_i = (RC_2)^{1/2} \qquad \text{for } M = M_{min} - r \qquad (14)$$

Substituting for M_i in equation (13) by means of equation (14) then yields the total variable mass minimized with respect to the mass of insulation (and the reliquefaction mass flow rate) -

$$M_{min - r} = 2\,(RC_2)^{1/2} \qquad (15)$$

The mass of the reliquefier for the conditions which minimize the total variable mass is equal to the insulation mass for the same conditions and is obtained by combining equations (8), (12), and (14) -

$$M_r = (RC_2)^{1/2} \qquad \text{for } M = M_{min} - r \qquad (16)$$

It should be noted that the total variable mass can not be minimized by the calculus with respect to the reliquefaction mass flow rate due to the fact that the value of the reliquefaction mass flow rate which minimizes the total

APPENDIX B (Continued)

Comparison of equations (14) and (17) reveals that the optimum insulation masses with and without a reliquefier are in the same ratio as the total variable masses. The employment of a lesser insulation thickness in conjunction with a reliquefier is thus indicated.

APPENDIX C

TRANSIENT THERMAL ANALYSIS OF THE STORAGE TANK

C-I. SUMMARY

The relationship between the amount of heat transferred to a tank containing liquid hydrogen and the pressure rise within the tank is derived herein from an energy balance. It is assumed that the hydrogen temperature is uniform. An evaluation of the order of magnitude of the terms appearing in the energy balance indicates that, in general, only the change of hydrogen internal thermal energy is significant; the changes of tank shell internal thermal energy and tank shell strain energy together contribute less 0.1 percent of the transient energy storage.

C-II. NOMENCLATURE

u	Hydrogen internal thermal energy, Btu/lb
v	Hydrogen specific volume, ft^3/lb
M	Mass of hydrogen, lbs
x	Quality of hydrogen (Mass fraction in vapor phase)
Q	Heat transferred to tank shell, Btu
P	Pressure, psi
V	Tank volume, cu ft
E	Young's modulus, psi
σ	Working stress, psi
μ	Poisson's ratio
u_s	Tank shell internal thermal energy, Btu/lb
ρ	Hydrogen density, lb/ft^3
ρ_s	Tank shell density, lb/ft^3
Δ	Increment

Subscripts

V	Saturated vapor
L	Saturated liquid
m	Maximum
i	Initial
f	Final

APPENDIX C (Continued)

C-III. ANALYSIS

An energy balance considering a control volume immediately outside the tank shell yields

$$dQ = M\,du + M_s\,d\,u_s + p\,dV \tag{1}$$

Equation (1) states that the heat transferred through the tank insulation to the tank shell is equal to the sum of the increments of the internal thermal energy of the stored hydrogen, the internal thermal energy of the tank shell, and the elastic energy of the tank shell.

From the definition of the specific volume,

$$V = M\,v$$

whence

$$dV = M\,d_v \tag{2}$$

Substituting Equation (2) in Equation (1) and integrating yields

$$Q = M\left\{(u_f - u_i) + \frac{M_s}{M}(u_{sf} - u_{si}) + \int_{v_i}^{v_f} P\,dv\right\} \tag{3}$$

As an aid in the evaluation of the second term in the braces in Equation (3), the internal thermal energy of parahydrogen is presented in Figure C-1 as a function of pressure and specific volume. The latter variable was selected because the heating of the hydrogen takes place at nearly constant volume conditions. (The volume of the tank increases very slightly due to the pressure rise during heating.) The saturated liquid and saturated vapor internal thermal energies and specific volumes of Reference 7 were employed in preparing Figure C-1. (The corrections to the saturated liquid internal thermal energy issued by the originating agency were incorporated in Reference 7). For selected values of the specific volume the quality (the mass fraction of the hydrogen in the vapor phase) was first determined for each pressure from

$$x = \frac{v - v_L}{v_v - v_L} \tag{4}$$

The internal thermal energy was then calculated using

$$u = x\,u_v + (1-x)\,u_L \tag{5}$$

MAC A639

APPENDIX C (Continued)

It is possible to show that for liquid hydrogen storage the changes of the tank shell internal thermal energy and strain energy (represented by the second and third terms within the braces in Equation (3)) are negligible. To do this an approximate value of the tank shell mass is required. This is estimated assuming a uniformly stressed spherical shell. The required shell thickness is given by

$$\delta = \frac{R\,d}{4\sigma} \tag{6}$$

Multiplying this by the shell surface area yields the volume of shell material. Multiplying this in turn by the density of the shell material yields the shell mass.

$$M_s = \frac{\pi P d^3 \rho}{4\sigma} \tag{7}$$

Multiplying the volume enclosed by the shell by the hydrogen density yields the mass of hydrogen stored.

$$M = \frac{\pi d^3 \rho}{6} \tag{8}$$

Dividing Equation (7) by Equation (8) then yields the ratio of the shell mass to the stored hydrogen mass.

$$\frac{M_s}{M} = \frac{3\rho_s P}{2\rho\sigma} \tag{9}$$

For 6061-T6 aluminum alloy at cryogenic temperatures,

$$\sigma \tilde{=} 40{,}000 \text{ psi}$$
$$\rho_s \tilde{=} 175 \text{ lb/ft}^3$$
$$\nu \tilde{=} 0.3$$
$$E \tilde{=} 10 \times 10^6 \text{ psi}$$

and for a typical tank shell design

$$P_m = 30 \text{ psi}$$
$$\rho = 4.2 \text{ lb/ft}^3$$

APPENDIX C (Continued)

whence

$$\frac{M_s}{M} = 0.0468$$

(The tank shell thickness for this design is 0.045 inch.) For a 20-foot diameter tank, the hydrogen hydrostatic head is 0.1 psi. Since this is small compared to the tank pressure, the assumption of a uniformly stressed shell should yield substantially correct estimates of the shell mass.

From Reference 10, the enthalpy change of aluminum from 1.8°R to 54°R is less than 0.1 Btu/lb. (The internal thermal energy change is slightly less.) For this temperature change the second term within the braces in Equation (3) is thus less than 0.005 Btu/lb (of hydrogen). The temperature change associated with a rise in tank pressure from 10 psia to 30 psia is from 34.3°R to 41.3°R; and, from Figure C-1, the associated change in hydrogen internal thermal energy amounts to 16.7 Btu/lb. The contribution of the change of tank shell internal thermal energy is thus entirely negligible even compared to the change of hydrogen internal thermal energy for a substantially smaller temperature change.

The order of magnitude of the contribution of the tank shell strain energy (the third term within the braces in Equation (3)) is estimated for the same change of tank pressure considered above as follows. The change of hydrogen specific volume is determined from the change in tank volume.

$$\frac{\Delta v}{v} = \frac{\Delta V}{V} = 3 (1 - \nu) \frac{\Delta \sigma}{E} \qquad (10)$$

The tank shell stress is directly proportional to the pressure.

$$\frac{\sigma}{\sigma_m} = \frac{P}{P_m} \qquad (11)$$

From Equations (10) and (11)

$$\frac{(\Delta v)}{v} = 3 (1 - \nu) \frac{\sigma_m}{E P} (\Delta P) \qquad (12)$$

For the properties of 6061-T6 aluminum alloy listed above and for the pressure change from 10 psia to 30 psia,

$$(\Delta v) = 1.333 \times 10^{-3} \text{ ft}^3/\text{lb}$$

Multiplying this change of specific volume by the maximum pressure of 30 psi (and converting to thermal units) yields a product which is greater than the third term within the braces in Equation (3), viz.

$$P(\Delta)v) = 0.0074 \text{ Btu/lb}$$

The contribution of the change in tank shell strain energy is thus entirely negligible compared to the change of hydrogen internal thermal energy.

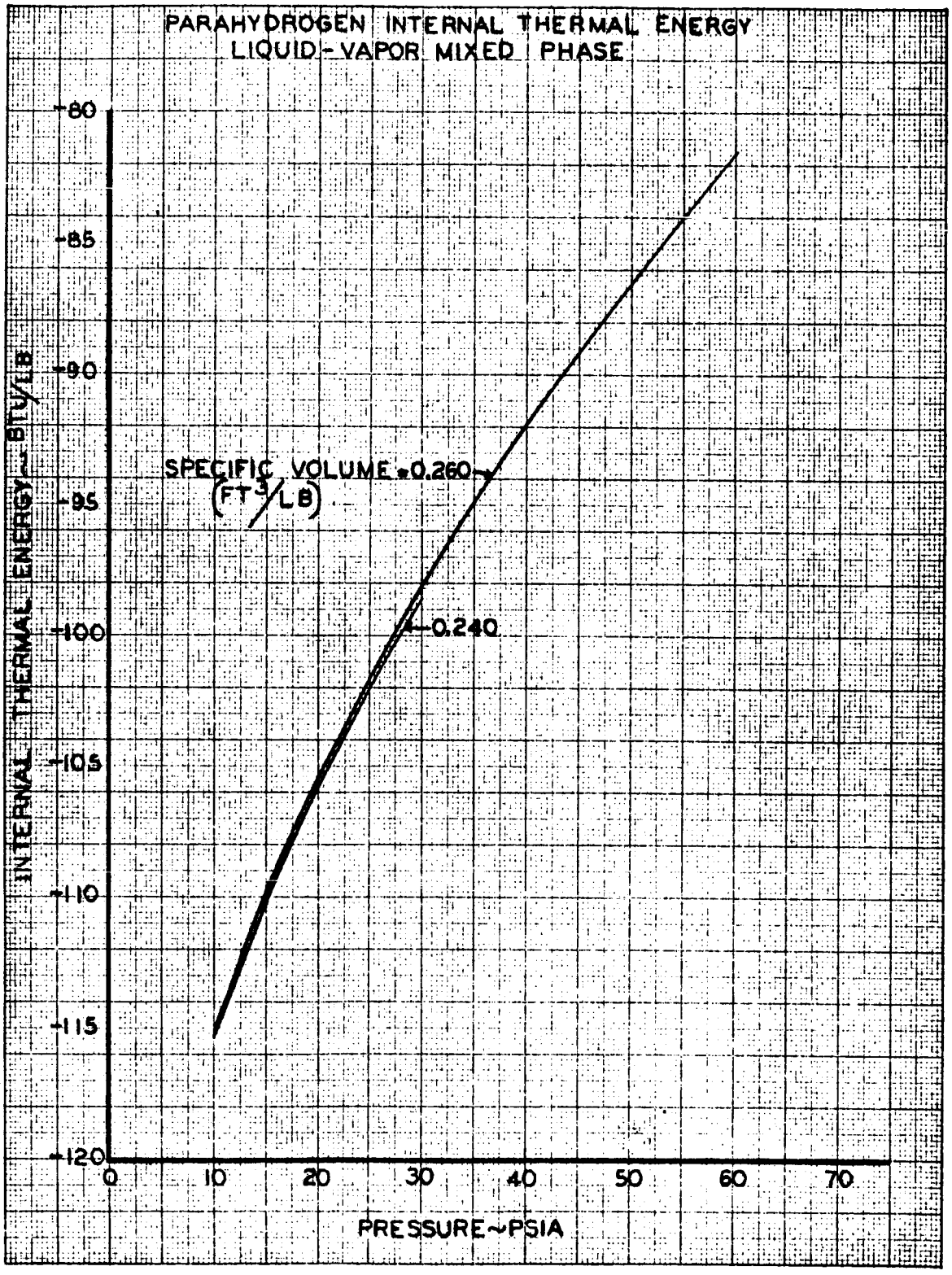

MAC A 673

FIGURE C-1

APPENDIX D

RADIATOR AREA REQUIREMENT

D-I. INTRODUCTION

As a fluid is cooled in passing through a radiator, the reduction in fluid temperature gives rise to a reduction in the radiant heat transfer rate per unit surface area. This effect is considered in a general analysis of radiator area requirements presented herein. To facilitate the application of the analysis, numerical results are also presented in both tabular and graphical forms.

D-II. ASSUMPTIONS

The following assumptions are made in the analysis:

1. Steady state
2. Gray body radiation
3. All portions of the radiator surface are exposed to the same radiation environment
4. Uniform surface heat transfer effectiveness
5. Constant specific heat of the fluid flowing through the radiator

D-III. NOMENCLATURE

A	Radiator surface area, ft^2
A_b	Radiator surface area for same heat transfer rate and uniform fluid temperature of T_b, ft^2
c_p	Specific heat at constant pressure, (Btu/lb)/°R
d	Differential
F	Radiation configuration factor between radiator and sink
h	Fluid enthalpy, Btu/lb
m	Mass flow rate of fluid passing through radiator, lb/hr
q	Heat transfer rate, Btu/hr
T_a	Bulk average temperature of fluid entering radiator, °R
T_b	Bulk average temperature of fluid leaving radiator, °R
T_o	Sink temperature (temperature to which radiator is radiating), °R
η	Surface heat transfer effectiveness
σ	Stefan-Boltzmann constant = 0.1714×10^{-8} (Btu/hr)/(ft^2 $°R^4$)

APPENDIX D (Continued)

D-IV. ANALYSIS

Consider an infinitesimal section of a radiator of surface area (dA) in which a fluid temperature change of (dT) is effected and from which heat is radiated at a rate of (dq). A steady-state energy balance on this section yields -

$$dq = -mdh \tag{1}$$

Substituting for (dq) by means of the rate equation for gray body radiation and substituting $c_p(dT)$ for (dh) yields -

$$\sigma F \eta (T^4 - T_o^4)\,(dA) = -mc_p\,(dT) \tag{2}$$

The surface heat transfer effectiveness, η, is by definition the radiant heat transfer rate divided by the radiant heat transfer rate that would prevail if the local radiator surface temperature were equal to the local fluid temperature. As such the surface heat transfer effectiveness includes the effects of the temperature differences associated with both the convection within the fluid passage and conduction from the walls of the fluid passage to the radiation surface elements. (The term "surface heat transfer effectiveness" is used herein since only the effect of the latter is included in the usual definition of fin heat transfer effectiveness.)

Solving equation (2) for the area (dA) required to effect a fluid temperature change (dT) and then integrating to obtain the total area required to cool the fluid from its inlet temperature, T_a, to its exit temperature, T_b -

$$A = \frac{-mc_p}{\sigma F \eta} \int_{T_a}^{T_b} \frac{dT}{T^4 - T_o^4} \tag{3}$$

Separation of the integrand into partial fractions and integrating yields -

$$A = \frac{-mc_p}{2\sigma F \eta T_o^3} \left[\arctan\left(\frac{T}{T_o}\right) - \operatorname{arctanh}\left(\frac{T}{T_o}\right) \right]_{T_a}^{T_b}$$

MAC A673

APPENDIX D (Continued)

whence -

$$A = \frac{mc_p}{2\sigma F \eta T_o^3}\left\{\text{arctanh}\left(\frac{T_o}{T_b}\right) - \arctan\left(\frac{T_o}{T_b}\right) - \text{arctanh}\left(\frac{T_o}{T_a}\right) + \arctan\left(\frac{T_o}{T_a}\right)\right\} \quad (4)$$

In the numerical results presented herein the radiator area is normalized with the radiator area, A_b, that would be required if the bulk average temperature of the fluid throughout the radiator were uniform and equal to the value at the exit, T_b. By definition then

$$A_b = \frac{q}{\sigma F \eta (T_b^4 - T_o^4)} \quad (5)$$

From an overall energy balance on the radiator -

$$q = mc_p (T_a - T_b) \quad (6)$$

Substituting for the heat transfer rate, q, in equation (5) by means of equation (6) and dividing equation (4) by the resulting equation then yields the expression employed in the numerical computations -

$$\left(\frac{A}{A_b}\right) = \frac{\left\{1 - \left(\frac{T_o}{T_b}\right)^4\right\}}{2\left(\frac{T_o}{T_b}\right)^3\left\{\left(\frac{T_a}{T_b}\right) - 1\right\}}\left\{\text{arctanh}\left(\frac{T_o}{T_b}\right) - \arctan\left(\frac{T_o}{T_b}\right) - \text{arctanh}\left(\frac{T_o}{T_a}\right) + \arctan\left(\frac{T_o}{T_a}\right)\right\} \quad (7)$$

In the special case of the sink temperature, T_o, approaching zero, equation (7) becomes an indeterminate form and hence can not be employed for numerical computations. This difficulty is circumvented by deriving the expression equivalent to equation (7) for this special case. This may be accomplished in either of two ways: setting the sink temperature, T_o, equal to zero in equations (3) and (5) and, beginning with equation (3), proceeding along the same general lines as in the development of equation (7) or by evaluating the limit of the right hand side of equation (7) from the calculus (using L'Hospital's rule). The result is, of course, the same, namely -

$$\left(\frac{A}{A_b}\right) = \frac{1}{3}\left(\frac{T_b}{T_a}\right)\left\{\left(\frac{T_b}{T_a}\right)^2 + \left(\frac{T_b}{T_a}\right) + 1\right\} \qquad \left(\frac{T_o}{T_b}\right) = 0 \quad (8)$$

MAC A673

APPENDIX D (Continued)

The former approach yields, as an intermediate result, the following expression for the radiator area -

$$A = \frac{mc_p}{3\sigma F \eta T_b^3} \left\{ 1 - \left(\frac{T_b}{T_a}\right)^3 \right\} \qquad \left(\frac{T_o}{T_b}\right) = 0 \qquad (9)$$

Application of Results

The first step in the application of the analysis results is the computation by means of equation (5) of the radiator surface area, A_b, that would be required if the bulk average temperature of the fluid throughout the radiator were uniform and equal to the value at the exit, T_b. The ratio of the actual radiator area to this radiator area, (A/A_b), is presented in tabular and graphical forms in Table D-I and Figure D-1, respectively, as a function of the inlet to exit and exit to sink temperature ratios, (T_a/T_b) and (T_b/T_o). The ratio, (A/A_b), is evaluated from a knowledge of the temperatures and then multiplied by A_b to yield the actual radiator area, A.

APPENDIX D (Continued)

TABLE D-I

RADIATOR AREA REQUIREMENTS

T_o Sink temperature

T_a Fluid temperature into radiator

T_b Fluid temperature out of radiator

A Radiator surface area

A_b Radiator surface area for same heat transfer rate and uniform fluid temperature of T_b

T_a/T_b	A/A_b				
	$\frac{T_o}{T_b} = 0$	$\frac{T_o}{T_b} = 0.4$	$\frac{T_o}{T_b} = 0.5$	$\frac{T_o}{T_b} = 0.6$	$\frac{T_o}{T_b} = 0.7$
1.0	1.0000	1.0000	1.0000	1.0000	1.0000
1.1	0.8289	0.8252	0.8205	0.8098	0.7897
1.2	0.7022	0.6973	0.6900	0.6756	0.6489
1.4	0.5296	0.5241	0.5164	0.5010	0.4733
1.6	0.4199	0.4149	0.4078	0.3938	0.3690
1.8	0.3452	0.3409	0.3345	0.3221	0.3005
2.0	0.2917	0.2878	0.2821	0.2713	0.2524
2.2	0.2517	0.2482	0.2433	0.2337	0.2170
2.4	0.2209	0.2178	0.2134	0.2048	0.1898
2.6	0.1965	0.1937	0.1897	0.1820	0.1686
2.8	0.1768	0.1741	0.1706	0.1636	0.1515
3.0	0.1605	0.1582	0.1549	0.1485	0.1374
3.2	0.1469	0.1448	0.1417	0.1359	0.1257
3.4	0.1354	0.1334	0.1306	0.1251	0.1158

MAC A673

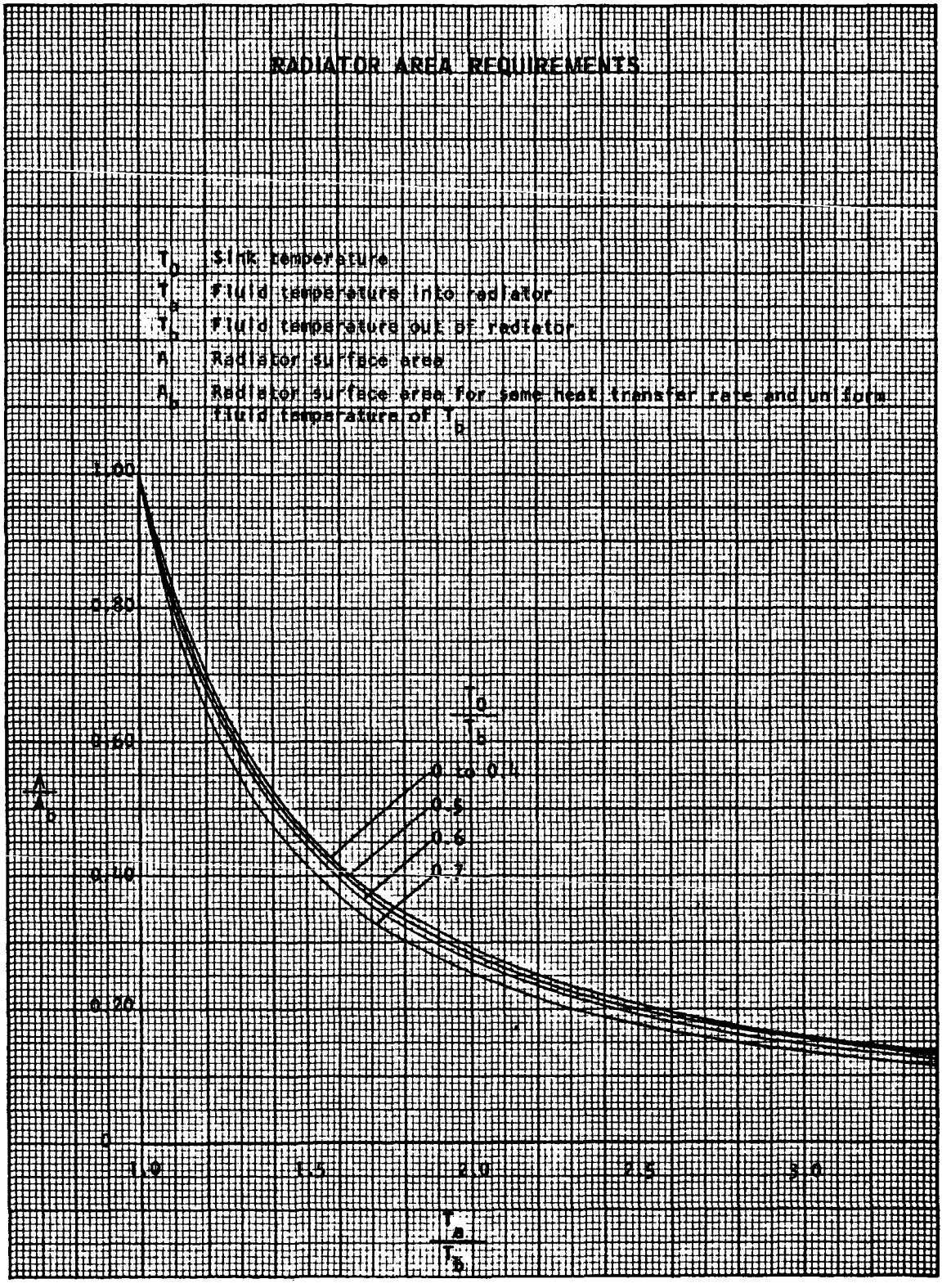

MAC A673

FIGURE D-1

DISTRIBUTION

Copy No.	Transmitted to
1 to 11 & Reproducible.	National Aeronautics and Space Administration George C. Marshall Space Flight Center Purchasing Office Huntsville, Alabama 35812 Attn.: PR-EC